

University of Alberta

***PASSIVITY DEGRADATION OF NICKEL ALLOY 690 IN
LEAD-CONTAINING ENVIRONMENTS***

by

BIN PENG

A thesis submitted to the Faculty of Graduate Studies and Research in partial fulfillment
of the requirements for the degree of **Master of Science**

in

Materials Engineering

Department of Chemical and Materials Engineering

Edmonton, Alberta

Spring, 2007



Library and
Archives Canada

Bibliothèque et
Archives Canada

Published Heritage
Branch

Direction du
Patrimoine de l'édition

395 Wellington Street
Ottawa ON K1A 0N4
Canada

395, rue Wellington
Ottawa ON K1A 0N4
Canada

Your file *Votre référence*
ISBN: 978-0-494-30003-9
Our file *Notre référence*
ISBN: 978-0-494-30003-9

NOTICE:

The author has granted a non-exclusive license allowing Library and Archives Canada to reproduce, publish, archive, preserve, conserve, communicate to the public by telecommunication or on the Internet, loan, distribute and sell theses worldwide, for commercial or non-commercial purposes, in microform, paper, electronic and/or any other formats.

The author retains copyright ownership and moral rights in this thesis. Neither the thesis nor substantial extracts from it may be printed or otherwise reproduced without the author's permission.

AVIS:

L'auteur a accordé une licence non exclusive permettant à la Bibliothèque et Archives Canada de reproduire, publier, archiver, sauvegarder, conserver, transmettre au public par télécommunication ou par l'Internet, prêter, distribuer et vendre des thèses partout dans le monde, à des fins commerciales ou autres, sur support microforme, papier, électronique et/ou autres formats.

L'auteur conserve la propriété du droit d'auteur et des droits moraux qui protègent cette thèse. Ni la thèse ni des extraits substantiels de celle-ci ne doivent être imprimés ou autrement reproduits sans son autorisation.

In compliance with the Canadian Privacy Act some supporting forms may have been removed from this thesis.

Conformément à la loi canadienne sur la protection de la vie privée, quelques formulaires secondaires ont été enlevés de cette thèse.

While these forms may be included in the document page count, their removal does not represent any loss of content from the thesis.

Bien que ces formulaires aient inclus dans la pagination, il n'y aura aucun contenu manquant.


Canada

Abstract

The electrochemical behavior of nickel-based alloy 690 was investigated in simulated steam generator crevice chemistries by electrochemical measurements and surface analyses. It was found that the role of lead in corrosion processes strongly depends on the pH value of testing solutions. The presence of lead substantially increases the anodic dissolution of nickel alloys in alkaline solution, but has no effect on the electrochemical behavior of the pre-formed passive film. SEM examination shows that the morphologies of oxide films formed at 300°C in high pH range are modified by lead incorporation. For surface films formed in alkaline chemistries, significant changes of the film composition by lead were observed. XPS analyses demonstrate that the ingress of lead accompanies an increase of hydroxide in the passive film. SIMS analysis also reveals that the presence of lead contamination in the alkaline chemistry increases not only hydroxyl but also hydrogen in the passive film. Furthermore, XRD results indicate that lead prevents the formation of spinel oxides in the passive film in alkaline solution. Nanoindentation shows the mechanical properties of passive films in acidic and alkaline solutions decrease with the presence of lead. These experimental observations suggest that the retarded dehydration process by lead may play an important role in the lead-induced passivity degradation. A film-rupture model has been proposed based on the experimental results.

Acknowledgements

I would like to thank my supervisor Dr. Jingli Luo for her encouragement and guidance throughout my master's program. Her advice and instruction are highly appreciated.

Special thanks are extended to Dr. Baotong Lu, who provided valuable suggestions during the course of this work.

My deepest thanks are for my wife, Li Lin, for her love, support and sacrifice throughout my study.

The financial supporters are sincerely appreciated. This project is sponsored by NSERC/AECL (Atomic Energy of Canada, Ltd) CRD Grant.

Contents

| | |
|--|----|
| 1. Introduction | 1 |
| 2. Literature review | |
| 2.1. Introduction of stress corrosion cracking..... | 5 |
| 2.1.1. Characteristics of SCC..... | 6 |
| 2.1.2. Mechanism of SCC..... | 7 |
| 2.2. Pb-induced SCC in nickel alloys..... | 10 |
| 2.2.1. Sources of lead impurities..... | 10 |
| 2.2.2. Lead behavior in SCC..... | 11 |
| 2.2.3. Environmental factors controlling PbSCC..... | 12 |
| 2.2.4. Features of PbSCC in nickel alloys..... | 12 |
| 2.2.4.1. Susceptible materials..... | 12 |
| 2.2.4.2. pH..... | 13 |
| 2.2.4.3. Potential..... | 15 |
| 2.2.5. Mechanism of lead-induced SCC..... | 16 |
| 2.3. Passivity of metals..... | 18 |
| 2.3.1. Definition of passivity..... | 18 |
| 2.3.2. Formation of passive films..... | 20 |
| 2.3.3. Models of passive films..... | 22 |
| 2.4. Passive films on nickel alloys..... | 25 |
| 2.4.1. Thermodynamic consideration..... | 25 |
| 2.4.2. Composition and structure of passive films..... | 25 |
| 2.4.3. Effect of pH and potential..... | 27 |
| 2.4.4. Effect of alloying elements..... | 27 |
| 2.5. Effect of lead on the passivation behavior of nickel alloys..... | 28 |
| 2.5.1. Effect of lead on the corrosion potential of nickel alloys..... | 28 |
| 2.5.2. Effect of lead on the anodic dissolution of alloy constituents..... | 29 |
| 2.5.3. Effect of lead on the polarization behavior of nickel alloys..... | 30 |

| | | |
|-----------|--|-----------|
| 2.5.4. | Effect of lead on the characteristics of passive films on nickel alloys..... | 31 |
| 2.5.5. | Interaction of lead and other species in the solution..... | 32 |
| 2.6. | Experimental techniques..... | 33 |
| 2.6.1. | Electrochemical methods..... | 33 |
| 2.6.1.1. | Dynamic polarization measurement..... | 33 |
| 2.6.1.2. | Cyclic polarization measurement..... | 34 |
| 2.6.1.3. | Mott-Schottky measurement..... | 34 |
| 2.6.2. | Surface analysis techniques..... | 36 |
| 2.6.2.1. | X-ray photoelectron spectroscopy..... | 36 |
| 2.6.2.2. | Secondary ion mass spectrometry..... | 38 |
| 2.6.2.3. | X-ray diffraction..... | 40 |
| 2.6.2.4. | Nanoindentation..... | 42 |
| 3. | Experimental..... | 45 |
| 3.1. | Selection of testing materials..... | 45 |
| 3.2. | Formulation of testing solutions..... | 46 |
| 3.3. | Experiment procedure..... | 47 |
| 3.3.1. | Electrochemical experiment..... | 47 |
| 3.3.2. | Surface analysis..... | 50 |
| 3.3.3. | Nanoindentation..... | 51 |
| 4. | Results..... | 52 |
| 4.1. | Electrochemical behavior of Alloy 690 in lead-containing environments..... | 52 |
| 4.1.1. | Effect of lead on the corrosion resistance of Alloy 690 in acidic chemistry..... | 53 |
| 4.1.2. | Effect of lead on the corrosion resistance of alloying elements in acidic chemistry..... | 54 |
| 4.1.3. | Effect of lead on the corrosion resistance of Alloy 690 in alkaline chemistry..... | 58 |
| 4.1.4. | Effect of lead on the corrosion resistance of alloying elements in alkaline | |

| | |
|--|------------|
| chemistry..... | 64 |
| 4.1.5. Cyclic voltammetry study of the effect of lead..... | 68 |
| 4.1.6. Effect of lead on the semiconductive behavior of Alloy 690..... | 75 |
| 4.2. Surface analysis of Alloy 690 in lead-containing environments..... | 79 |
| 4.2.1. Effect of lead on the surface morphology of passive films..... | 79 |
| 4.2.2. Effect of lead on the composition and structure of passive films..... | 79 |
| 4.2.3. Effect of lead on the thickness of passive films..... | 87 |
| 4.2.4. Distribution of lead in the passive film..... | 88 |
| 4.2.5. Effect of lead on the chemical state of oxygen in the passive film..... | 89 |
| 4.2.6. Effect of lead on the chemical state of chromium in the passive film..... | 92 |
| 4.2.7. SIMS analysis..... | 96 |
| 4.2.8. XRD analysis..... | 99 |
| 4.3. Effect of lead on mechano-mechanical properties of passive films..... | 103 |
| | |
| 5. Discussion | 108 |
| 5.1. Mechanism of lead-induced passivity degradation..... | 108 |
| 5.2. Film rupture model of lead-induced SCC..... | 115 |
| | |
| 6. Conclusions..... | 118 |
| | |
| References..... | 121 |
| | |
| Appendix..... | 131 |

List of tables

| | | |
|-----------|---|-----|
| Table 2-1 | Relative ranking of PbSCC resistance of candidate SG tubing alloys..... | 13 |
| Table 3-1 | Nominal composition of Nickel Alloy 690 (UNS N6690)..... | 46 |
| Table 3-2 | Concentrations of species in simulated CANDU SG crevice chemistries..... | 47 |
| Table 4-1 | Passive current density of Alloy 690 and Ni in alkaline SG chemistries..... | 65 |
| Table 4-2 | Effect of lead on the Mott-Schottky measurements..... | 77 |
| Table 5-1 | Equilibrium constants for the deprotonation reactions..... | 113 |

List of figures

| | |
|---|----|
| Figure 2-1 Tubing materials in U.S. recirculating SGs in 2001..... | 6 |
| Figure 2-2 Schematic diagram of typical crack-propagation rate..... | 7 |
| Figure 2-3 Schematic representation of crack propagation by the film-rupture model..... | 9 |
| Figure 2-4 Ratio of concentration of species in deposits from occluded heat transfer crevices vs. those from adjacent free span surface..... | 11 |
| Figure 2-5 Dependence of PbSCC for Alloys 600MA, 600TT, and 690TT on pH in the alkaline, neutral and acidic regions..... | 14 |
| Figure 2-6 Depth of penetration determined metallographically and by polarization current density..... | 15 |
| Figure 2-7 Schematic diagram for a metal exhibiting passivity of type 1..... | 19 |
| Figure 2-8 Schematic diagram for a metal exhibiting passivity of type 2..... | 19 |
| Figure 2-9 Schematic models of passive film formation..... | 22 |
| Figure 2-10 Schematic of physical-chemical processes that occur within a passive film according to PDM model..... | 24 |
| Figure 2-11 Layer model used for the calculation of the different layer thicknesses of the passive film formed on the Ni-Cr-Fe alloy in high temperature and high pressure water..... | 26 |
| Figure 2-12 Effect of Pb on passive film composition of Alloy 690 at different pHs..... | 32 |
| Figure 2-13 Schematic of main components of XPS system..... | 38 |
| Figure 2-14 Schematic of main components of SIMS system..... | 40 |
| Figure 2-15 Basic features of a typical XRD experiment..... | 41 |
| Figure 2-16 Typical load vs. depth curve in indentation tests..... | 43 |
| Figure 3-1 Setup of electrochemical cell..... | 49 |
| Figure 3-2 Setup of electrochemical cell for sample transfer experiment..... | 49 |
| Figure 4-1 Polarization plots of Alloy 690 in acidic simulated SG crevice solutions with and without PbO..... | 54 |

| | |
|--|----|
| Figure 4-2 Effect of lead on the polarization behavior of pure nickel in acidic SG chemistries..... | 55 |
| Figure 4-3 Effect of lead on the polarization behavior of pure chromium in acidic SG chemistries..... | 56 |
| Figure 4-4 Effect of lead on the polarization behavior of pure iron in acidic SG chemistries..... | 57 |
| Figure 4-5 Effect of lead on the magnitude of current peak 1 in acidic SG chemistries.. | 58 |
| Figure 4-6 Polarization plots of Alloy 690 in alkaline simulated SG crevice solutions with and without PbO..... | 59 |
| Figure 4-7 Concentration effect of lead on polarization behavior of Alloy 690 in alkaline simulated SG crevice..... | 61 |
| Figure 4-8 Effect of PbO concentration and the current density of peak 1..... | 61 |
| Figure 4-9 Polarization curves of Alloy 690 prepassivated at $-0.3 V_{SCE}$ for (1) 15 minutes, (2) 30 minutes and (3) 60 minutes..... | 62 |
| Figure 4-10 Polarization curves of Alloy 690 in alkaline SG crevice chemistry with 0.44 mM PbO, the samples were preconditioned at $-1 V_{SCE}$ for (1) 1 minute, (2) 15 minutes and (3) 60 minutes..... | 63 |
| Figure 4-11 Effect of lead on the polarization behavior of pure nickel in alkaline SG chemistries..... | 64 |
| Figure 4-12 Effect of lead on the polarization behavior of pure chromium in alkaline SG chemistries..... | 66 |
| Figure 4-13 Effect of lead on the polarization behavior of pure iron in alkaline SG chemistries..... | 67 |
| Figure 4-14 Effect of lead on the magnitude of current peak 1 in alkaline SG chemistries..... | 67 |
| Figure 4-15 Effect of deposited lead on the voltammetric behavior of Alloy 690 in alkaline SG chemistry..... | 69 |
| Figure 4-16 Voltammetric behavior of Alloy 690 in Pb-free alkaline crevice solution... | 71 |
| Figure 4-17 Effect of dissolved Pb^{2+} (added at $-0.795 V_{SCE}$) on the voltammetric behavior of Alloy 690..... | 73 |

| | |
|---|----|
| Figure 4-18 Effect of dissolved Pb^{2+} (added at $-0.7 V_{SCE}$) on the voltammetric behavior of Alloy 690..... | 73 |
| Figure 4-19 Effect of dissolved Pb^{2+} (added at $-0.2 V_{SCE}$) on the voltammetric behavior of Alloy 690..... | 74 |
| Figure 4-20 Mott-Schottky plots of Alloy 690 prepassivated in acidic SG crevice chemistry with and without Pb at $300^{\circ}C$ | 77 |
| Figure 4-21 Mott-Schottky plots of Alloy 690 prepassivated in neutral SG crevice chemistry with and without Pb at $300^{\circ}C$ | 78 |
| Figure 4-22 Mott-Schottky plots of Alloy 690 prepassivated in alkaline SG crevice chemistry with and without Pb at $300^{\circ}C$ | 78 |
| Figure 4-23 SEM images of passive films formed on Alloy 690 in acidic conditions..... | 80 |
| Figure 4-24 SEM images of passive films formed on Alloy 690 in neutral conditions.... | 81 |
| Figure 4-25 SEM images of passive films formed on Alloy 690 in alkaline conditions...82 | |
| Figure 4-26 Composition-depth profile of the passive film on Alloy 690 prepassivated at $300^{\circ}C$ in acidic SG crevice chemistry free of lead..... | 84 |
| Figure 4-27 Composition-depth profile of the passive film on Alloy 690 prepassivated at $300^{\circ}C$ in acidic SG crevice chemistry with lead | 84 |
| Figure 4-28 Composition-depth profile of the passive film on Alloy 690 passivated at $300^{\circ}C$ in the neutral SG crevice chemistry free of lead | 85 |
| Figure 4-29 Composition-depth profile of the passive film on Alloy 690 passivated at $300^{\circ}C$ in the neutral SG crevice chemistry with lead..... | 85 |
| Figure 4-30 Composition-depth profile of the passive film on Alloy 690 prepassivated at $300^{\circ}C$ in alkaline SG crevice chemistry free of lead..... | 86 |
| Figure 4-31 Composition-depth profile for the passive film on Alloy 690 prepassivated at $300^{\circ}C$ in alkaline SG crevice chemistries with lead..... | 86 |
| Figure 4-32 Passive film thickness on Alloy 690 obtained at $300^{\circ}C$ in different crevice chemistries..... | 87 |
| Figure 4-33 Depth profiles of Pb in the passive films on Alloy 690 prepassivated at $300^{\circ}C$ in different pH conditions..... | 88 |
| Figure 4-34 Estimated distribution of OH^{-} and O^{2-} in the passive film obtained in acidic crevice chemistries at $300^{\circ}C$ with and without lead..... | 89 |

| | |
|--|-----|
| Figure 4-35 Estimated distribution of OH ⁻ and O ²⁻ in the passive film obtained in neutral crevice chemistries at 300°C with and without lead..... | 90 |
| Figure 4-36 Estimated distribution of OH ⁻ and O ²⁻ in the passive film obtained in alkaline crevice chemistries at 300°C with and without lead..... | 90 |
| Figure 3-37 Effect of lead on the dehydration degree of passive films in different pH values..... | 91 |
| Figure 4-38 Decomposition of XPS Cr 2p _{3/2} spectra for samples prepassivated in acidic chemistry at 300°C (a) without and (b) with lead..... | 93 |
| Figure 4-39 Decomposition of XPS Cr 2p _{3/2} spectra for samples prepassivated in neutral chemistry at 300°C (a) without and (b) with lead..... | 94 |
| Figure 4-40 Decomposition of XPS Cr 2p _{3/2} spectra for samples prepassivated in alkaline chemistry at 300°C (a) without and (b) with lead..... | 95 |
| Figure 4-41 Composition profile of Cr in alkaline solution (a) by SIMS and (b) by XPS..... | 97 |
| Figure 4-42 Distribution profiles of OH and H in samples immersed in alkaline solution at 300°C (a) with lead (b) without lead..... | 98 |
| Figure 4-43 XRD patterns of samples prepassivated in acidic chemistry at 300°C (a) without and (b) with lead..... | 100 |
| Figure 4-44 XRD patterns of samples prepassivated in neutral chemistry at 300°C (a) without and (b) with lead..... | 101 |
| Figure 4-45 XRD patterns of samples prepassivated in alkaline chemistry at 300°C (a) without and (b) with lead..... | 102 |
| Figure 4-46 Reduced modulus of the passive film on Alloy 690 prepassivated in acidic SG crevice chemistry with and without Pb at 300°C..... | 105 |
| Figure 4-47 Hardness of the passive film on Alloy 690 prepassivated in acidic SG crevice chemistry with and without Pb at 300°C..... | 105 |
| Figure 4-48 Reduced modulus of the passive film on Alloy 690 prepassivated in neutral SG crevice chemistry with and without Pb at 300°C..... | 106 |
| Figure 4-49 Hardness of the passive film on Alloy 690 prepassivated in neutral SG crevice chemistry with and without Pb at 300°C..... | 106 |

| | |
|---|-----|
| Figure 4-50 Reduced modulus of the passive film on Alloy 690 prepassivated in alkaline SG crevice chemistry with and without Pb at 300°C..... | 107 |
| Figure 4-51 Hardness of the passive film on Alloy 690 prepassivated in alkaline SG crevice chemistry with and without Pb at 300°C..... | 107 |
| Figure 5-1 The gel-like structure of Pb-doped passive film..... | 111 |

Abbreviation

| | |
|-------|---|
| AcSCC | Acidic SCC |
| AFM | Atomic force microscope |
| AkSCC | Alkaline SCC |
| AVT | All volatile treatment |
| BWR | Boiling water reactor |
| DSSCC | Doped steam SCC |
| IGSCC | Intergranular stress corrosion cracking |
| IGA | Intergranular Attack |
| ISE | Indent size effect |
| HPSCC | High-potential SCC |
| HSAB | Hard and soft acid and base |
| LME | Liquid metal embrittlement |
| LPSCC | Low-potential SCC |
| LTSCC | Low-temperature SCC |
| MA | Mill and annealed |
| MOD | Metal-organic decomposition |
| OCP | Open circuit potential |
| OgSCC | Organic SCC |
| PDM | Point defect model |
| PbSCC | Lead-induced SCC |
| PWR | Pressurized water reactor |
| SCC | Stress corrosion cracking |
| SCE | Saturated calomel electrode |
| SEM | Scanning electron microscope |
| SG | Steam generator |
| SIMS | Secondary ion mass spectrometry |
| SME | Solid metal embrittlement |

| | |
|-------|---|
| SS | Stainless steel |
| SySCC | Reduced sulfur SCC |
| TGSCC | Transgranular stress corrosion cracking |
| ToF | Time-of-flight |
| TT | Thermally treated |
| UPD | Underpotential deposit |
| XPS | X-ray photoelectron spectroscopy |

Chapter 1

1. Introduction

Nuclear energy has become one of the most important and reliable energy sources in the world since the 1960's. Unlike any other fuels it is clean and renewable. Millions of Canadians use energy generated by nuclear resources every day even though they are not aware of this fact. In Canada nuclear power provides 14% of the electricity supply for the country. Today there are 16 reactors operating in Ontario, one in Quebec and one in New Brunswick. In Ontario in 1997 the sources of electricity were nuclear 48%, hydro 27%, fossil 24% and other 1% (Electric Power in Canada 1997, Natural Resources Canada). Nuclear energy has proved to be an effective, efficient fuel source with enormous potential and already has become an indispensable source of energy in the world.

However the safety issue and potential dangers of nuclear power are always of great concern to the public. The production of nuclear energy must be safe to both the society and the environment, and any potential risk has to be avoided. In 1986 the worst nuclear accident in the world took place at Chernobyl, Ukraine. A huge nuclear reactor exploded without any warning. This disaster caused a huge number of fatal cancer cases. Over one million people were estimated to be affected by radiation, and the irradiative impact will last for hundreds of thousands of years.

Although many problems encountered in the safe operation of nuclear reactors have been gradually solved or abated, some of them still last after so many years. Stress corrosion cracking (SCC) in nickel-based alloys, which are used as steam generator (SG) tubing materials, has been reported as a major degradation mode in operating plants for decades. This type of premature failure could be a catastrophe and cause inestimable health, financial and environmental loss. In Canada, at Ontario Hydro's Bruce Nuclear Generating Station A (BNGS A) the leakage of nickel alloy tubing materials produced by SCC resulted in the shutdown of an operating unit in September 1995 (Wright et al.

1999). Therefore, the study of SCC in SG tubing materials has special economic and environmental significance.

The steam generator is a tubular heat exchanger in a pressurized water reactor (PWR) system, designed to withstand the thermal stresses associated with thermal cycling from cold to hot operating conditions. In addition to heat transfer, radioactive and non-radioactive sides of the system are separated by steam generators. A typical PWR system consists of three loops. In the primary loop, the coolant (such as gas, water) takes heat away from the reactor and enters the second stage. Steam is produced in the secondary loop by exchanging the heat in steam generators. In the tertiary loop, the steam is used to drive high pressure turbines and produce electricity. A typical steam generator consists of thousands of thin tubes operating in a temperature range of about 300°C.

BNGS A in Ontario, Canada has four 760 MW reactor units. Every one comprises eight recirculating steam generators. Each generator has 4200 tubes with a dimension of 0.5 inch (Mirzai et al. 1997). Given that leakage or failure of any of these tubes will cause the unit to shut down to replace the damaged parts, the regular safety inspection and exchange are absolutely a big challenge to avoid huge labor and capital cost.

SG tubing materials are mainly nickel-based alloys because this type of material possesses excellent corrosion and SCC resistance at elevated temperatures. Alloy 800 and nickel alloys 600 and 690 are widely used in the nuclear industry in many countries. In order to improve their in-plant performance, great effort has been made to optimize the metallurgical characteristics of these materials. However, the persistence of SCC still appears in nickel alloys. Different types of SCC cracks have been identified according to specific operation conditions. Among those, the occurrence of SCC in the lead-contaminated environment is of special concern.

Lead has been generally considered as one of the primary sources to increase the susceptibility of SCC in the second side of steam generators. Pb-induced SCC (PbSCC) was first reported by Copson and Dean in 1965 (Copson and Dean, 1965). It was found

that lead oxide could accelerate the occurrence of SCC in aerated and ammoniated water. With increasing application of nickel-based alloys, especially in modern nuclear power plants, SCC resistance evaluation on nickel alloys in lead-containing environments has increased. Pb-caused degradations of steam generators were reported in St. Lucie-1 (1987), in EDF plants (1990-1993), in Doel-4 (1992), in Oconee (1999) (Staehele 2003b). In Canada, corrosion cracking of Alloy 690 SG tubes at BNGS A was attributed to lead contamination (King et al. 1993). In Korea transgranular SCC failure was observed at nuclear power plant B, and it was also suggested to be related to lead pollution (Hwang et al. 2003). Many plants claimed the identification of lead contamination in their steam generators. Within unplugged tubes lead was detected throughout stress corrosion cracks and at the crack tip in tubing materials (Staehele 2004b). Laboratory studies revealed that Pb initiates SCC in the full pH range for most nickel alloys used as tubing materials; the threshold of Pb concentration to produce SCC is considered to be very low, because SCC of nickel alloys was reported in a solution with a Pb concentration as low as 0.1 ppm (Staehele 2003b). Modes of SCC failure caused by Pb are varied, including intergranular stress corrosion cracking (IGSCC), transgranular stress corrosion cracking (TGSCC) and intergranular attack (IGA). It is a fact that PbSCC has become a matter of increasing concern in SG tubing materials.

On the other hand lead as a contaminating species is far from well defined unlike some other mineral ions in aqueous system. Although some studies of PbSCC have been carried out, the nature of this phenomenon has not been elucidated to date. Modes such as liquid/solid metal embrittlement (LME/SME), hydrogen embrittlement, selective/grain boundary oxidation, slip dissolution/oxidation and dealloying were proposed, but none of them has been widely accepted. Based on the work of Kilian, who pointed out there is a relation between SCC and polarization behavior of nickel alloys, it was hypothesized that lead can induce passivity degradation on nickel alloys and further lead to the increasing possibility of SCC (Staehele 2004b). This idea has been supported by more and more experimental observations in recent years.

However, these basic concepts are far from enough to clarify the role of lead in the initiation and propagation of SCC. Nickel-based alloys mainly consist of Ni, Cr and Fe, but the interaction of Pb and alloying elements has not been systematically discussed. Although it is quite clear that Pb can be involved in the surface film formation (Staehele 2004b, Hwang et al. 2002, Costa et al. 1995), the mechanism of Pb ingress has not been illuminated. Moreover, mechano-chemical characteristics of Pb-modified passive films on nickel alloys, which are of essential importance in SCC nucleation and crack growth, have never been examined. Therefore, further investigation is necessary to obtain a better understanding of PbSCC. On the other hand, it is also important to realize that the contribution of lead is complicated. Contradictory effects of lead may be observed because SCC is a synergistic result of metallurgical, mechanical and corrosive factors. Under certain conditions, other parameters may become dominant, rather than the effect of lead contamination. Even though the possible role of lead should be addressed in the investigation, it is wise to reckon the impact of lead is always associated with other environmental factors.

In the present research, the main objective is to identify the role of lead on the instability of passive films on nickel alloys and provide in-depth discussion of the mechanism of PbSCC in nickel alloys. Special testing solutions, CADUN* simulated SG crevice chemistries, were used in this work. Electrochemical techniques were employed to investigate effects of lead on the corrosion resistance of nickel alloys. Surface analyses were implemented to distinguish the compositional and structure modification of passive films by lead. Nanoindentation experiments were performed to provide information regarding mechano-chemical properties of passive films formed in lead-containing environments. Great efforts were made to evaluate the influence of lead on the passivation process of nickel alloys. Special attention was paid to analyze the correlation between surface mechanical properties and surface compositions. Based on experimental results, a possible mechanism of Pb-induced passivity degradation of nickel alloys was proposed and the film rupture model of PbSCC was discussed.

* CADUN is the trade mark of Atomic Energy of Canada, Ltd.

Chapter 2

2. Literature review

In this chapter, basic concepts of SCC are first introduced. Parameters affecting the PbSCC susceptibility of nickel alloys are reviewed with emphasis on the role of lead. Thereafter fundamental aspects of passivity of metals are reviewed because lead is suspected to induce passivity degradation on nickel alloys, which finally increases the susceptibility to SCC. At the end of this chapter important experimental techniques are briefly described.

2.1 Introduction of stress corrosion cracking

Typically, SCC is the service failure of materials resulting from a combined interaction of environmental, metallurgical and mechanical factors. Nickel and nickel-based alloys were found to sustain SCC in fluosilicic acid in the 1950's. Since then a number of aggressive chemical systems such as chromic acid, acetic acid, caustic solutions, H₂O-Cl⁻ solutions and organic liquids have been reported to be able to cultivate SCC in nickel alloys since 1978. With the increasing application of nickel-based alloys, the number of environments inducing SCC in nickel alloys has steadily expanded. Although SCC susceptibility for a given metal can be approximately outlined by the potential-pH framework nowadays, in-depth investigation of SCC mechanisms in nickel alloys is still of great importance in terms of prevention and prediction needs in practice (Jones 1992).

Nickel-based alloys have been used as SG tubing materials in power plants since the late 1960s. Figure 2-1 shows the types of tubing materials used in U.S. in 2001. In certain conditions it has been found that nickel alloys undergo serious SCC problems. The study of SCC for high nickel alloys started in 1959. An alloy similar to Alloy 690 was first investigated in pure deoxygenated water (Staehle, 2004b). With the advance of SCC monitoring and analysis techniques, different types of SCC in nickel alloys under various

conditions were revealed. To date SCC in nickel alloys has been found to be one of the most dangerous failures in nuclear power plants. Nine SCC submodes have been classified according to various parameters determining the susceptibility of SCC in nickel alloys as tubing materials (Staehe 2003a), named as alkaline SCC (AkSCC), low-potential SCC (LPSCC), acidic SCC (AcSCC), high-potential SCC (HPSCC), lead SCC (PbSCC), reduced sulfur SCC (Sy-SCC), doped steam SCC (DSSCC), organic SCC (OgSCC) and low-temperature SCC (LTSCC).

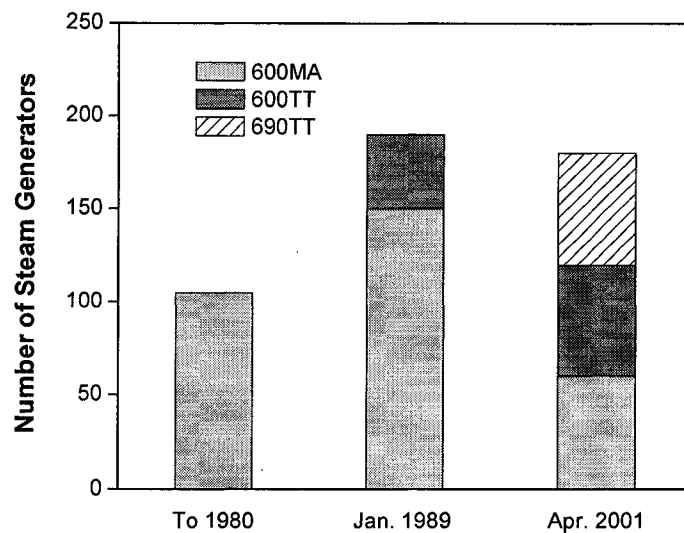


Figure 2-1 Tubing materials in U.S. recirculating SGs in 2001 (from Harrod et al. 2001).

MA: Mill and annealed; TT: Thermally treated

2.1.1 Characteristics of SCC

SCC is characterized by delayed failure. A typical SCC process consists of three stages as shown in Figure 2-2: (1) stage 1 represents crack initiation; (2) stage 2 corresponds to steady state crack propagation; (3) stage 3 indicates final mechanic failure (Jones 1992).

The critical value of the stress leading to initiation and propagation of SCC is usually far less than the mechanical fracture strength of most materials. Although the final failure caused by SCC often exhibits itself as brittle and prompt fracture of materials, the nucleation and growth of cracks are very slow and undetectable at the beginning. This is the main reason that SCC problems should be under control in operation to avoid disasters.

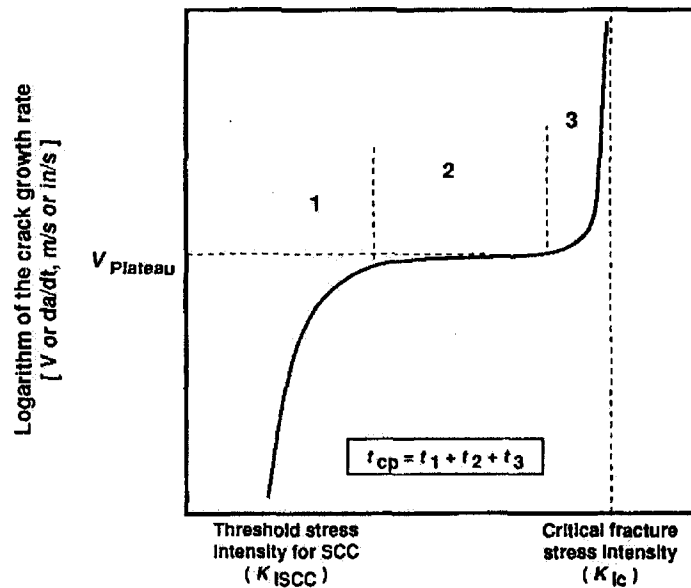


Figure 2-2 Schematic diagram of typical crack-propagation rate as a function of crack-tip stress-intensity behavior illustrating the regions of stage 1, 2, and 3 crack propagation as well as identifying the plateau velocity and the threshold stress intensity (from Jones 1992).

2.1.2 Mechanisms of SCC

To produce SCC, cracks must first initiate on the materials surface in a corrosion environment under constant stress. In general crack initiation take place easily at weak sites such as grain boundaries, surface discontinuities and corrosion pits. The

intergranular corrosion or slip dissolution can also result in the formation of cracks. Although it is well recognized that crack initiation has some favorite sites, the fact is that there is a lack of well-developed SCC initiation models (Jones, 1992). Since there are no standard criteria to measure and evaluate the nucleation of cracks, the evaluation of SCC resistance is commonly based on the assumption that the cracks already preexist in the materials in industry and in laboratories.

Current SCC mechanisms only concentrate on the second stage of the SCC process—cracking propagation due to the complexity of crack nucleation. Film rupture and hydrogen embrittlement are two basic models among mechanisms of SCC. Each model may give reasonable interpretation for certain material/environment combinations, but the application is still confined to a certain range due to the complexity of SCC processes.

(1) Film rupture model

This model hypothesizes that a crack propagates by preferential dissolution at its tip. It is assumed there is a passive film formed on the metal surface. Stress causes plastic deformation and the emergence of slip steps ruptures the thin passive film. Bare metal is thereby exposed to the corrosive environment. Because the crack tip is more anodic than the wall, the crack front advances by anodic dissolution while the crack wall is repassivated during this course. Repetition of this process eventually leads to discontinuous or continuous cracking.

In this model, the crack growth rate with a limited velocity can be calculated from the dissolution current density measured on bulk materials. Thus the crack growth rate under pure anodic dissolution can be described as Equation 2-1 according to Faraday's law:

$$\frac{da}{dt} = \frac{i_a M}{zF\rho} \quad (2-1)$$

where i_a is the anodic current density, M the atomic weight, z the valence of solvated species, F the Faraday's constant, and ρ the density of the metal. SCC experiments have

confirmed that the calculated propagation rate is consistent with the estimated one (Parkins 1995, 2000).

According to Equation 2-1, there are a number of factors controlling the crack advance such as crack tip strain rate, film fracture strain, corrosion rate of the bare metal, repassivation rate of the surface, the diffusion rate of corrosion products and crack geometry. In general, the crack propagation rate is determined by a competition between the rupture and recovery rate of the surface film. The schematic illustration of this model is shown in Figure 2-3. It is important that the crack wall must maintain a relatively more inactive state compared with the electrochemical state of the crack tip. The kinetics of the repassivation process plays a crucial role in this model.

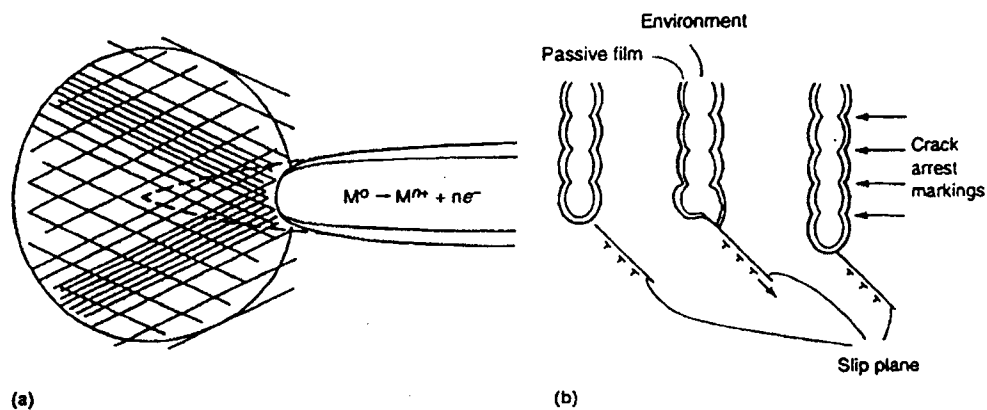


Figure 2-3 Schematic representation of crack propagation by the film-rupture model. (a) Crack tip stays bare as a result of continuous deformation. (b) Crack tip passive and is ruptured repeatedly (from Jones 1992).

(2) Hydrogen embrittlement model

The hydrogen embrittlement model postulates the crack propagates by a high stress concentration at the crack tip which exceeds the yield or fracture strength of a given material. In a corrosive system atomic hydrogen can be generated by chemical reactions

at the crack tip. It is well known that hydrogen atoms have smaller size than most metallic atoms. Therefore, it is easy for small hydrogen atoms to enter interstitial sites and grain boundaries of metals. Because of their high diffusion rate in metals, the accumulation of hydrogen atoms can take place near the crack tip. High local concentration of atomic hydrogen reduces the bond strength between metal atoms, resulting in embrittlement of the deformation zone around the crack tip. Thus crack propagation occurs when high local stress surpasses the yield or fracture strength at the embrittled area (Anderson 2005).

2.2 Pb-induced SCC in nickel-based alloys

Most nickel alloys are used in execrable environments such as high pressure and high temperature due to their high cost. Although nickel alloys exhibit better SCC resistance than carbon steels and some stainless steels (SS) at high temperatures, the immunity of SCC is still impossible taking into account their serious service conditions. For the sake of safety issues, special attention has been paid to SCC problems for nickel alloys in nuclear power plants. In the following section, previous studies of SCC in lead-containing environments are reviewed.

2.2.1 Sources of lead impurities

SCC in steam generators mainly occurs on the heat transfer crevice such as tube supports, sludge and tops of the tubesheets, because dilute species can be concentrated to produce high local concentrations of aggressive chemicals. Even in well-controlled water chemistry, impurities can accumulate to a significant extent at these locations as shown in Figure 2-4. On the other hand, the source of lead contamination is wide. Lead impurities in the second side may come from the water chemistry of the plant, condenser cooling water leaks, copper alloys in condensers and feed water heaters, and seals and gaskets in pump and pipe fittings (Stahle 2003b). Accumulated lead species may remain in sludge or form insoluble chemical compounds, which are difficult to remove by chemical

cleaning. Under certain conditions lead ions in these compounds can be released and promote SCC.

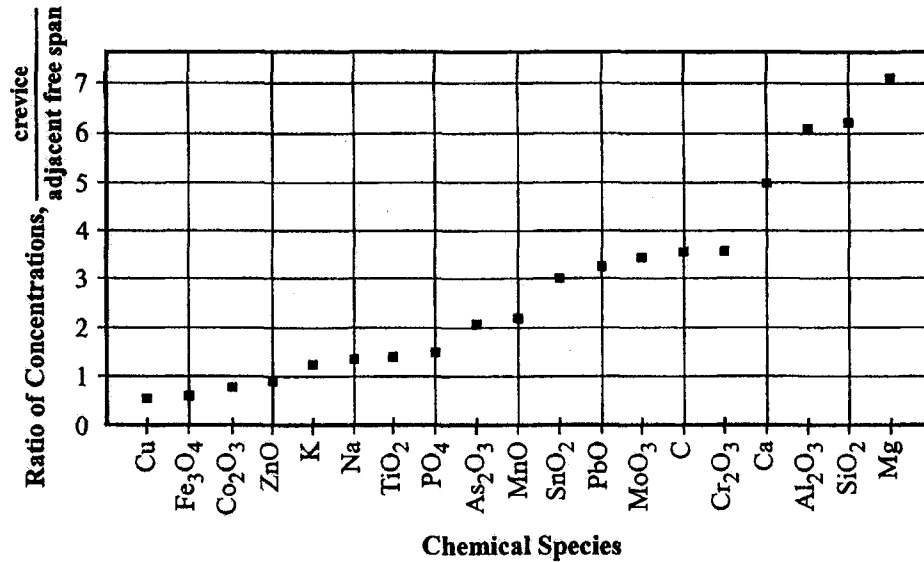


Figure 2-4 Ratio of concentration of species in deposits from occluded heat transfer crevices vs. those from adjacent free span surface (from Staehle 2003b).

2.2.2 Lead behavior in SCC

Basically there are three strong proofs indicating lead is involved in the occurrence of SCC of SG tubing materials. One is that lead has been detected throughout cracks and at crack tips. The crack wall usually contains the highest amounts of lead contamination, followed by the mouth, and a small amount of lead can be found at the crack tip (Thomas et al. 2005). The most common lead compound in cracks is oxide (Mirzai et al. 1997), which is also the common lead impurity found in the deposits on pulled SG tubes.

Another feature of PbSCC is that lead alone, without any other complex chemistries or heat flow conditions, can produce IGSCC and TGSCC in nickel alloys (Staehle 2004b, Thomas et al. 2005). In recognition of the fact of the wide existence of lead impurities in

SG water chemistry and the impossibility to totally remove these hazardous species, the potential danger of PbSCC must be seriously taken into account in plant operation.

Furthermore it has been reported that in the lead-containing environment the crack velocity is much higher than that in the lead-free environment (Staehele 2003b). Under some laboratory tests, the crack growth rate is ten times higher with the presence of lead (Lumsden et al. 2005).

2.2.3 Environmental factors controlling PbSCC

According to Staehele, there are seven primary parameters affecting the PbSCC resistance of nickel alloys in service conditions (Staehele 2004b). These parameters can be expressed as the following equation with respect to the penetration depth of PbSCC.

$$X = A[H^+]^n [x]^p \sigma^m e^{\frac{E-E_0}{b}} e^{\frac{Q}{RT}} t^q \quad (2-2)$$

where X is depth of SCC penetration, A alloy composition and structure, H the pH value, x environmental species, σ stress, E electrochemical potential, E_0 determined by alloy composition and structure, T temperature and t represents the time. N , p , m , b and q are all constants. The main parameters are discussed in the following sections.

2.2.4 Features of PbSCC in nickel alloys

2.2.4.1 Susceptible materials

Nickel-based Alloy 600 (Ni-16Cr-9Fe), Alloy 690 (Ni-30Cr-10Fe) and stainless steel Alloy 800 (Fe-33Ni-22Cr) are commercially available as SG tubing materials in most nuclear power plants around the world. It has been reported that high chromium content can improve PbSCC resistance, and this beneficial effect was supported by both experimental observation and industrial practice (Helie 1993, Lumsden et al. 2005, Harrod et al. 2001, Rosecrans et al. 2001). The SCC resistance of nickel-based alloys in

lead-containing environments is summarized in Table 2-1(Harrood et al. 2001). It can be seen Alloy 600 is susceptible to all the test conditions; Alloy 690, with higher chromium content, demonstrates better performance in most aggressive environments. This is the main reason that Alloy 690 has replaced Alloy 600 in industry today. However, Alloy 690 still sustains high risk of PbSCC in caustic environments. Alloy 800, with 22% chromium, displays lower PbSCC proneness than Alloy 690 under certain conditions.

Table 2-1 Relative ranking of PbSCC resistance of candidate SG tubing alloys

| | Alloy 600 | | Alloy 690 | 800 SS | 304 SS |
|---------------------|-----------|----|-----------|--------|--------|
| | MA | TT | TT | MOD | |
| Acid | 4 | 4 | 1 | 3 | (4) |
| Neutral (or AVT) | 3-4 | 3 | 1 | 1 | 1 |
| Alkaline | 3-4 | 3 | 4-5 | 5 | 5 |

Rankings: 1 - Best; 5 - Worst; () - Estimates

MA: Mill and annealed; TT: Thermally treated; MOD: Metal-organic decomposition

AVT: All volatile treatment

2.2.4.2 pH

Lead is soluble within the full pH range at elevated temperatures and PbSCC for nickel alloys has been observed in acidic, neutral and alkaline environments (Staehele 2003b, Mirzai et al. 1997, Castano-Marin et al. 1993). Its severity tends to increase with the pH value as shown in Figure 2-5. In acidic conditions the chemistry may play an important role in SCC susceptibility. Sulfate seems to be more aggressive to promote PbSCC at low pH range than chloride, and nickel alloys may have less risk of PbSCC in neutral conditions. It was reported that Alloy 690 MA is immune to SCC in a pH 7 solution with 10000 ppm PbO, while SCC occurs in pH 4 and pH 10 solutions, respectively, under the same test condition (Hwang et al. 1999).

The pH value, together with potential, determines the stability of the passive film developed from chemical reactions between metals and electrolytes. Protective quality of passive films is closely related to the SCC resistance in nickel alloys (Hiroshi et al. 1990). Hence, it is suggested that lead may incorporate into the passive film, decrease its protective characteristics and increase PbSCC susceptibility (Staehle 2004b). Hwang et al. investigated the composition profile of passive films formed on Alloy 690 in acidic, neutral and caustic solutions with lead. It was found lead reduces chromium content in passive films formed over the entire pH range. The facilitation of SCC in a Pb-contaminated environment was attributed to the poor quality of passive films due to the loss of chromium (Hwang et al. 1999).

On the other hand, the mechanical properties, such as ultimate tensile strength (UTS) and strain at fracture, may also change with the pH in lead-containing conditions (Hwang et al. 1999). The degradation of mechanical properties may also contribute to the decrease of PbSCC resistance.

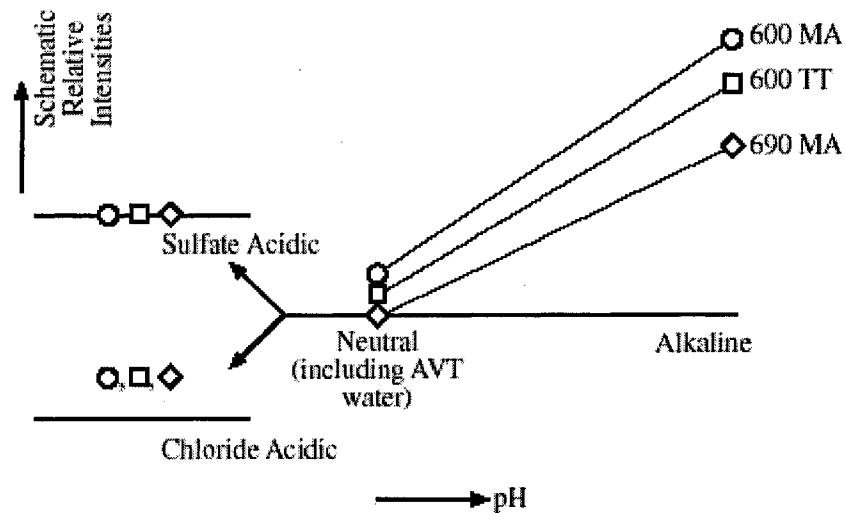


Figure 2-5 Dependence of PbSCC for Alloys 600MA, 600TT, and 690TT on pH in the alkaline, neutral and acidic regions. Horizontal reference lines are for zero PbSCC (from Staehle 2003b).

2.2.4.3 Potential

Figure 2-6 is an experimental result which shows the potential dependence of crack depth in Alloy 690 and Alloy 800 in 1M NaOH + 0.1% PbO solution. The intensity of PbSCC in Alloy 800 reaches a maximum value around the anodic current peak, and the coverage of PbSCC extends from open circuit potential (OCP) up to about 700 mV in the noble direction. Above this region, PbSCC gradually diminishes. Alloy 690 demonstrates a similar behavior in this environment. This phenomenon was also reported by Lumsden et al., who found the most severe PbSCC cracking was around the OCP in oxidation conditions (Lumsden et al. 2005). It is suggested the preference of PbSCC in the low potential region can be related to the active/passive transition of the materials in corrosive environments. Violent changes of the lattice structure are expected in this transition region, resulting in increasing SCC susceptibility at local sites.

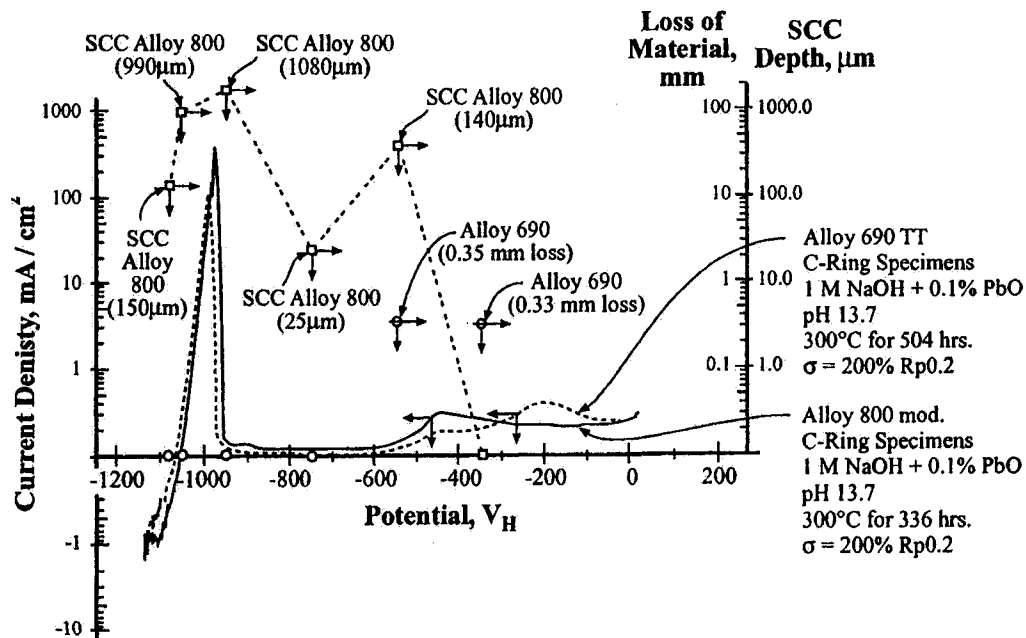


Figure 2-6 Depth of penetration determined metallographically and by polarization current density for (a) Alloy 800mod (336 hrs) and (b) Alloy 690TT (504 hrs) exposed at twice the 0.2% Y.S. to 1M NaOH at 300°C (from Kilian, 1993).

2.2.5 Mechanism of lead-induced SCC

The mechanism of PbSCC has been under controversy for decades. Even analyzed with modern instruments and techniques, it still remains a puzzle. One of the most important reasons is that the role of lead on corrosion resistance of metals in aqueous or gaseous systems has never been systematically investigated.

In the early stages, the model of LME was prevalent because the melting temperature of lead (327°C) is close to the operating temperature in the second side of steam generators. LME is the phenomenon where a metal experiences brittle fracture or loss of ductility in the presence of a liquid metal. Lead was suspected to have a similar embrittlement effect as that of Zn and Al. Experimental observation indicated Alloy 690 is sensitive to molten lead at 350°C (Helie 1993), and Alloy 690 is also susceptible to SCC in a metallic lead plus chloride environment (Chung 1996). To identify the role of metallic lead, SCC tests of Alloy 690 MA, 600 TT, Alloy 690 TT and Alloy 800 were performed at 350°C and 320°C in caustic, acid and AVT environments (Castano-Marin et al. 1993). The former testing temperature is higher than the melting temperature of lead and the latter is lower. SCC cracks were detected for both temperatures, but the susceptible materials were different. This model has mainly been criticized in two aspects. LME is usually considered to take place within a monoatom layer on the surface. But the composition profiles obtained from lead-incorporated surface films show that the penetration depth of lead is much higher than this magnitude (Staehele 2004b). Although metallic lead could accumulate on the metal surface by underpotential deposition (UPD) or displacement reaction with nickel at low potentials, nickel alloys still sustain PbSCC at potentials several hundred mVs higher than OCP (Kilian 1993). Furthermore, it has been pointed out that crack growth rate in liquid lead is ten times lower than that of water + PbO (Staehele 2004b).

Hydrogen embrittlement is also a popular mechanism of SCC. It was suggested that lead may act as a hydrogen poison, which facilitates hydrogen uptaking on the nickel-based alloy surface and promotes of hydrogen into alloys (Psaila-Dombrowski et al. 1999). However, there is a lack of direct evidence for this hypothesis.

Based on the film rupture model, a few interpretations of the lead effect have also been given with respect to PbSCC. It was suggested that lead lowers the global activation energy of the repassivation process, resulting in enhanced anodic dissolution and increasing SCC susceptibility (Helie et al. 1995). However, in this explanation mechanical properties of the lead-incorporated passive film were not discussed. Lumsden and co-workers assumed that displacement plating of metallic lead takes place prior to the passive film formation when bare metal surface is exposed. The repassivation process with an oxide film is retarded by the lead deposition layer. As a consequence, the enhanced anodic dissolution increases the probability of crack initiation and propagation (Lumsden et al. 2005). This assumption emphasizes the potential dependence of PbSCC, because the reduction reaction is not thermodynamically possible at anodic conditions.

According to the work of Kilian, which gives a relationship between the SCC crack penetration depth and polarization behavior of nickel alloys, it was proposed that lead can produce passivity degradation on nickel alloys and further lead to the increasing possibility of SCC (Staehele 2004b). Lead was assumed to be incorporated during the formation of passive films on alloys, resulting in the instability of the passive film. This assumption was supported by most laboratory observations, in which lead decreases corrosion resistance of nickel alloys (Sakai et al. 1998, Costa et al. 1995, Lu 2005, Ahn et al., 2005). Surface analysis confirmed that lead can modify the thickness and composition as well as structure of the passive film (Hwang et al. 1997). In addition, the occurrence of SCC caused by the lead-contaminated oxide film in a lead-free environment was also reported (Takamatsu et al. 1997). As a result, it is gradually accepted that lead may undertake electrochemical reaction on the alloy surface and migrate into the passive film. The degradation of passive films by lead increases the susceptibility of SCC in nickel alloys.

However, how lead promotes the instability of the passive film is still in debate and the validation of current theories is very limited. Chung et al. investigated SCC susceptibility of Alloy 690 in acidic NaCl solutions with different PbCl₂ concentrations and proposed a synergism of lead and chloride ions. It was suggested a crack may initiate at pits caused

by chloride ions, because lead thins the passive film and acts as a crack initiation promoter. The crack advance was attributed to the dissolution of nickel at the crack tip (Chung et al. 1995). However, most PbSCC cracks were observed near OCP. Pits are not likely to be produced in such a low electrochemical potential range. It was also postulated that the low SCC resistance of nickel alloys is a result of the lead promoted chromium depletion from the outer surface film (Hwang et al. 2002), but this work is not consistent with other experimental observations.

2.3 Passivity of metals

2.3.1 Definition of passivity

Corrosion is the mass loss and intrinsic properties degradation of a material resulting from its chemical reaction with the environment. Many metals and alloys, such as iron, nickel, chromium and stainless steels, exhibit a substantial decrease of corrosion rate in certain conditions due to surface films formed on their surface, which significantly reduce their chemical reactions with environments. This phenomenon is called passivity. According to (Uhlig and Revie 1985), there are two types of passivity in general.

Type 1: “A metal is passive if it substantially resists corrosion in a given environment resulting from marked anodic polarization”, as shown in Figure 2-7.

Type 2: “A metal is passive if it substantially resists corrosion in a given environment despite a marked thermodynamic tendency to react”, as shown in Figure 2-8.

Corrosion products are usually chemical compounds. An insoluble corrosion product may precipitate on the metal surface or form a protective surface layer. As a consequence, the corrosion rate of the metal will decrease by the presence of this film. Because the surface film acts as a physical barrier, diffusion of metal ions from bulk material to the electrolyte will be reduced. Local corrosion or breakdown of the surface film will lead to the exposure of fresh metal to the corrosive environment, generating abruptly accelerated anodic dissolution. In this process pitting or crack nucleation can be produced. Obviously,

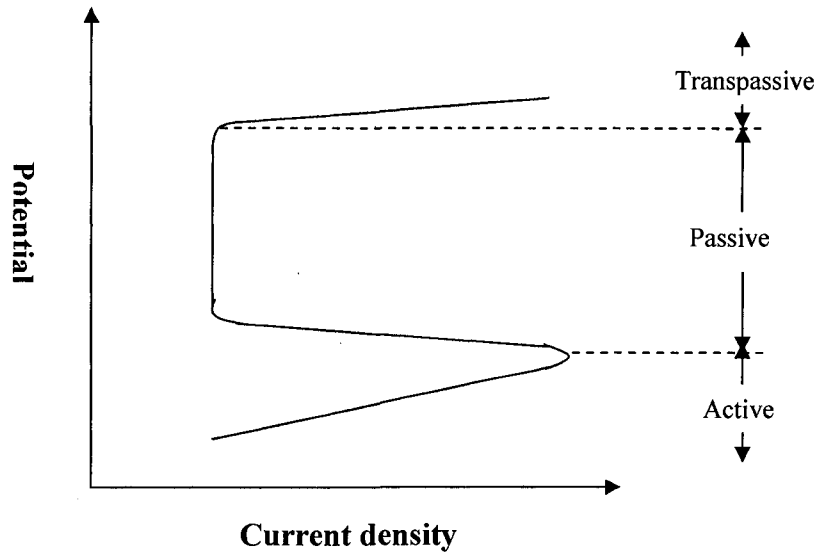


Figure 2-7 Schematic diagram for a metal exhibiting passivity behavior of type 1.

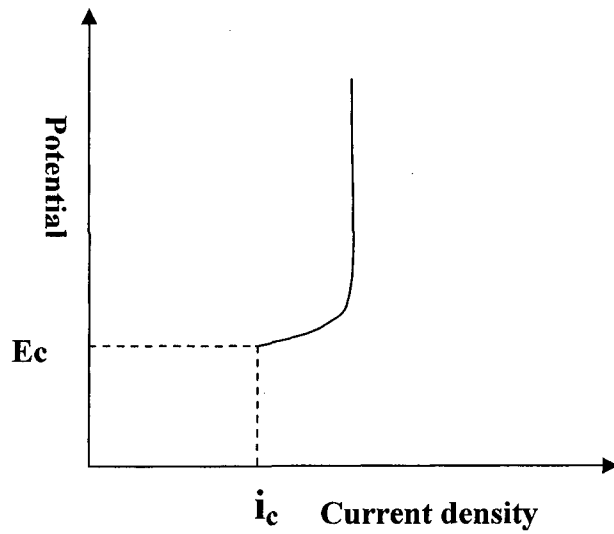


Figure 2-8 Schematic diagram for a metal exhibiting passivity behavior of type 2.

the protective quality of passive films remarkably influences the probability of potential corrosion failure. Pitting, SCC, corrosion fatigue and other corrosion problems must be controlled in service; therefore, it is essential to study the passivity behavior of materials.

2.3.2 Formation of passive films

The nature and properties of passive films are fundamental aspects of corrosion science and engineering. Accordingly study on the growth, kinetics, stability and breakdown of passive films has been intensively carried out.

A classic model for stainless steels was proposed by Okamoto et al. with emphasis on a dehydration reaction in the film formation process (Okamoto et al. 1978). It has been assumed that the passive film on stainless steels is composed of hydrated oxide at the beginning of corrosion with a gel-like structure. Deprotonation takes place in the film during aging under anodic polarization, resulting in the formation of MOH^+ ions. This type of ion precipitates on the bare surface after arrested by surrounding H_2O molecules, and forms a solid film. Therefore, there are three types of bonds in the film structure: $\text{H}_2\text{O-M-O}_2\text{H}$, HO-M-OH and O-M-O . The ratio of these bonds depends on the degree of the deprotonation reaction. Among these oxygen bonds, the $\text{H}_2\text{O-M-O}_2\text{H}$ bonds are the most reactive, followed by the HO-M-OH bonds, while the O-M-O bonds are the most stable. Hence, at the early stage of passivation, the freshly formed film contains a large amount of bound water. During the aging process, the film will change to a less hydrated structure. The number of $\text{H}_2\text{O-M-O}_2\text{H}$ bonds and HO-M-OH bonds will be reduced, eventually leading to the formation of a perfect oxide (O-M-O).

With the application of advanced surface analysis techniques, this model has been further developed by Marcus and co-workers. The formation of a passive film has been described as a process of nucleation and growth of oxide at the metal/electrolyte interface. At the initial stage, there are two approaches to develop a mature oxide film after the hydroxylation of the metal surface. One path assumes oxide islands nucleate

simultaneously with the surface hydroxylation. A full monolayer of oxide must be achieved before lateral growth of this oxide layer occurs to reach the stationary state of passivity. Another path requires the formation of a complete hydroxide on the metal surface before the nucleation of oxide. Subsequent nucleation and growth of an oxide layer form the inner part of the passive film (Marcus et al. 2001). The schematic illustration of this model is shown in Figure 2-9.

The importance of aging in the passivation process has been emphasized by modern theories. Corrosion resistance of metals can be affected by composition and structure alteration of the passive film during the aging process. This effect is attributed to the anodic reaction of dehydroxylation (or deprotonation, dehydration) in the passive film. Prolonged aging treatment will generally lead to the crystallization of passive films in aqueous solutions for stainless steels (Marcus et al. 2001). In Ni-Cr-Fe alloys, it has been pointed out that the film maturation process with time will result in the formation of spinel oxides such as NiFe_2O_4 phase, which are thermodynamically more stable (Rosecrans et al. 2002).

The spinel oxide is a particular protective phase formed at the surface in aqueous environments or at elevated temperatures. The spinel structure is essentially cubic, containing oxygen ions in a fcc lattice. Normally this type of oxides is described by the general formula AB_2O_4 , in which the valences of the metal ions A and B can be (a) A^{II} , B^{III} ; (b) A^{IV} , B^{II} ; (c) A^{VI} , B^{I} . Its crystallographic structure is based on a closed-packed cubic arrangement. The A cations occupy tetrahedral sites, while the allocation of B cations are in octahedral sites. Some spinels have an inverse structure, in which only half of the B cations are located tetrahedral positions, the rest of X cations and B cations randomly fill all octahedral sites (Shreir et al. 1994).

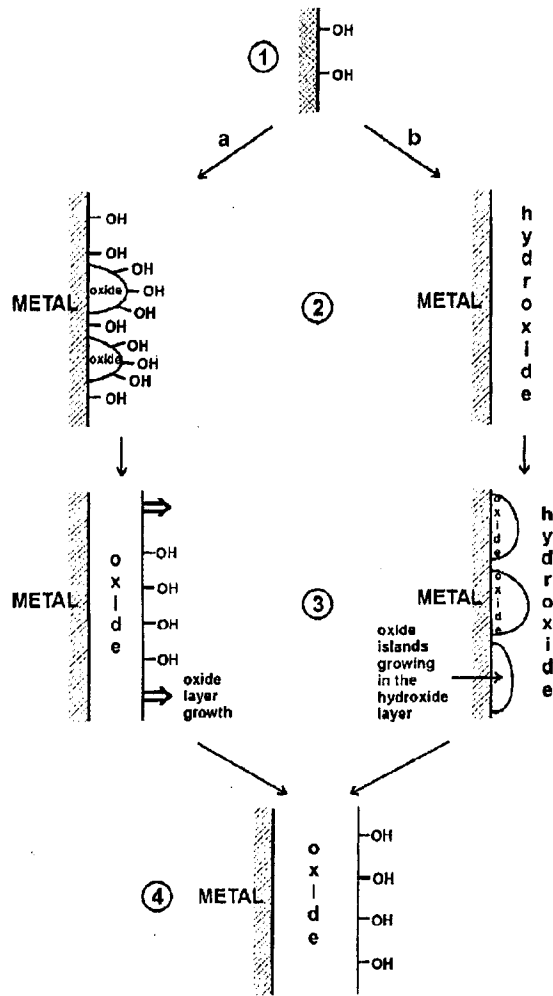


Figure 2-9 Schematic models of passive film formation. Path (a): the nucleation and completion of a full monolayer of oxide before growth of a multilayer film of oxide to reach a steady state passive film; Path (b): the growth of a passive layer of hydroxide with subsequent nucleation and growth of a layer of oxide in the inner part (from Marcus et al. 2001).

2.3.3 Models of passive films

The composition and structure of the passive film are key factors determining the mass transport, i.e., oxygen atoms move from the solution into the film while cation species

migrate from the metal matrix to the film. Many models have been proposed over time with emphasis on the transport of mass and charge in the film. Some of the important models are briefly introduced as follows.

Mott-Cabrera model

In this model it is postulated that the film growth is due to the transport of metal cations across the oxide film to the film/solution interface where they react with the electrolyte.

The penetration of cations is driven by a high electric field, which is constant through the oxide film and independent of the film thickness. The rate-limiting step for film growth is believed to be the emission of metal cations from metal into the film at the metal/film interface (Chao et al. 1981). Based on assumptions, an inverse logarithmic rate law was created to determine the film growth. This model is criticized by not taking into account the contribution of film dissolution at low pH and anion transport to the film growth.

Sato and Cohen's model

In this model, a so-called "place-exchange" mechanism was hypothesized. A layer of oxygen is adsorbed on the metal surface. Oxygen atoms can exchange their positions with underlying metal atoms under certain conditions. After this shift a new layer of oxygen is adsorbed again and two M-O pairs rotate simultaneously. Repetition of this process results in the film thickening (Chao et al. 1978). This model is difficult to evaluate for a film with a thickness of more than one or two monolayers. Meanwhile, the result of radioactive markers indicates that anion transport is mainly responsible for film growth.

Point Defect Model (PDM)

The Point Defect Model was developed by Macdonald to interpret the growth, breakdown and impedance characteristics of passive films on Ni, Fe and Fe-base alloys (Macdonald 1992, Chao et al. 1981). A schematic illustration is shown in Figure 2-10.

This model is based on the following assumptions:

- i. When the external potential is nobler than the Flade potential in the passive region, a continuous passive film with $MO_{x/2}$ oxide will form on the metal surface.

2.4 Passivity of nickel alloys

2.4.1 Thermodynamic consideration

From the thermodynamic point of view, corrosion and immunity of a given metal can be predicted by means of a potential-pH diagram (Pourbaix diagram). This work for a Ni-Cr-Fe-H₂O system at 25°C and 300°C was theoretically accomplished by Beverskog and Puigdomenech (Beverskog et al. 1999). Three spinel oxides are found stable in the aqueous environment, which are trevorite (NiFe₂O₄), chromite (FeCr₂O₄) and nichromite (NiCr₂O₄). According to the calculation, (NiFe₂O₄) is the most stable phase at the operating temperature for SG tubing materials. It is also possible to generate ternary metallic oxides taking into account the crystal structure, nonstoichiometry and surface energy of spinel oxides.

Based on experimental data Chen et al. constructed a potential-pH diagram for Alloy 690 in 5M NaCl solution at 25°C (Chen et al. 2005). In his work, corrosion behavior such as immunity, passivation and pitting can be predicted by means of the specific diagram. Another systematic thermodynamic analysis of Alloy 690 in a high temperature aqueous system was also available, in which the stabilization or destabilization of chromium, iron and nickel in the alloy has been evaluated by a modified solution theory (Lemire et al. 2001). Based on a theoretical calculation, it is expected that for near-neutral and mildly basic conditions, chromium is destabilized in Alloy 690 and readily oxidized. Iron and nickel are stabilized and more resistant to oxidation. γ -CrOOH is likely to be the equilibrium solid phase and form a surface film at 300°C. Under more oxidizing conditions, Cr³⁺ ions can be further oxidized to Cr⁶⁺ species, and the stable surface phases are anticipated to be a mixture of NiO and NiFe₂O₄.

2.4.2 Composition and structure of passive films

The passivation behavior of nickel-based alloys has not been well-defined. It is difficult to clearly describe the inherent nature and characteristics of passive films on nickel-based alloys to date. Machet et al. investigated the behavior of Alloys 600, 690 and 800

exposed to simulated primary water at 325°C and compared passive films obtained on different alloys (Machet et al. 2002). It was found that all alloys present a duplex structure. The outer layer consists of Fe-rich crystals and covers a compact Cr-rich inner layer. The film thicknesses are 4-20 nm for Alloy 600 with 0-400 hour exposure time, 4-40 nm for Alloy 690 with 0-400 hour exposure time, and 4-150 nm for Alloy 800 with 0-150 hour exposure time. It was suggested that the formation of a Cr-rich inner layer is a result of preferential dissolution of iron and nickel at the early stage of film growth.

Further investigation reveals at the onset of passivation an ultra –thin Cr_2O_3 layer (1 nm) is formed with an external layer of $\text{Cr}(\text{OH})_3$ and a very small amount of $\text{Ni}(\text{OH})_2$. The thickening of the inner layer consumes the outer layer in the aging process (Machet et al. 2004). A structural model has been proposed based on the experimental observations as shown in Figure 2-11.

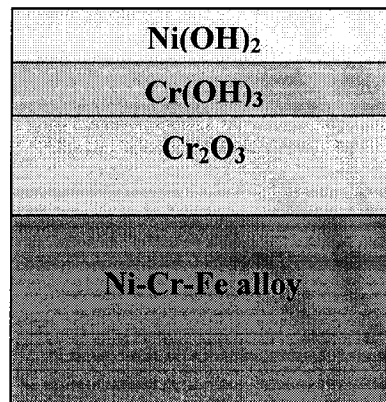


Figure 2-11 Layer model used for the calculation of the different layer thicknesses of the passive film formed on the Ni-Cr-Fe alloy at high temperature and high pressure water (revised from Machet et al. 2004).

2.4.3 Effect of pH and potential

In Ni-Cr-Fe systems, the stability of alloying elements varies at different pH. Montemor et al. evaluated oxide films formed on Alloy 600 and Alloy 690 in high temperature aqueous environments of pH 5, 8 and 10 (Montemor et al. 2003). It was found there is a high pH dependence on the film composition. At pH=5, the film is rich in chromium oxide, while at pH=10 the film contains mixed iron-nickel oxides. The electronic structure is also modified by means of the composition changes.

The passivation potential is critical to the deprotonation process because it governs the oxidation state of the metal, which in turn governs its solubility. XPS analysis revealed that the composition of passive films formed on Alloy 690 in 0.5M H₂SO₄ + 0.5M NaCl solution varies for different potential ranges (Dutta et al. 2002). At the onset of passivity (+100 mV_{SCE}) the surface film is enriched with Cr(OH)₃ but without any Fe³⁺/Fe²⁺, while at higher anodic potential, the passive film consisted only of Cr₂O₃ without any Fe and Ni compounds.

2.4.4 Effect of alloying elements

Alloying elements thermodynamically account for the composition and corrosion behavior of the protective film formed on the alloy. It was found that in a borate solution the electrochemical behavior of a passive film on a Ni-20%Cr alloy resembles that on pure Cr, whereas the film on a Ni-10%Cr alloy is similar to that on pure Ni (Bojinov et al. 2001). By further studies with pure Ni, pure Cr and three Ni-Cr alloys (10, 15 and 20 wt% Cr) in 0.1M Na₂B₄O₇ solution at 200°C, it was suggested that in the passive zone chromium determines the corrosion resistance of these alloys, while in the transpassive zone the critical element is nickel. This experimental result is consistent with the pitting potentials of pure Cr and Ni (Bojinov et al. 2003).

2.5 Effect of lead on the passivation behavior of nickel alloys

Although SG tubing materials demonstrate intensive SCC proneness in lead-containing environments, a literature review shows that there is no systematic laboratory study concerning the impact of lead on corrosion susceptibility and passivity of nickel alloys. This is partially due to the fact that the mechanism of PbSCC is still under debate. To date it is still difficult to predict the electrochemical performance of nickel alloys in lead-containing environments, because most research was conducted under different test conditions. Based on the available field and experimental observations, effects of lead on the corrosion behavior of nickel alloys are briefly described in the following sections.

2.5.1 Effect of lead on the corrosion potential of nickel alloys

Corrosion potential reflects the spontaneous corrosion tendency of engineering materials. It has been reported that corrosion potential of nickel alloys can be modified in lead-containing solutions based on testing conditions. Psaila-Dombrowski et al. investigated the effect of lead on the electrochemical behavior of Alloy 690 TT and Alloy 600 MA in 10% NaOH solution. It was found that the corrosion potential in lead-containing solutions is strongly dependent upon time, temperature and pH. The corrosion potential generally decreases with increasing temperature (25-225°C) for both alloys, but lead mitigates this tendency especially at intermediate temperatures (100-175°C). A maximum value of corrosion potential difference was obtained in this temperature range. At high temperature this difference gradually diminished (Psaila-Dombrowski et al. 1999), while in a mild acidic solution at 280°C, no corrosion potential difference was monitored between solutions with and without lead for Alloy 690 TT, 600 TT and 600 MA. However, a decrease of corrosion potential in AVT water for these alloys was detected with the presence of lead (Sakai et al. 1998). In a solution with combined lead and chloride ions at pH 4.5 and 288°C, anodic polarization measurements indicated that the corrosion potential of Alloy 690 shifted in the negative direction with increasing lead concentration (Chung et al. 1995).

Although corrosion potential does not directly reflect corrosion resistance of materials and the stability of passive films, it is a fact that fluctuation of corrosion potential caused by lead can be observed. It is evident that the surface condition of nickel alloys can be modified by lead species in the solution even at the OCP, which may fundamentally play an important role in the formation of passive films on nickel alloys.

2.5.2 Effect of lead on the anodic dissolution of alloy constituents

Effect of lead on the stability of alloying elements in aggressive environments is important to the passivation of SG tubing materials, since the characteristics of passive films on nickel alloys may significantly change according to different active dissolution patterns of alloys. In mild acidic to neutral solutions (pH 3-7), it was reported that nickel depletion and chromium enrichment were monitored in this pH range after Alloy 600 specimens were immersed in an autoclave at 280°C for one week. Increasing lead concentration accelerated this tendency, especially in acidic condition. Quantitative analysis of the dissolved metal ions revealed that lead promoted active dissolution of nickel and iron. It was pointed out that such a result indicated an enhanced selective dissolution of alloy constituents in lead-containing environments (Sakai et al. 1992a). The same effect of lead was detected in mild acidic and caustic solutions at 250°C (Hwang et al. 1997). Further investigation revealed that lead can also produce chromium depletion from the outer film of Alloy 600 and 690 in a pH 10 solution (Hwang et al. 2002).

The superimposed potential-pH Pourbaix diagrams of Ni and Pb indicate that in the pH range of 8-14, the equilibrium potential of lead is higher than that of nickel. Hence it is possible that the reduction of dissolved Pb species can enhance the oxidation of metallic Ni. In other words, there is a displacement reaction between lead and nickel as Equation 2-3 (Sakai et al. 1992b, Lumsden et al. 2005). This hypothesis is technically based on a thermodynamic consideration and plausible in high pH conditions. However, selective dissolution of nickel and iron induced by lead was also observed at low pH range. It means the phenomenon of selective dissolution of alloying elements may not be

controlled by Equation 2-3. The incorporation of lead and other environmental or metallurgical factors may also have a great influence on the stability of alloy constituents.



2.5.3 Effect of lead on the polarization behavior of nickel alloys

The detrimental effect of lead on the corrosion behavior of nickel alloys has been recognized with laboratory evidence (Staehele 2003b, Lu 2005). However, some contradictory experimental results were presented which make the investigation more complicated. In a NaOH solution with pH 10 at 90°C both passive current densities and critical current densities of Alloy 600 and 690 increased with lead concentration. It was suggested that the increasing anodic dissolution resulted from (1) the dissolution of metallic lead deposited on the electrode during the cathodic process and (2) the lead-enhanced electrochemical attack of constituents. However, in a pH 4 solution the passive current density and critical current density were not simply a function of lead content. In addition, the transpassive potential generally decreased with lead concentration under this condition, especially for Alloy 600 (Hwang et al. 2002). Newman and co-workers investigated the effect of UPD of lead on the passivation of nickel and Ni-21Cr by means of introducing Pb^{2+} impurities into the electrochemical system at different electrode potentials. It was found in acetic acid and perchloric acid, lead species strongly inhibited active dissolution of Ni at a low potential. This was attributed to a stable lead UPD adlayer formed on Ni which is against anodic dissolution. On the other hand, Pb was observed to activate the anodic dissolution of Ni in the passive region. With the addition of the alloying element chromium, both effects of lead were suppressed. In the same testing solution (perchloric acid), Costa et al. performed regular anodic polarization measurements and found that lead enhanced anodic dissolution of nickel and alloy 600, but had no effect on chromium and Alloy 690 (Costa et al. 1995).

In most electrochemical experiments lead impurities are added into the solution before the measurements start. Therefore, it is important to realize that for a different potential range lead may not always act as a corrosion promoter for nickel alloys. In the Ni-Cr-Fe alloy system, the role of one or two alloying elements may be dominant in certain conditions; the dominant factor controlling the electrochemical behavior of alloys is likely to shift at different potential, pH or in different chemistries.

2.5.4 Effect of lead on the characteristics of passive films on nickel alloys

In a lead-containing environment, the integrity of the passive film may be modified by the incorporation of lead. It was pointed out that the impact of lead on the composition of passive films on Alloy 600 varied at different pH values (Hwang et al., 2002). In his work, the film composition was analyzed after immersion tests were performed at 250°C with lead concentrations of 0, 25 and 250 ppm at pH 4 and 10. It was reported that in the outermost layer of the passive films, Cr enrichment and Ni depletion were observed at both pH 4 and 10. The inner layer has an opposite distribution of Ni and Cr at high pH value and this effect is enhanced by lead in the alkaline solution. In addition, it was found the stability of passive films decreases as a function of lead content, and increasing lead concentration leads to thicker passive films under the testing conditions. The effect of lead on the film structure and composition on Alloy 600 is summarized in Figure 2-12. It was suggested that the protective quality of a passive film on nickel alloys is determined by the nature of the inner layer. The increasing corrosion and SCC susceptibilities of nickel-based alloys in lead-containing caustic environments are due to enhanced Cr depletion in the inner layer.

However, the depletion of Cr instead of enrichment is observed in the lead-free solution at pH 4 in Figure 2-12. For stainless steels it is well known that chromium promotes passivity especially in acidic condition. The bleach of chromium at the surface of stainless steels in acidic media is not likely to occur from a thermodynamic view. It is highly possible that lead may not be the only contributor to degrade the stability of passive films on nickel-based alloys in some specific conditions.

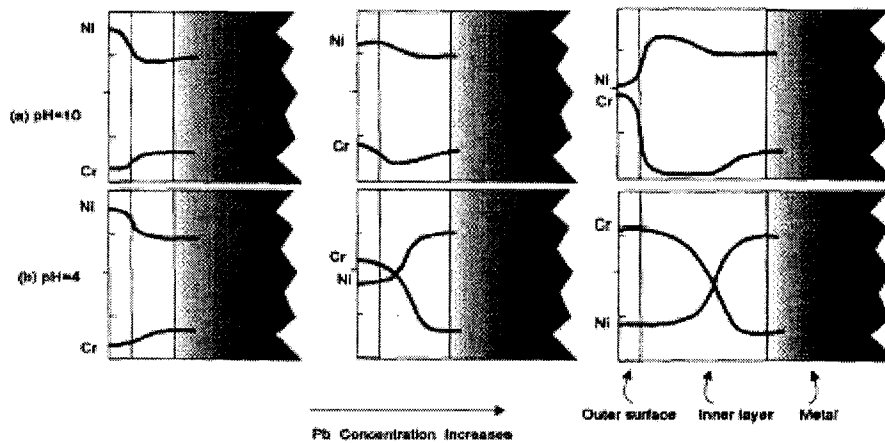


Figure 2-12 Effect of Pb on passive film composition of Alloy 690 at pH 4 and 10 (from Hwang et al. 1997).

2.5.5 Interaction of lead and other species in the solution

It is believed that a water chemistry containing some impurities is considered to be beneficial to reduce the risk of PbSCC. The reason is that the contaminating species such as P, S and C may form insoluble compounds with lead. After such chemical reactions the lead is immobilized and the probability of Pb SCC will decrease (Staehle 2004b).

On the other hand, the presence of some impurity ions in a pressurized water system, such as halide and sulfate ions, can efficiently modify the corrosion properties of oxide films at high temperature. When Pb ions are released from insoluble compounds in certain conditions, the detrimental effect of lead can be enhanced or inhibited by other species. Lu investigated the synergistic interaction of two coupled species, $\text{SO}_4^{2-}/\text{PbO}$ and SiO_2/PbO , on the polarization behavior of Alloy 800 in simulated crevice solutions at 300°C . It was found the anodic dissolution rate decreases with the pH value by the coexistence of $\text{SO}_4^{2-}/\text{PbO}$, while it increases with the pH value by the presence of

SiO₂/PbO (Lu 2005). It has been reported that TiO₂ and CeB₆ act as inhibitors on SCC for nickel alloys (Kim et al. 2005); some insight may be provided if the effect of such species can be evaluated in lead-containing solutions.

2.6 Experimental techniques

2.6.1 Electrochemical methods

2.6.1.1 Dynamic polarization measurement

Polarization measurement is a typical and mature electrochemical technique to evaluate corrosion resistance of materials. In this approach three electrodes are used in the electrochemical cell known as the working electrode, reference electrode and counter electrode. The reference electrode potential is comparatively stable during measurement in such an electrochemical system. A potentiostat is used to control the current across the working/counter electrode pair and maintain the potential difference between the working and reference electrodes. Any desired potential can be reached at the working electrode by this potentiostat. Since the responding current is a unique function of the potential, complete electrochemical behavior of a system can be obtained by sweeping the potential and recording the current-potential curve. The potential change can be set up in a predetermined manner; usually it has a linear relationship with time. From the current-potential curve, some important information can be derived such as OCP, active/passive state region, passive current density and transpassive potential.

Polarization measurements can also be performed by controlling current step instead of potential step. This method is not commonly used because of some fundamental disadvantages. The interference of the double-layer charging effect takes place through the experiment and is difficult to correct. The responding potential is not a single function of the controlled current. In addition the data gathered from this approach are less well-

defined than those from potential controlled curves. But in the case of a background process study, the application of the controlling current method is more convenient.

2.6.1.2 Cyclic electrochemical measurement

Cyclic voltammetry is an important transient analysis approach in the electrochemical measurement family. It is an effective technique for an initial study of an unknown electrochemic system and provides information about electrochemic reactions and interface structure on the electrode.

In this technique, the electrode potential is reversed periodically over a number of cycles at a fixed scanning rate. An upper limit of potential and a lower limit of potential are usually predetermined in the experiment. Usually potential vs. current curves are plotted for all the cycles in the same figure. It should be noted that the scan rate has a great influence on the shape of the forward and backward curves.

In principle, the data obtained from cyclic voltammetry are much easier to analyze than the complete i - E - t map for a new system. The impact of potential and time on the current is relatively direct in a single experiment. Usually this method is the first step to explore the reaction mechanism of electrochemical processes on the electrode. Cyclic voltammetry also provides semiquantitative results for kinetic parameters for electrode reactions. More accurate and precise evaluation of these kinetic values can be further acquired by other electrochemical methods such as chronocoulometry.

2.6.1.3 Mott-Schottky measurement

It has been well established that capacitive behavior of most passive films between the metal/electrolyte interface is similar to a semiconductor. The electronic properties of a semiconductor/electrolyte interface can be described by Mott-Schottky theory, in which some basic assumptions must be obeyed (Di Quarto et al. 2004):

- The semiconductor is homogeneously doped and the charge carriers are completely ionized in the bulk.
- The semiconductor is not degenerate so that Maxwell-Boltzmann statistics hold.
- The electrode potential is quite anodic so that $\Delta U_{SC} \gg kT$.

For a Schottky contact, a complex impedance $R + (i\omega C_{SC})^{-1}$ is produced across the metal/electrolyte junction where C_{SC} corresponds to the space charge capacitance and R is the ohmic part. By superimposing an ac voltage with frequency ω over a dc bias applied across the interface, the ohmic part R and space charge capacitance C_{SC} can be evaluated.

When the capacitance of the Helmholtz layer is fairly large compared to that of the space charge region, a simplified Mott-Schottky equation can be given as follows, depending on the nature of the semiconductor. This relationship describes the potential dependence of C_{SC} of a semiconductor electrode under the depletion condition.

$$\frac{1}{C_{SC}^2} = \frac{2}{\epsilon\epsilon_0 q N_A} \left(U - U_{FB} - \frac{kT}{q} \right) \quad \text{for n-type passive film} \quad (2-4)$$

$$\frac{1}{C_{SC}^2} = \frac{2}{\epsilon\epsilon_0 q N_A} \left(U_{FB} - U - \frac{kT}{q} \right) \quad \text{for p-type passive film} \quad (2-5)$$

where ϵ is the dielectric constant of the passive film, ϵ_0 the vacuum permittivity, N_A the charge carrier density, q the elementary charge, T the temperature, k the Boltzmann constant, U the applied potential and U_{FB} is the flatband potential.

According to the equation, the capacitance, $1/C_{SC}^2$, has a linear relationship with the applied potential, U , when the flat band potential is fixed. In the Mott-Schottky plot ($1/C_{SC}^2$ vs. U), a straight line with positive slope indicates a n-type semiconductor; a straight line with negative slope indicates a p-type semiconductor. The flat band potential

can be derived from the intersection of the curve with the axis of the applied potential, and donor/accepter density can be calculated from the slope.

2.6.2 Surface analysis techniques

The nature and characteristics of passive films play a critical role in passivity. Therefore, it is essential to analyze the surface response of metals and alloys in corrosive environments in order to control corrosion problems. Currently, a variety of surface analytical equipment and techniques are available to explore physical and chemical properties of a solid surface. Among them, X-ray photoelectron spectroscopy (XPS), secondary ion mass spectrometry (SIMS) and X-ray diffraction (XRD) are three powerful techniques for surface chemical analysis, providing thickness, composition, structure, chemical state of elements, element distribution and other important information for industrial and academic studies.

2.6.2.1 X-ray photoelectron spectroscopy

XPS is a quantitative spectroscopy technique in surface and thin film analysis. The strength of XPS is chemical analysis as it yields both compositional and chemical information. All elements except hydrogen and helium can be analyzed by XPS. It is not a destructive method with very low sample damage. The collected spectra are easy to interpret, and the operation of XPS equipment is not difficult. Thus XPS has been extensively used since it was invented.

The principle of XPS involves the interaction of incident X-ray photoelectrons and the sample surface. The schematic of this emission process is shown in Figure 2-13(a). When a solid surface is irradiated with X-ray photons, the energy of a photon $h\nu$ can be transferred to an electron with binding energy E_B , resulted in the ejection of a photoelectron. The photoelectron emitted is given with certain kinetic energy E_k . The relationship of these energies can be express as the following equation, where $h\nu > E_B$.

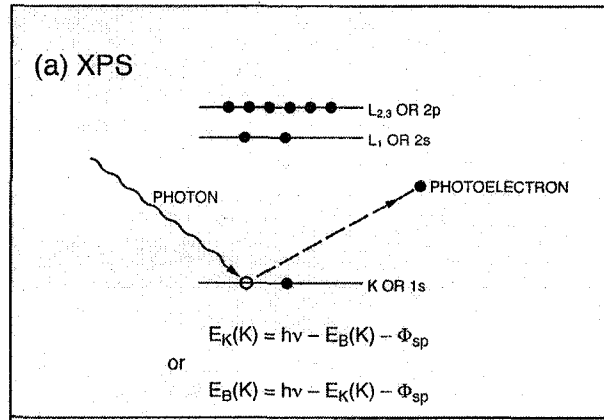
$$E_k = h\nu - E_B - \Phi_s \quad (2-6)$$

where Φ_s is a constant term corresponding to the work function and can be eliminated. Rearranging Equation 2-6 gives

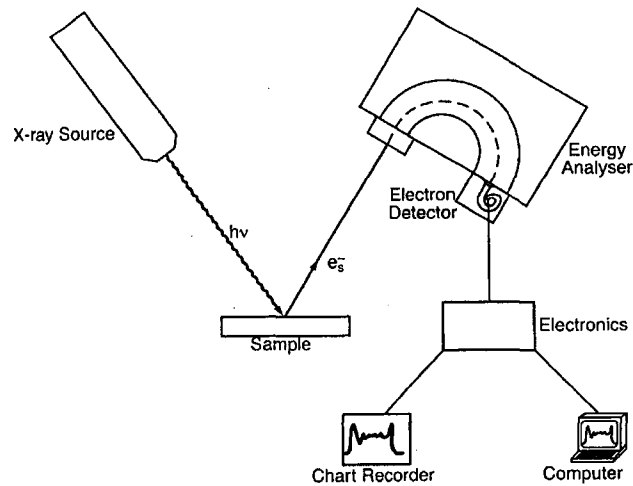
$$E_B = h\nu - E_k \quad (2-7)$$

Since the binding energy of electrons in core levels is unique for each element, identification of elements can be achieved by measurement of kinetic energies of the photoelectrons. Moreover, the fluctuation in E_B reflects the change of the chemical state of atoms. According to Equation 2-7, any energy fluctuation in E_B can induce changes in E_k . Interpretation of this effect successfully leads to the generation of chemical information.

A basic X-ray photoelectron spectroscopy system is mainly composed of an X-ray source, a sample stage, an electron energy analyzer and an electron detector and data processing system as shown in Figure 2-13(b). XPS is usually an ex-situ technique and requires a solid sample because it must be carried out under ultra-high vacuum (less than 10^{-8} Pa). Application of XPS covers many areas of materials science. Metals, catalysts, semiconductors, ceramics, biomaterials, nanomaterials and many other materials can be analyzed by means of XPS. It has become an indispensable surface analytical technique in modern analytical laboratories.



(a)



(b)

Figure 2-13 (a) Schematic illustration of X-ray photoelectron emission process; (b) Schematic of main components of XPS system (from O'Connor et al. 2003).

2.6.2.2 Secondary ion mass spectrometry

SIMS is usually considered as the most sensitive surface technique for surface compositional analysis. Its element sensitivity is as low as the ppb-ppm level due to its high signal-to-background ratio. Although XPS and SIMS are both spectroscopy techniques and have similar element detection capabilities, only SIMS can exam all the elements in the periodic table including hydrogen. The increasing application of SIMS is

also attributed to its capabilities of isotope identification of the element and chemical bonding determination at the surface. Besides, lateral resolution of SIMS is higher than that of XPS.

In SIMS analysis, heavy energetic primary particles such as the argon ion are used as primary ion sources. Thus penetration depths of incident ions are very large with an evident scattering effect. A variety of secondary particles such as secondary electrons, Auger electrons, photons, positive secondary ions and negative secondary ions are emitted from their original positions due to collisions with incident particles and the interaction among themselves. The last two particles are collected by a mass spectrometer and converted to positive or negative mass spectra. The main components in a SIMS system consist of ion sources, energy analyzer, mass analyzer, ion detector and electronic devices shown in Figure 2-14.

Time-of-flight (ToF) is a method used in SIMS analysis to measure the mass-to-charge ratio of particles emitted from the analyzed surface. When charged ions are collected into the mass spectrometer and accelerated by an electric field, all ions with the same charge are given the same kinetic energy. However, different types of ions naturally have various masses. Therefore, the velocity of a particular particle is determined by its mass-to-charge ratio, resulting in the exclusive time it takes to reach the detector. Based on this method, almost any combination of elements or compounds can be distinguished.

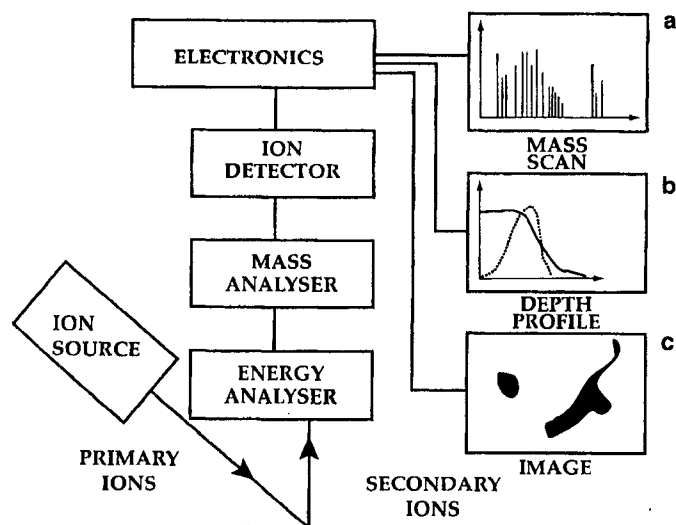


Figure 2-14 Schematic of main components of SIMS system (from O'connor et al. 2003).

In general, the application of SIMS is more qualitative than quantitative in nature. High detection sensitivity gives this technique priority to be used to identify surface composition and contamination for all kinds of materials. In addition, it also covers many other areas such as surface phenomena, coatings and nanoelectronics. In the case of corrosion processes, SIMS is also a powerful tool in many aspects. A “map” of local corrosion can be generated with this method; compositional profile can be created as a function of depth; the existence of hydrogen, which is an important element in corrosion studies, can also be analyzed. Due to their advantages, ToF instruments have demonstrated growing application in surface and near-surface analysis.

2.6.2.3 X- ray diffraction

XRD is a popular method to determine crystalline phases and lattice parameters of solid materials. It is also used to obtain information such as thickness and atomic arrangement of amorphous materials. XRD is an inexpensive, nondestructive method and the preparation of samples is not difficult. The elemental sensitivity of XRD is very high, because all the elements can be studied. However the diffraction intensity measured with XRD is strongly dependent upon the nature of materials. High-Z elements usually

generate larger signals, thus leading to higher surface sensitivity. Thin films with a thickness of 50 Å or even less can be effectively studied by means of this technique. Typically, the limitations of XRD are the lack of spatial resolution information and weak signals when compared with other surface analysis methods.

Principally, application of the XRD technique is based on the Bragg Equation 2-8, which is schematically shown in Figure 2-15.

$$\lambda = 2d \sin \theta \quad (2-8)$$

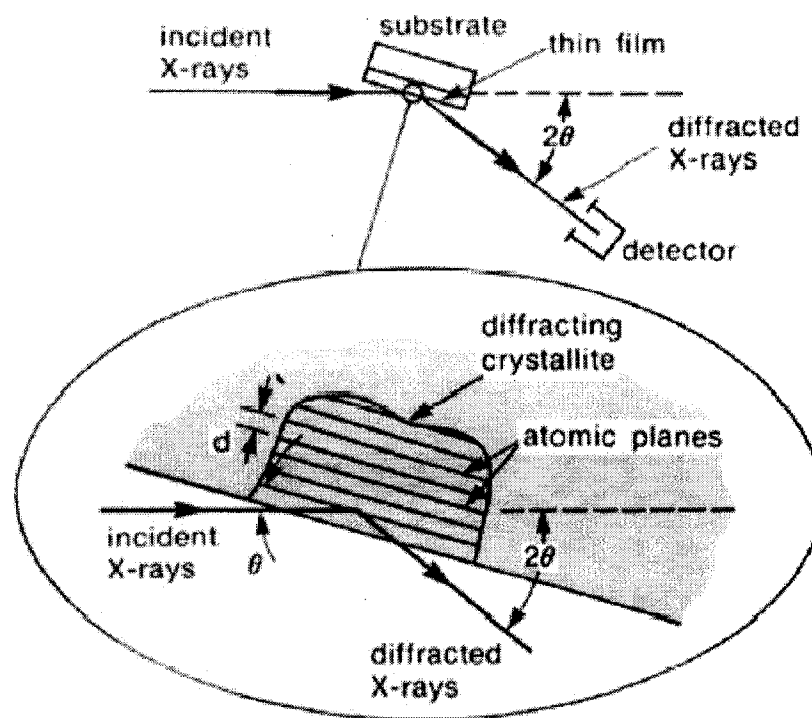


Figure 2-15 Basic features of a typical XRD experiment (from Brundle et al., 1992).

where λ is the wave length of the X-ray radiation, θ the Bragg angle (the angle between the incident X-ray beam and the atomic planes) and d the inter-planar distance between the planes causing diffraction. When a sample surface is irradiated with monochromatic

X-rays, the detector must be positioned at a certain angle to collect signals from specific atomic planes. By recording the intensities with corresponding diffraction angles (2θ), the value of d can be evaluated according to the Bragg equation.

XRD is widely used to evaluate the characteristics of thin films and multilayer coatings, such as phase identification, determination of strain and crystallite size. The unique and accurate measurement of this radiation technique makes it an important family member of surface science.

2.6.2.4 Nanoindentation

The nanoindentation technique was established in the 1970's with the purpose of providing mechanical information of coatings and thin films with a micro- and nanometer resolution. In corrosion studies, the synergistic interaction between mechanical and chemical factors is of great interest. In many conditions, the breakdown of a passive film is suspected to be controlled by this mechano-chemical effect. The application of nanoindentation makes it possible to better understand the relationship between mechanical properties at local sites of the surface and corrosion resistance. Besides, in situ nanoindentation can be performed under electrochemically controlled conditions. These experiments are fundamentally important to clarify the mechanism of passivity and local corrosion of metal and alloys. The popularity of nanoindentation has increased rapidly with the combination of other surface analytical techniques such as atomic force microscopy (AFM).

In the indentation test, an indenter penetrates into the material with increasing load, holds at the peak value for a period of time, and then is withdrawn with decreasing load. The curve of penetration depth vs. load is recorded to determine the hardness. Elastic modulus can also be evaluated by the projected area. A typical load/depth curve is shown in Figure 2-16.

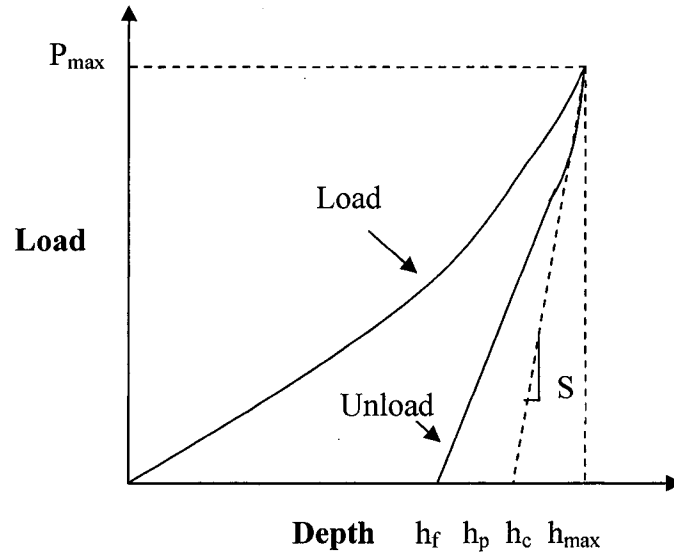


Figure 2-16 Typical load vs. depth curve in indentation tests.

The hardness H is defined by the ratio of the maximum load P_{\max} to the projected contact area A ,

$$H = \frac{P_{\max}}{A} \quad (2-9)$$

The contact area A is a function of the contact depth h_c , given by,

$$A = c_0 h_c^2 \quad (2-10)$$

where c_0 is a constant depending on the type of indenter. The geometry of indenter shape plays a key role in the accurate measurement of contact depth. The contact depth h_c varies at different indentation depth h_{\max} . Fused quartz is used as a standard specimen in calibration because its hardness and modulus are known. For calibration, a correction equation for h_c is given by

$$h_c = h_{\max} - \frac{0.75P_{\max}}{S_{\max}} \quad (2-11)$$

Where S_{\max} ($\frac{dP}{dh}$) is the unload stiffness.

Combining Eq. 2-10 and Eq. 2-11, the projected contact area can be expressed as

$$A = \left(\frac{\pi}{4}\right) \left(\frac{S_{\max}}{E_r}\right)^2 \quad (2-12)$$

where E_r is the reduced modulus, which can be interpreted as

$$\frac{1}{E_r} = \left(\frac{1-\nu^2}{E}\right)_{\text{specimen}} + \left(\frac{1-\nu^2}{E}\right)_{\text{indenter}} \quad (2-13)$$

where E and ν are the elastic modulus and Poisson ratio of the fused quartz and the indenter, respectively. The contact area A can be fitted by the following equation, which is called area function.

$$A = c_0 h_c^2 + c_1 h_c + c_2 h_c^{1/2} + c_3 h_c^{1/4} + c_4 h_c^{1/6} + c_5 h_c^{1/8} \quad (2-14)$$

where c_0 is a constant depending on the type of indenters, c_1 to c_5 are fitted constant.

In the indentation test with a given tip, the modulus and Poisson ratio are known. Thus the modulus of the specimen can be calculated.

Chapter 3

3. Experimental

3.1 Selection of testing materials

Three types of nickel alloys are commonly used as steam generator tubing materials. They are Alloys 600, 690 and 800. The first used nickel-based alloy was Alloy 600 (UNS N06600). However, this alloy soon was found to sustain PbSCC heavily. Alloy 690 with high chromium content, which demonstrates much better PbSCC resistance than that of Alloy 600 in operation, was then developed to replace Alloy 600 in most plants. However, laboratory experiments discovered the susceptibility of PbSCC is still high in alkaline media. To date there is no widely accepted explanation, and the study of this phenomenon would be extremely helpful to better understand the mechanism of PbSCC. Therefore Alloy 690 was selected as the main testing material in this work.

Nickel-based Alloy 690 (UNS N06690) as received was used in most electrochemical and surface analysis experiments. The nominal composition of alloy 690 in weight percent is 0.02C, 30Cr, 10Fe, 0.5Mn, 0.5Si and balance Ni, as shown in Table 3-1. Pure metals of nickel, chromium and iron were also used in electrochemical experiments to identify the effect of Pb on the electrochemical behavior of alloying elements. The pure nickel is 1.0 mm foil from Aldrich Chemical Company, Inc. Its nominal purity is 99.98% with trace amount of impurities (less than 100 ppm level). The composition of commercial pure iron in weight percent is C 0.003, Si 0.01, Mn 0.12, P 0.006, Cr 0.01, B 0.009, Al 0.32 and Fe balance. The purity of chromium is 98%.

For electrochemical experiments, all the testing materials were cold mounted by epoxy. One surface of the mounted samples was ground with silicon paper up to 600-grit, then cleaned in de-ionized water and degreased with acetone.

For surface analysis, Alloy 690 specimens were cut into 1x2 cm² pieces. The specimens were ground with silicon paper up to 600-grit, cleaned in distilled water and degreased with acetone. Then the specimens were divided into 6 groups according to the different testing chemistries (see section 3.2). Each group of specimens was put into an autoclave and immersed in the corresponding solution for 24 hours at 300°C. During this process, surface films were formed on the specimen surfaces. After being taken out of the autoclave all the specimens were cleaned in acetone by an ultrasonic machine, and were ready for XPS and SIMS analyses.

For nanoindentation experiments, the same procedure of sample preparation was used as that for surface analysis.

Table 3-1 Nominal composition of Nickel Alloy 690(UNS N6690)

| C | Cr | Fe | M | Si | Ni |
|------|----|----|-----|-----|------|
| 0.02 | 30 | 10 | 0.5 | 0.5 | Bal. |

3.2 Formulation of testing solutions

Field and laboratory examinations revealed that in SCC of tubes at the Ontario plant five elements were detected at or near the crack tip: O, S, Cl, Ca and Pb. Thus the laboratory test requires a chemical solution to simulate the typical crevice environment in the plant. Under operating condition, the crevice in tubes has a pH range of 4-9 with deaeration. PbO is selected as the lead impurity added in this testing solution because it is the only lead compound detected in the Ontario plant. The concentration of lead contamination, 500 ppm, is considered the upper limit of lead species in a normal condition based on previous experiments and field observations.

Thus, a set of special solutions were designed to simulate CANDU SG crevice chemistries, as shown in Table 3-2. To investigate the effect of lead on the electrochemical performance of the samples, 2.2 mM PbO (equal to 500 ppm) was added as Pb contamination to basic solutions. All the tests carried out in the lead-containing solutions were accompanied with this concentration of PbO unless otherwise stated. It should be noted that the concentration of PbO is a nominal value because solubility data for PbO at high temperature are not available at present. The actual amount of dissolved lead species is determined by pH value and temperature.

Table 3-2 Concentrations (Mole) of species in simulated CANDU SG crevice chemistries

| | NaCl | KCl | Na ₂ SO ₄ | CaCl ₂ | NaHSO ₄ | NaOH | PbO | pH ₂₅ ^o C | pH ₃₀₀ ^o C |
|----------|------|------|---------------------------------|-------------------|--------------------|------|--------|---------------------------------|----------------------------------|
| Acid | 0.3 | 0.05 | 0.15 | 0.15 | 0.05 | - | - | 1.5 | 3.22 |
| | 0.3 | 0.05 | 0.15 | 0.15 | 0.05 | - | 0.0022 | 1.5 | 3.31 |
| Neutral | 0.3 | 0.05 | 0.15 | 0.15 | - | - | - | 5.14 | 6.10 |
| | 0.3 | 0.05 | 0.15 | 0.15 | - | - | 0.0022 | 5.12 | 6.88 |
| Alkaline | 0.3 | 0.05 | 0.15 | 0.15 | - | 0.4 | | 12.7 | 9.26 |
| | 0.3 | 0.05 | 0.15 | 0.15 | - | 0.4 | 0.0022 | 12.7 | 9.26 |

3.3 Experiment procedure

3.3.1 Electrochemical Experiment

A typical three-electrode system was used in the electrochemical experiments. A platinum wire acts as the counter electrode. The reference electrode is a saturated calomel electrode (SCE) connected with a capillary. All experiments were carried out at room temperature (23°C) with continuous deaeration by pure nitrogen gas. The setup of the electrochemical cell is shown in Figure 3-1.

In the electrochemical experiments, a Gamry 3.2 system was used for polarization measurements and a Solartron 1287B system was used for voltammetry measurements.

Before polarization measurements, the test solutions were deaerated by bubbling pure nitrogen for one hour. Then the sample was conditioned at a cathodic potential ($-1.0 V_{SCE}$) for 15 minutes to remove air-formed oxides unless otherwise stated. Because this potential is lower than the equilibrium potential of Pb/Pb^{2+} , the deposition of metallic lead on the electrode surface is expected to take place at the same time when the preconditioning is carried out in Pb-contaminated solutions. The potential dynamic scanning was started at $-0.2 V$ below the OCP with a scanning rate of $1 mV/s$.

To investigate the effect of metallic Pb produced during the preconditioning on the polarization behavior, a group of samples was transferred into the Pb-free solution after preconditioning in the Pb-contaminated solution. This experiment was done by replacing the test solution after preconditioning. After the Pb-contaminated solution was drained, the electrochemical cell was refilled with de-ionized water and then, the water was drained again. This procedure was repeated three times to clean the cell and electrodes. The setup of electrochemical cell is shown in Figure 3-2.

To investigate the effect of dissolved Pb species on the corrosion and repassivation behaviour of Alloy 690, Pb contamination was added to the cell at different potentials after the samples were preconditioned in Pb-free solutions for voltammetry measurements. Three potentials (-0.795 , -0.70 and $-0.20 V_{SCE}$) were designated according to the equilibrium potential of Pb/Pb^{2+} . After preconditioning at $-1.0 V_{SCE}$ for 15 minutes in the Pb-free solutions, the electrode potential was raised to an assigned potential and kept at this value for 60 seconds. $1.1 mM PbO$ was added to the test solution and mixed rapidly during this period. Then voltammetry measurements were started at this assigned potential with a scanning rate of $3 mV/s$. Each test lasted 5 cycles. For comparison, every test was performed once without Pb addition following the same procedure.

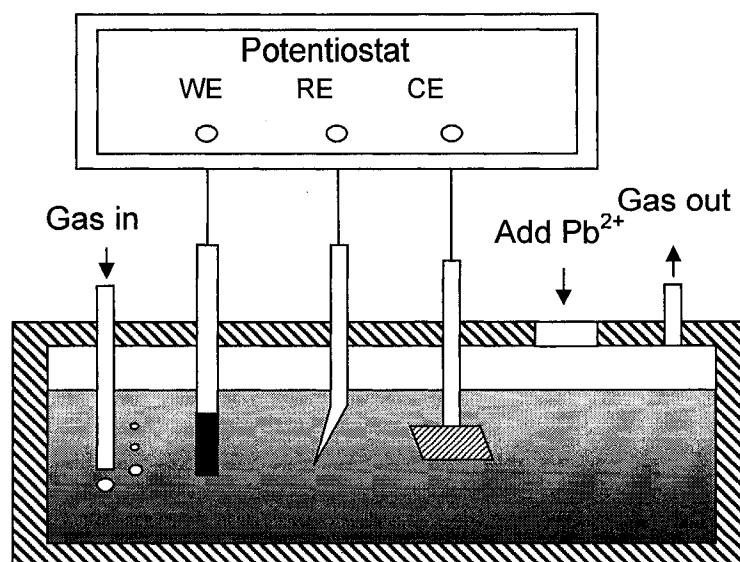


Figure 3-1 Setup of electrochemical cell

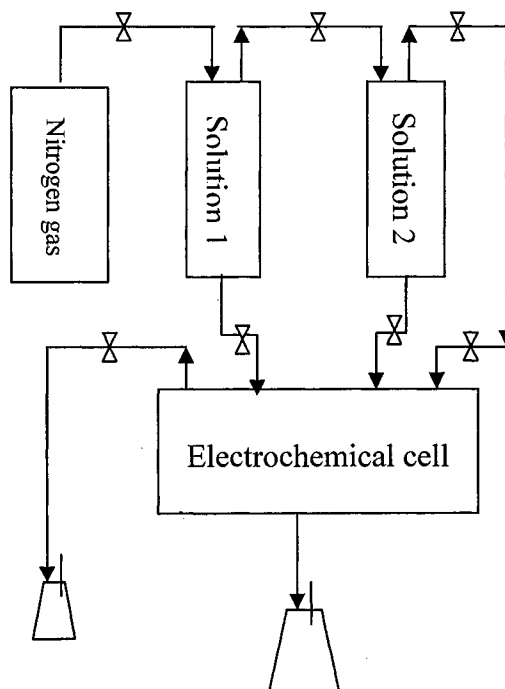


Figure 3-2 Setup of electrochemical cell for sample transfer experiment. Solution No.1 is Pb-free solution and No. 2 is Pb-containing solution.

3.3.2 Surface analysis

(1) XPS analysis

The XPS measurements were performed using an Axis-ULTRA (Kratos Analytical) spectrometer controlled by a SUN workstation. Photoelectron emission was excited by an aluminium (monochromatized) source operated at 210W with initial photon energy 1486.71 eV. The survey spectra were recorded at steps of 0.33 eV using 160 eV pass energy, whereas high-resolution spectra were taken at steps of 0.1 eV using 20 eV pass energy. The base pressure was approximately $5\sim 10^{-10}$ Torr. The C1s peak from adventitious carbon at 284.6 eV was used as a reference to correct the charging shifts. The photoelectrons were collected at a take-off angle of 90° with respect to the sample surface. Depth profiling was performed over an area of $1.5 \times 1.5 \text{ mm}^2$ under 3 keV Ar-ion sputtering and the sputter rate was estimated to be 3 nm/min. Casa XPS software was used in XPS spectra decomposition. The high resolution spectra were fitted according to the Gaussian-Lorentzian lineshape, and the Shirley approach was used to subtract backgrounds. Before XPS analysis, the morphologies of the same samples were examined with JEOL Field Emission SEM.

(2) SIMS analysis

The same samples in XPS analysis were used for ToF SIMS testing. SIMS analysis was carried out with ToF SIMS IV instrument (ION-TOF GmbH). All ions were detected with extreme sensitivity to small amounts of impurities, 1 ppm to ppb depending on the element. In the current work, the analysis source used was Ga^+ , operation at 15 kV; the sputtering source is Cs^+ , operating at 1 kV.

(3) XRD analysis

The X-ray diffraction experiment was carried out by using a Rigaku rotating anode RU-200B system equipped with a cobalt anode as X-ray source. Alloy 690 samples prepassivated in different SG crevice chemistries for 24 hours at 300°C were cut and thinned to an approximate thickness of 1 mm. The sample surfaces were cleaned with acetone in an ultrasonic cleaning machine prior to the XRD experiment. Thin film setup (vs. wide angle) was used in this study. The theta angle was 0.5 degree.

3.3.3 Nanoindentation

The nanoindentation apparatus (Hysitron Co., Ltd., Triboscope®) was attached with AFM (Digital Instruments, Nanoscope E) to control the positioning and displacement of the indenter on the specimen surface. A diamond cube corner indenter was used in the experiment. Prior to any indentation experiment, the instrument was calibrated with the standard fused quartz sample. A triangular load function was employed for the indentation consisting of a 5 seconds loading segment and a 5 seconds unloading segment. The peak value of the load ranged from 500 – 3000 μN

For comparison, the surface of an Alloy 690 sample without any treatment was also examined. Before tests, this specimen was first mechanically ground with silica paper up to grit 600, and manually polished with 6 μm diamond paste and 0.05 μm alumina particles.

The measurement of reduced modulus and hardness is sensitive to the surface condition of samples. For Alloy 690 samples prepassivated at high temperature, the surface is not uniform and smooth. Considering that these factors may affect the experimental result, nanoindentation was conducted at comparatively smooth sites, and average values were calculated after the experiments.

Chapter 4

4. Results

4.1 Electrochemical behaviors of Alloy 690 in lead-containing environments

It is reasonable to assume that there is an air-formed oxide film on the surface of SG tubes after manufacturing. In operation there exists a passive film on the alloy surface. Under certain stress, the passive film will rupture at the weakest sites and may initiate PbSCC or lead to the propagation of cracks. Therefore three types of surface condition were considered and evaluated independently in this work: (1) the fresh alloy surface; (2) the oxide film surface; (3) the passive film surface.

In order to investigate the effects of lead on the corrosion resistance of nickel alloys, polarization measurements were carried out in acidic and alkaline solutions. Neutral condition was skipped because of the solubility limitation of lead oxide in this pH range at ambient temperature. Alloy 690 is mainly composed of nickel (~60%), chromium (~30%) and iron (~10%) by weight percentage. The stability of alloying elements plays an essential role in the nature and characteristics of passive films on the alloy. However, few investigations systematically took into account the effect of lead on alloying elements and the consequent influence on the protective properties of passive films. In the present work electrochemical performance of the pure metals Ni, Cr and Fe were studied separately in lead-containing simulated SG crevice chemistries with different pH values.

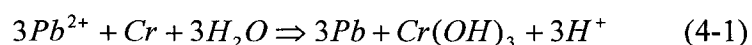
Prior to the electrochemical measurements, cathodic preconditioning was carried out to remove the oxide film on the sample surface formed in air unless otherwise stated. During low potential preconditioning, metallic lead is expected to deposit on the sample surface. To separate the interference of the plated lead from anodic dissolution of pure

alloying elements, a gold coated silicon wafer was used as an inert electrode in this experiment. The electrochemical response on such an electrode can be solely attributed to the oxidation of the metallic lead. The measured curves are marked as control and superimposed on corresponding figures for comparison.

4.1.1 Effect of lead on the corrosion resistance of Alloy 690 in acidic chemistry

Figure 4-1 shows the polarization curves of Alloy 690 in simulated SG crevice solutions at pH 1.5 with and without lead. The results indicate the impact of lead is limited in acidic chemistry. In the lead-containing solution, the OCP only slightly shifts in the negative direction. An anodic current peak was observed at $-0.5 V_{SCE}$, which represents the lead oxidation according to the potential-pH diagram (See Appendix A). The passive current density slightly increases with lead, but the transpassive potential is almost the same regardless of lead impurities. In the cathodic branch, the reaction on the working electrode is the reduction of hydrogen in a lead-free solution. A decrease of cathodic current density is detected in the lead-containing solution.

At low pH range lead is completely soluble. To date there is no evidence showing that the activity of dissolved Pb species is related to anodic dissolution of nickel-based alloys. However, it was theoretically postulated that, under certain conditions, lead may enhance the anodic dissolution of nickel alloys via the displacement reactions according to Equation 4-1 to 4-3 (Zhou 2005). Thus further investigation is demanded with respect to the anodic dissolution of pure Ni, Cr and Fe in a lead-contaminated environment.



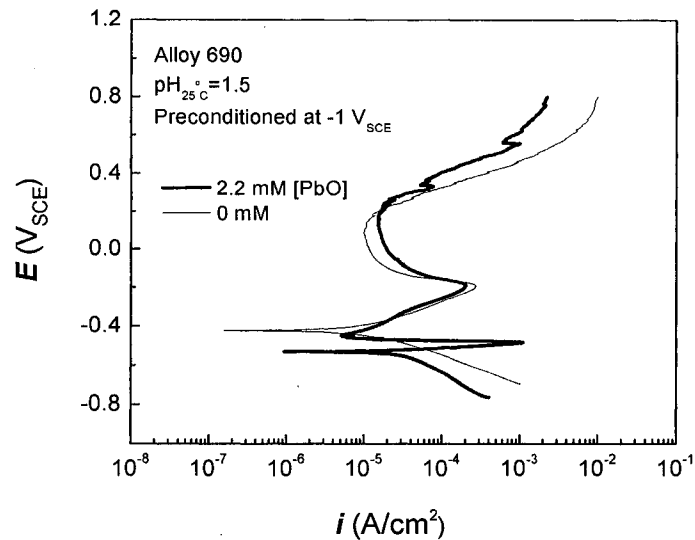


Figure 4-1 Polarization plots of Alloy 690 in acidic simulated SG crevice solutions with and without PbO.

4.1.2 Effect of lead on the corrosion resistance of alloying elements in acidic chemistry

To identify the anodic dissolution of plated lead, a polarization curve was measured on the control electrode, as shown in Figure 4-2. A current peak around $-0.5 V_{SCE}$ appears with the presence of lead. This potential represents the equilibrium potential of lead at pH 1.5. Above this potential, Pb is not stable and will be oxidized. After preconditioning, the same current peak is also detected in the polarization curves of all three pure metals, as shown in Figures 4-2, 4-3 and 4-4.

Figure 4-2 also shows the effect of lead on the passivity behavior of pure nickel in an acidic crevice solution. It is worthy to note the oxidation potential of lead is in the cathodic branch of the polarization curve of Ni. In this figure, lead slightly decreases the anodic dissolution of nickel in acidic solution rather than promotes it. A similar phenomenon was also reported in 0.1 M perchloric acid and acetic acid/sodium acetate

buffer solution, and it is suspected that the inhibit effecting of lead is related to the UPD of element lead (Radhakrishnan et al. 2005). The exact mechanism is still uncertain and no literature provides a widely accepted interpretation to date.

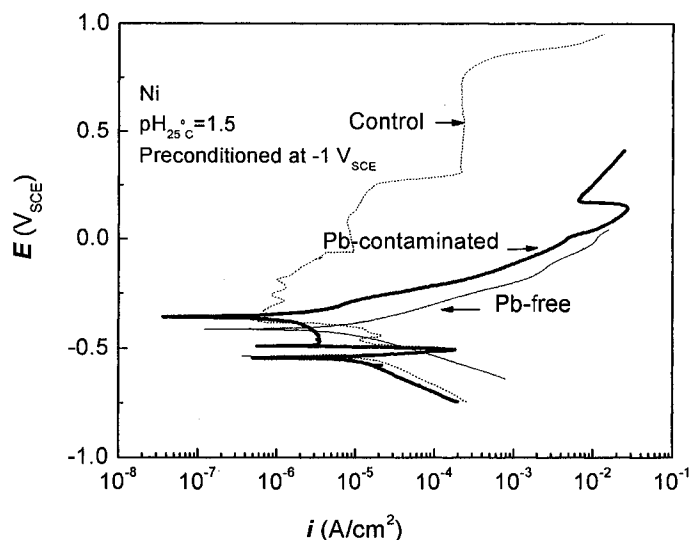


Figure 4-2 Effect of lead on the polarization behavior of pure nickel in acidic SG chemistries.

Chromium is an element added to increase oxidation resistance of alloys. Pure chromium exhibits excellent corrosion resistance in acidic solutions as shown in Figure 4-3. There is no effect of lead that can be seen except the additional oxidation current peak of lead. The OCP, passive current and transpassive potential of chromium retain the same values even with the presence of lead. This may ascribe to the rapid formation of a stable oxide film on the surface (Costa et al. 1995). Figure 4-4 shows that iron suffers active dissolution in acidic media and no effect of lead is demonstrated.

By comparison of Figures 4-1 through 4-4, it can be seen the passivation of Alloy 690 is mainly determined by nickel and chromium. The OCP of Alloy 690 is close to nickel. But the polarization curve of Alloy 690 exhibits a stable passive region during anodic

polarization, which is similar to that of chromium. However, the passive range is smaller, implying that the beneficial effect of chromium is affected by other factors in the high potential range. Iron is unstable in acidic solution irrespective of lead impurities, as shown in Figure 4-4. The polarization curves with and without lead almost overlap with each other. Surface analysis also indicated that iron has little contribution, if any, to the passivation on nickel alloy 600 and 690 in acidic media (Montemor et al. 2003, Hwang et al. 1997).

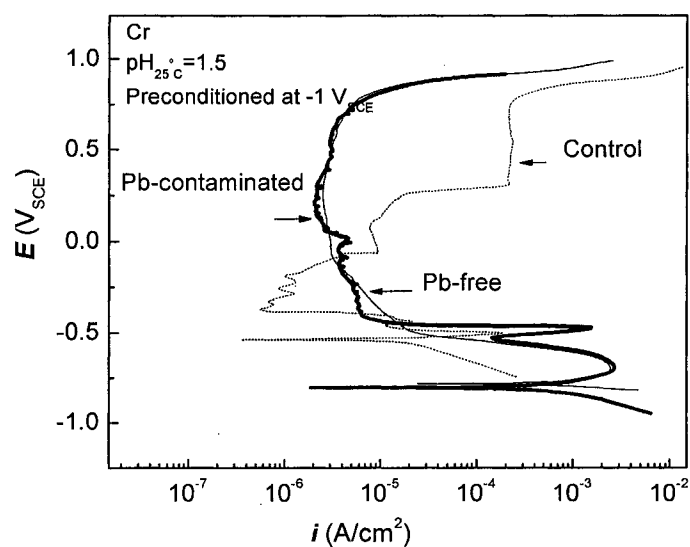


Figure 4-3 Effect of lead on the polarization behavior of pure chromium in acidic SG chemistries.

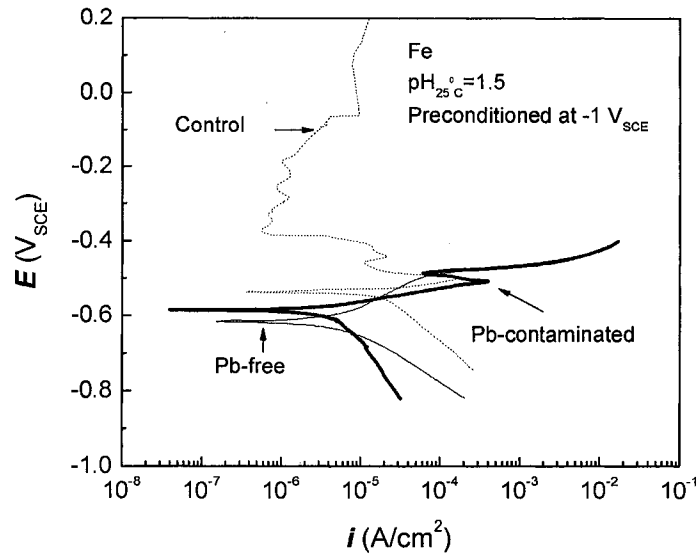


Figure 4-4 Effect of lead on the polarization behavior of pure iron in acidic SG chemistries.

The current peak in polarization measurements is a result of the oxidation of lead. In Figure 4-5, by comparing the magnitudes of peak current densities on the control electrode and pure metals, it is found that lead increases anodic dissolution of iron but has no influence on the dissolution of chromium and nickel. The potential of lead oxidation is around $-0.5 V_{SCE}$ in acidic crevice solution, which is higher than the OCP of iron and chromium. The oxidation of metallic lead may weaken the lattice structure of iron and promotes anodic dissolution. In this pH range pure chromium already turns into a passive state. Therefore, the effect of lead is not evident due to a stable passive film developed on the chromium surface. In the case of nickel, this potential is lower than its OCP as discussed above. When lead oxidation begins around $-0.5 V_{SCE}$, nickel is still immune from corrosion. Thus no accelerated anodic dissolution of nickel was observed.

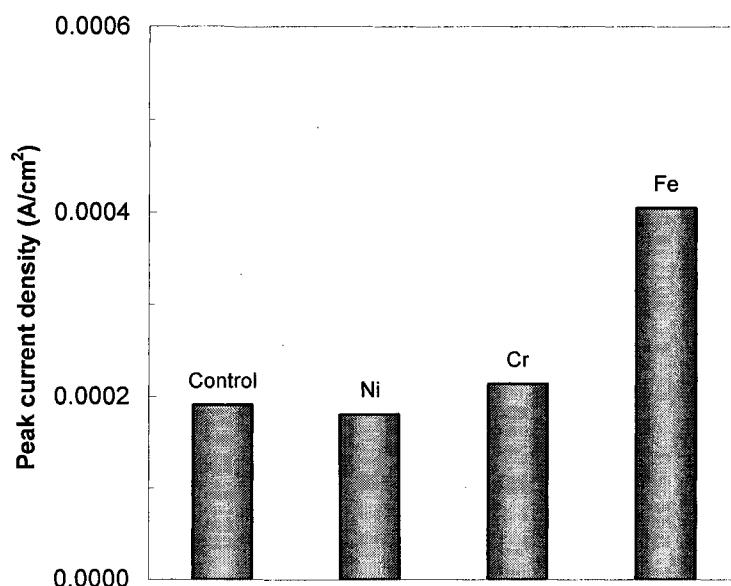


Figure 4-5 Effect of lead on the magnitude of current peak in acidic SG chemistries.

4.1.3 Effect of lead on the corrosion resistance of Alloy 690 in alkaline chemistry

Since nickel alloys sustain serious PbSCC in caustic media, three experiments were designed to probe the impact of lead on the stability of passive films in alkaline chemistry.

(1) The specimen was preconditioned at $-1 V_{SCE}$ in the lead-free solution and tested in the same solution, noted as curve 1; (2) The specimen was preconditioned at $-1 V_{SCE}$ in the lead-containing solution and tested in the same solution, noted as curve 2; (3) The specimen was preconditioned at $-1 V_{SCE}$ in the lead-containing solution and tested in the lead-free solution, noted as curve 3.

Figure 4-6 shows the polarization curves 1, 2 and 3 of Alloy 690 in simulated SG crevice solutions. In curve 2, the cathodic current density rises markedly in the lead-containing solution, implicating high reaction rate of lead reduction. A nearly vertical slope of the cathodic branch indicates this process is controlled by diffusion. The most possible species of lead at this pH range is $Pb(OH)_2$ or $HPbO_2^-$. They can be reduced to Pb within

the potential region of -1 to -0.7 V_{SCE} according to Equation 4-4 and 4-5 (Staehle 2003a, 2004b; Pourbaix 1974).

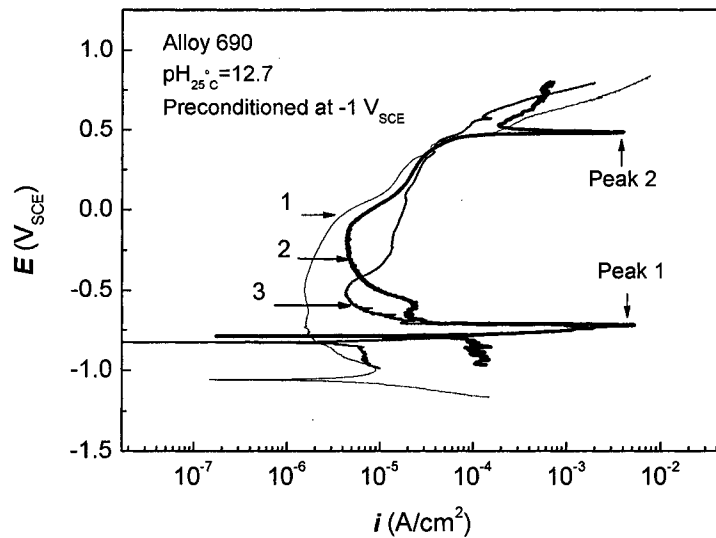
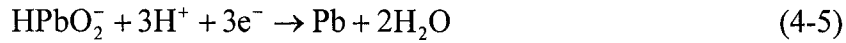
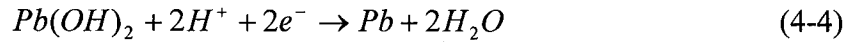


Figure 4-6 Polarization plots of Alloy 690 in alkaline simulated SG crevice solutions with and without Pb.

Comparing with curve 1, the OCP of curve 2 is shifted 200 mV in the noble direction by lead. The passive current density also substantially increases with the incorporation of lead. These observations indicate that the presence of lead can reduce the protective nature of the passive film on Alloy 690 under these test conditions. In addition, two current peaks are detected in curve 2. Current peak 1, which is also observed in curve 3, appears around -0.7 V_{SCE}, while current peak 2 appears around 0.45 V_{SCE}. The

magnitudes of peak 1 in curve 2 and curve 3 are very close. As mentioned before, metallic lead is expected to be plated on the electrode in the lead-containing solution in preconditioning. This current peak (around $-0.7 V_{SCE}$) indicates the oxidation of lead at this electrode potential. At high potential region (around $0.45 V_{SCE}$) the current peak 2 in curve 2 implies further oxidation of certain elements in the passive film to a higher valence. The disappearance of peak 2 in curve 3 implies that (1) peak 1 is affected by preconditioning in Pb-containing solution; (2) peak 2 appeared only when Pb was in the testing solution. A similar current peak was also observed on Alloy 690 in lead-containing NaOH solution with a pH value of 10, and it was attributed to the lead-promoted transpassive dissolution of chromium (Ahn et al. 2005). However, this phenomenon was found to be associated with the concentration of lead contamination in the following experiments and will be further discussed below.

Both field and laboratory evidence reveal that PbSCC is more intensive for Alloy 690 in alkaline conditions (Staehle 2003b, Lumsden et al. 2005, Wright et al. 1999); therefore, further electrochemical experiments concerning the effects of lead in corrosion susceptibility of Alloy 690 were conducted in high pH solutions.

Figure 4-7 shows the effect of lead concentration on the electrochemical behavior of Alloy 690 in alkaline solutions. Experimental results indicate that the corrosion susceptibility of Alloy 690 steadily increases with lead concentration. This effect was also reported at high temperature condition (Lu 2005). The magnitude of peak 1 proportionally increases with lead concentrations as shown in Figure 4-8, where a functional relationship has been demonstrated. When lead concentration is low (0.0044 mM), the shift of OCP and appearance of peak 2 can't be detected, suggesting the amount of lead in the solution must accumulate to make a perceptible influence on the OCP and promote peak 2. Based on the present results that (1) there is no peak 1 in Pb-free solution; (2) the magnitude of peak 2 increases with lead concentration, it is more likely that the appearance of peak 2 is promoted by lead on the electrode.

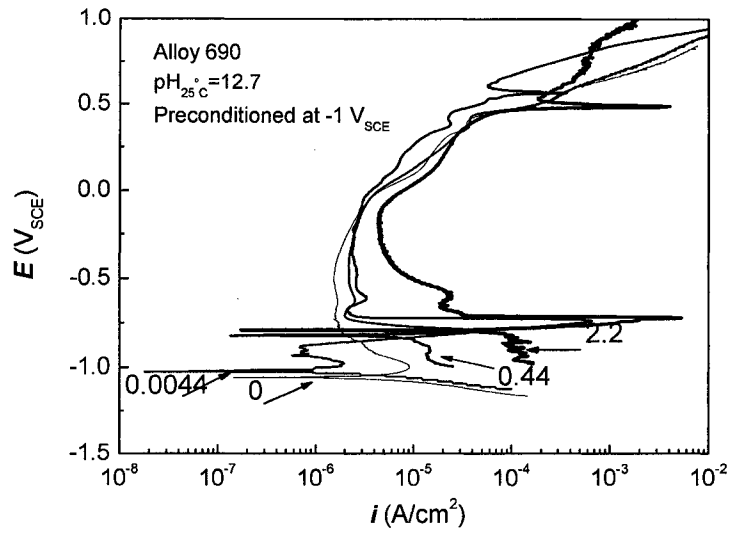


Figure 4-7 Concentration effect of lead on polarization behavior of Alloy 690 in alkaline simulated SG crevice.

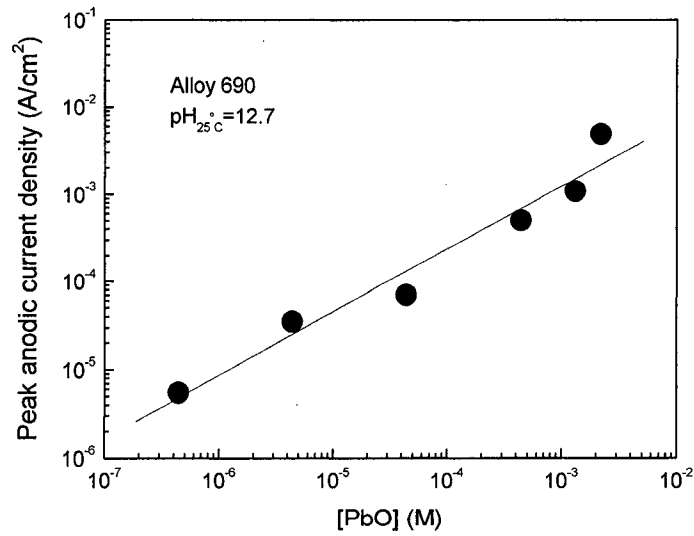


Figure 4-8 Effect of PbO concentration and the current density of peak 1.

Since lead has demonstrated significant impact on the passivity of fresh alloy surface, it is necessary to investigate the interaction between dissolved lead species and a pre-formed passive film. The effect of prepassivation time on the corrosion behavior of Alloy 690 in alkaline lead-containing solution is shown in Figure 4-9. With increasing prepassivation time at $-0.3 V_{SCE}$, all the specimens manifest the same passive current density in this potential region. Since all the OCPs in Figure 4-9 are quite high, peak 1 can't be observed in this test. However, the anodic current peak 2 is still exhibited when the prepassivated time is long enough. The enhanced peak implies that the ingress of lead into the passive film increases with time. On the other hand, the detrimental effect of lead seems to be not as obvious as that on the fresh alloy surface, although dissolved lead species can be continuously involved in the formation process of passive films. The interaction of Pb^{2+} and an existing passive layer is also denied by Costa et al. In his work, two nickel alloys were passivated in lead-free $0.1M HClO_4$ for 30 minutes, and then PbO was introduced as lead impurities in the solution. No difference of passive current was observed after the addition of lead (Costa et al. 1995).

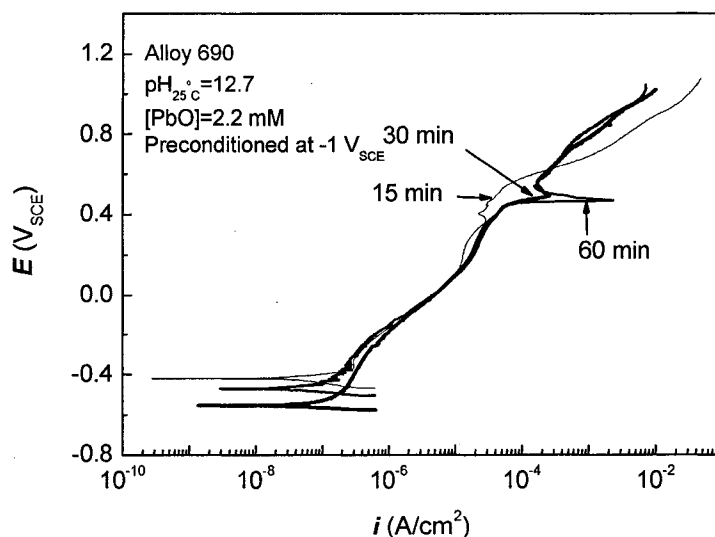


Figure 4-9 Polarization curves of Alloy 690 prepassivated at $-0.3 V_{SCE}$ for (1) 15 minutes in lead-free solution, (2) 30 minutes in $2.2 mM PbO$ solution and (3) 60 minutes in $2.2 mM PbO$ solution.

Although cathodic preconditioning is a common technique used in laboratories to remove the air-formed oxide film on a sample surface, it is impossible to do so during equipment installation or in plant operation. For Alloy 690 preserved in air, there is a spontaneous oxide film on the surface. To evaluate the effect of the Alloy 690 sample with air-formed oxide, a cathodic potential was applied to this type of sample. The integrity of the surface film is controlled by the time and potential of this reduction process. Obviously, longer cathodic preconditioning results in a lower degree of residual surface oxide. Figure 4-10 shows the effect of preconditioning duration, in other words the degree of residual oxide film on the polarization curves of Alloy 690 in alkaline solution containing 0.044 mM PbO. It can be seen that the passive current density increases with preconditioning time, suggesting that, with an air-formed oxide film, corrosion resistance of Alloy 690 increases in lead-containing alkaline solution. Although the lead concentration is very low, peak 1 still can be observed and passive current density gradually increases when the preconditioning duration is long. This result is in support of field observations that PbSCC can take place in dilute solutions with lead concentration as low as 0.1 ppm (Staehele 2003b).

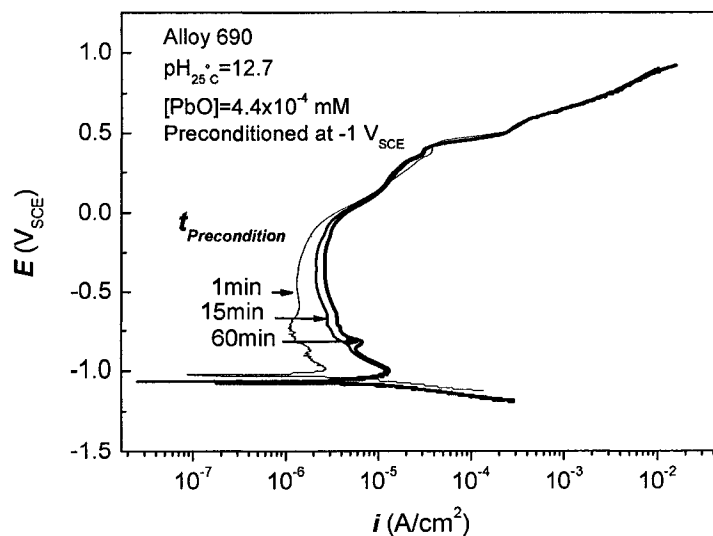


Figure 4-10 Polarization curves of Alloy 690 in alkaline SG crevice chemistry with 0.44 mM PbO, the samples were preconditioned at $-1 V_{SCE}$ for (1) 1 minute, (2) 15 minutes and (3) 60 minutes.

4.1.4 Effect of lead on the corrosion resistance of alloying elements in alkaline chemistry

To explore the effect of lead on the passivation behavior of pure metals in alkaline condition, polarization curves of Ni, Cr and Fe are presented in this section. Similar to the acidic condition, a control curve of lead was obtained to isolate the electrochemical response of pure lead and has been superimposed in Figures 4-11 through 4-13.

The electrochemical behavior of pure nickel is presented in Figure 4-11. The influence of lead is mainly displayed at the low potential range. The passive current densities and passive regions obtained in solutions with and without lead are close. But the passive current density of pure nickel in lead-free solution is higher than that of Alloy 690, as listed in Table 4-1, which clearly shows the superior corrosion resistance of Alloy 690 due to the beneficial effect of alloying elements, especially in a lead-free environment. However, the alloy suffers more than pure nickel when lead is added, suggesting some alloying elements can actively interact with lead and promote anodic dissolution of the alloy.

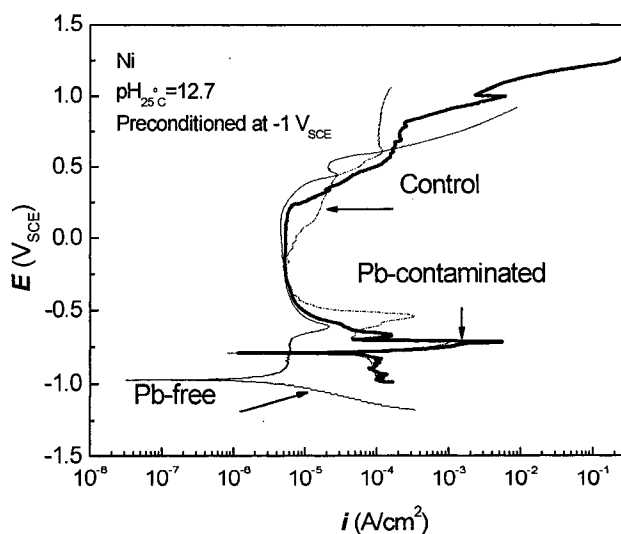


Figure 4-11 Effect of lead on the polarization behavior of pure nickel in alkaline SG chemistries.

Table 4-1 Passive current densities of Alloy 690 and pure metals at -0.25 V_{SCE} in alkaline SG crevice chemistries (μA/cm²)

| Chemistry Element | Pb-free solution | Pb-contaminated solution | $\Gamma = \frac{I_{Pb\text{-containing solution}}}{I_{Pb\text{-free solution}}}$ |
|----------------------|------------------|--------------------------|--|
| Ni | 5.0 | 5.2 | 1.04 |
| Cr | 2.7 | 16.9 | 6.26 |
| Fe | 56 | 75 | 1.34 |
| Alloy 690 | 2.1 | 4.6 | 2.19 |

Chromium is usually considered as a common passivity promoter for alloys (Marcus, 1994), which plays an important role in the SCC resistance and corrosion properties of alloys. In Figure 4-12 the passive current density increases sharply by lead, showing that lead significantly alters anodic polarization behavior of chromium in alkaline crevice solution. This deleterious effect is also shown in Table 4-1. It was suggested that three redox reactions, shown as Equation 4-6 through 4-8, are thermodynamically possible at 300°C for nickel-based alloys in a lead contaminated environment, and selective attack of chromium by lead seems most likely to occur in Ni-Cr-Fe alloys (Helie et al. 1995). But this assumption has not been widely accepted.



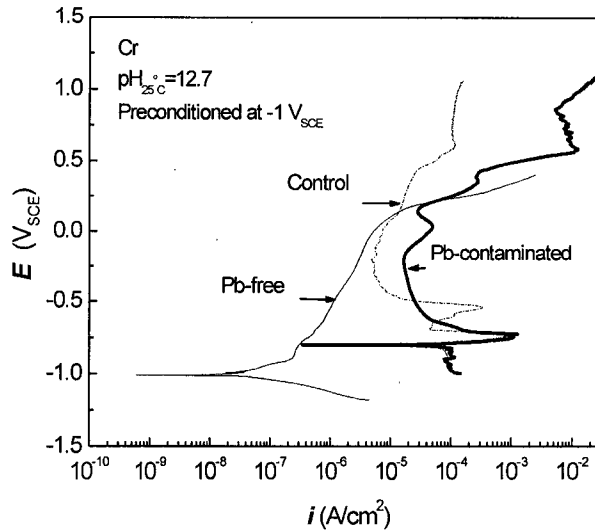


Figure 4-12 Effect of lead on the polarization behavior of pure chromium in alkaline SG chemistries.

In most laboratory experiments carried out in acidic conditions for nickel alloys, chromium concentration in passive films always increases (Montemor et al. 2003, Garcia-Mazario et al. 1996, Sakai et al. 1992a). This phenomenon may be associated with the increasing PbSCC intensity in high pH environments. In the present work, the different anodic behavior of chromium in alkaline and acidic solutions is a strong argument in support of this observation.

The influence of lead on iron in Figure 4-13 is not as significant as that on chromium. The passive current density in the lead solution slightly increases, and the transpassive potentials are almost the same regardless of the presence of lead. But the current peak 2 appears at high anodic potential on iron, which does not appear in nickel and chromium. This can be attributed to the fact that nickel and chromium are in the transpassive region at this peak potential. Thus the current peak 2 can't be seen due to high current density caused by uniform active dissolution of nickel and chromium.

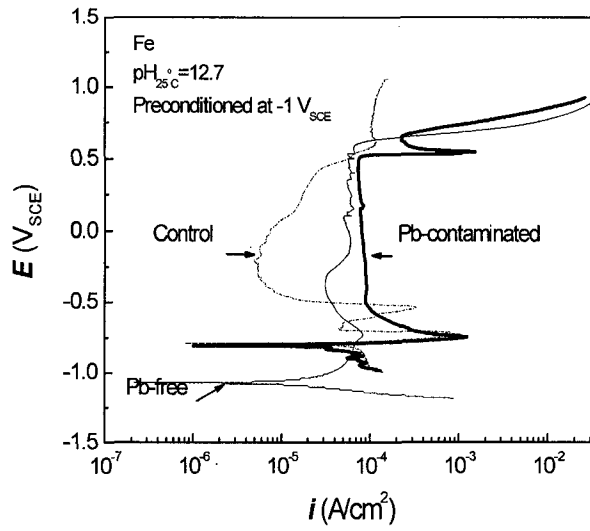


Figure 4-13 Effect of lead on the polarization behavior of pure iron in alkaline SG chemistries.

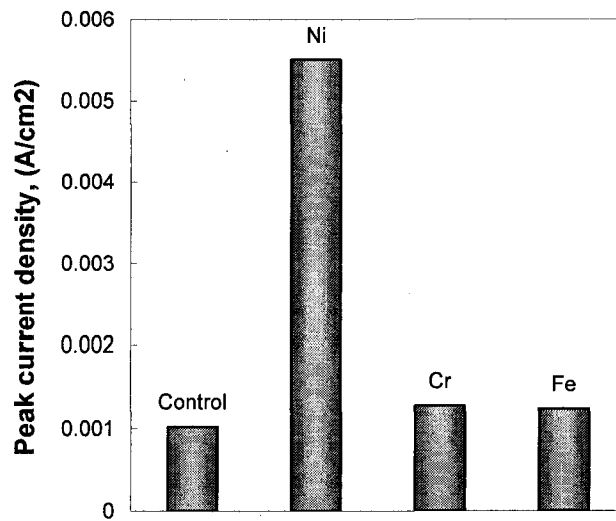


Figure 4-14 Effect of lead on the magnitudes of current peak 1 for Ni, Cr, Fe and Au in alkaline SG chemistries.

In the control curve, current peak 1 is observed around $-0.7 V_{SCE}$, which represents the oxidation of lead. This peak is also detected in polarization curves of all the pure metals as shown from Figures 4-11 through 4-13. However, the magnitude of this peak varies with respect to different electrode materials. In Figure 4-14, it can be seen the peak current densities of chromium and iron are almost equal to that of the control curve, suggesting there is no lead-induced anodic dissolution of pure chromium and iron at this potential. However, the value of the peak current density is much higher on nickel, indicating lead promotes anodic dissolution of nickel and results in selective dissolution on Alloy 690.

In the cathodic branch, the control curve is almost vertical in the lead-containing solution. It means this process is controlled by diffusion of lead species. At this potential, $Pb(OH)_2$ or $HPbO_2^-$ is unstable and can be reduced to metallic Pb (Pourbaix 1974). The cathodic current density of the control curve in alkaline lead-containing solution also significantly increases, suggesting the reduction of lead occurs readily in high pH solution.

It has been suggested that the preferential dissolution on nickel alloy in the presence of lead can be interpreted from a thermodynamic point of view (Staehele 2003b). Superposition of Pourbaix diagrams of Ni and Pb shows that the equilibrium potential of Pb/Pb^{2+} is higher than that of Ni/Ni^{2+} in the pH range of 8 to 14. Thus the displacement reaction between dissolved Pb^{2+} and Ni is thermodynamically possible in caustic solution. As a consequence, nickel atoms act as an electron donor and leave the bulk metal, while the dissolved lead ions enter the nickel lattice and accumulate on the surface.

4.1.5 Cyclic voltammetry study of the effect of lead

During plant operation, the rupture of passive films is a repeating process, which leads to frequent exposure of bare metals. It is necessary to investigate the effect of lead on this process because crack advance is closely related to the rupture of corrosion film. Figure 4-15 shows the voltammetry curve of Alloy 690 obtained in the alkaline crevice solution with lead. In every cycle, metallic lead is expected to be plated on the electrode surface

during the cathodic process. The current peak 1 again appears around $-0.7 \text{ V}_{\text{SCE}}$. A noticeable feature is that the anodic current density of the first scan is much higher than the rest of the cycles. The decreasing oxidation peak is obviously due to the decreasing amount of metallic lead on the electrode, which is proportional to the time during which the electrode potential stays in the cathodic branch. The preconditioning time before the experiment is much longer than the cathodic duration in each cyclic scan. Therefore, the magnitude of peak 1 current in the first scan is the highest one.

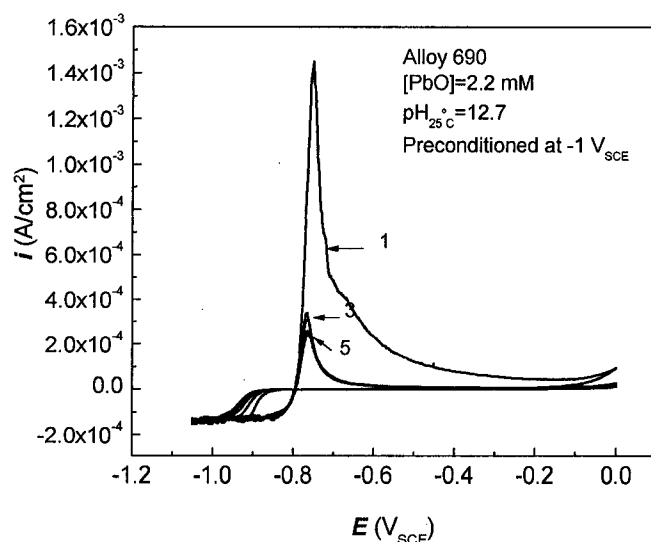


Figure 4-15 Effect of deposited lead on the voltammetric behavior of Alloy 690 in alkaline SG chemistry.

Figure 4-15 also shows that the passive current densities decrease with increasing cycle numbers. This may be related to the effect of lead on a pre-existing passive layer. Only in the first scan cathodic preconditioning can lead to the exposure of fresh metal surface. During the reverse scan, it is impossible to remove the oxide film completely in such a short time on the Ni-Cr-Fe alloy specimen. In the rest of the scans, it is evident the influence of lead is reduced on a prepassivated surface. This phenomenon is in agreement

with the prepassivation experiment (Figure 4-9) and other published reports. It was reported that there was no observed interaction of Pb^{2+} with a pre-formed passive film on Alloy 600, 690, pure Ni and Cr. Also it has been pointed out that the existence of a lead complex in the passive layer has never been detected, and the reaction between lead and nickel or chromium oxide, such as Equation 4-9, is not likely to take place. In other words, lead is not likely to react with oxides on the alloy surface (Costa et al. 1995, Helie et al. 1995).



Figure 4-16 shows 1, 3, 5 voltammetry cycles of Alloy 690 in Pb-free alkaline crevice solution. Comparing with Figure 4-15, the passive current densities are very close for all cycles. Without the interference of the plated lead, voltammetric behavior of Alloy 690 seems to be very stable. Only the cathodic current densities in reverse scan slightly increase with cycle numbers, which may reflect the thickening of the oxide layer during increasing anodic scan cycles.

In lead-containing solutions, the dissolved Pb^{2+} is suspected to be replaced as metallic lead onto the fresh metal surface by UPD and damage the integrity of subsequently formed oxide (Zhou 2005, Radhakrishnan et al. 2005). The phenomenon of UPD is the electrochemical formation of two-dimensional sub or monolayer surface coverage by the adsorption of metal atoms at potentials more positive than their equilibrium potential. Also it is suspected that replacement reaction between Pb and Ni can take place, and the reduction of dissolved Pb species gives rise to enhancing anodic dissolution of metallic Ni (Lumsden et al. 2005). Therefore it is important to identify the influence of dissolved lead species in the electrolyte on the corrosion resistance of nickel alloys.

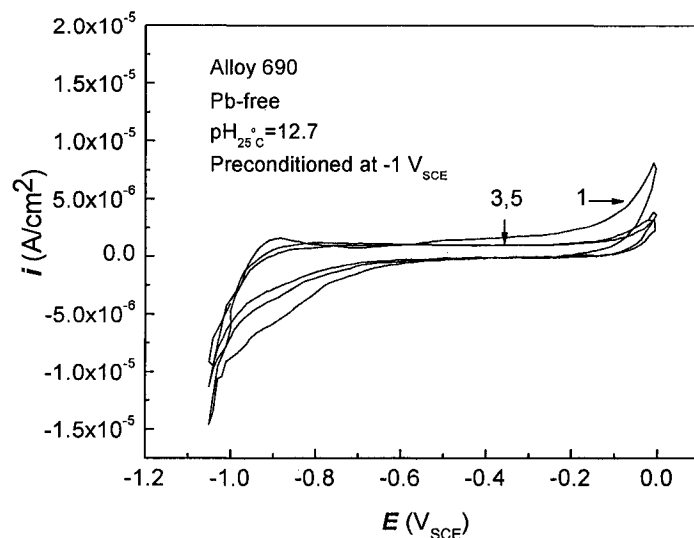


Figure 4-16 Voltammetric behavior of Alloy 690 in Pb-free alkaline crevice solution.

To avoid the formation of metallic lead during preconditioning, Pb^{2+} impurities were inoculated in the test solution at different potentials in the following experiments to further evaluate the effect of dissolved Pb^{2+} species.

According to the voltammetry curve of Alloy 690 in Figure 4-15, three potential zones can be divided with respect to the oxidation potential of lead at $-0.7 \text{ V}_{\text{SCE}}$.

- Zone 1 is from the OCP ($-0.795 \text{ V}_{\text{SCE}}$) to $-0.7 \text{ V}_{\text{SCE}}$. Alloy 690 suffers active dissolution within this potential range.
- Zone 2 is from $-0.7 \text{ V}_{\text{SCE}}$ to $-0.2 \text{ V}_{\text{SCE}}$. Alloy 690 is in the passive state within this potential range.
- Zone 3 is the potential range higher than $-0.2 \text{ V}_{\text{SCE}}$. Further oxidation to a higher valence of chromium will take place above this potential.

Based on these three potential zones, it was decided to deliberately add Pb^{2+} impurities into electrolytes at the three potentials -0.795 , -0.7 and $-0.2 \text{ V}_{\text{SCE}}$. All Alloy 690 specimens were first preconditioned at $-1.0 \text{ V}_{\text{SCE}}$ in alkaline crevice solution without lead.

Then electrode potential was shifted to a pre-designated value and kept at this potential for 1 minute. 250 ppm Pb^{2+} was added into the electrolyte and rapidly mixed up in this period. After that, cyclic voltammetry measurement started from this potential to 0 V_{SCE} . Because the susceptibility of PbSCC is very low in the high potential range, the potential region higher than 0 V_{SCE} was not taken into account. The same procedures and cyclic voltammetry measurements were repeated in the Pb-free solution for comparison.

(1) Dissolved lead species added at -0.795 V_{SCE}

Figure 4-17 shows 1, 3, 5 cycles of cyclic voltammograms after dissolved Pb^{2+} species was added at -0.795 V_{SCE} . With the presence of lead anodic dissolution of Alloy 690 only slightly increases in the first positive scan within low potential range (from -0.75 to -0.4 V_{SCE}). This increment results from the oxidation of lead and the lead-enhanced anodic dissolution of Alloy 690 as discussed before, because lead can be reduced during the one minute blackout of scanning. In the rest of the scanning, the impact of lead can't be detected. This phenomenon may be related to the stability of the oxide film formed on the specimen surface. The corrosion film containing chromium oxide is difficult to remove in reverse scan. As indicated above, there is no influence of lead on the pre-formed passive films. The anodic current densities in the rest of the cycles are, therefore, lower than the first cycle. The rapid increase of anodic current near 0 V_{SCE} can be attributed to the transpassive dissolution of chromium from Cr^{3+} to Cr^{6+} .

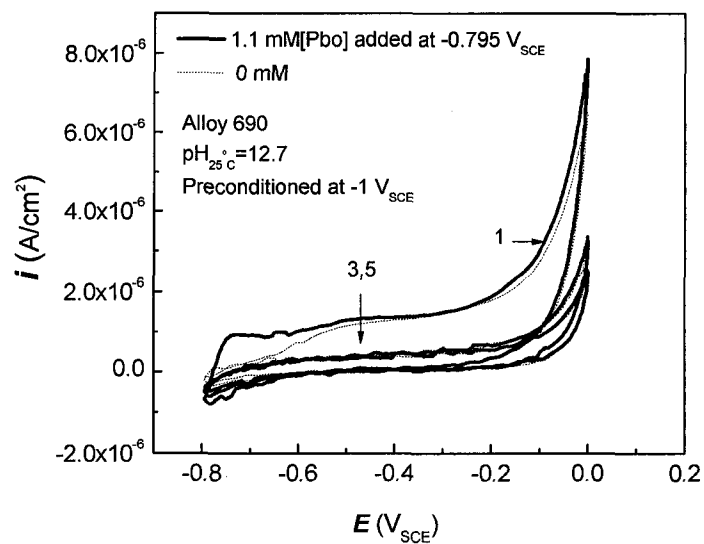


Figure 4-17 Effect of dissolved Pb^{2+} (added at -0.795 V_{SCE}) on the voltammetric behavior of Alloy 690.

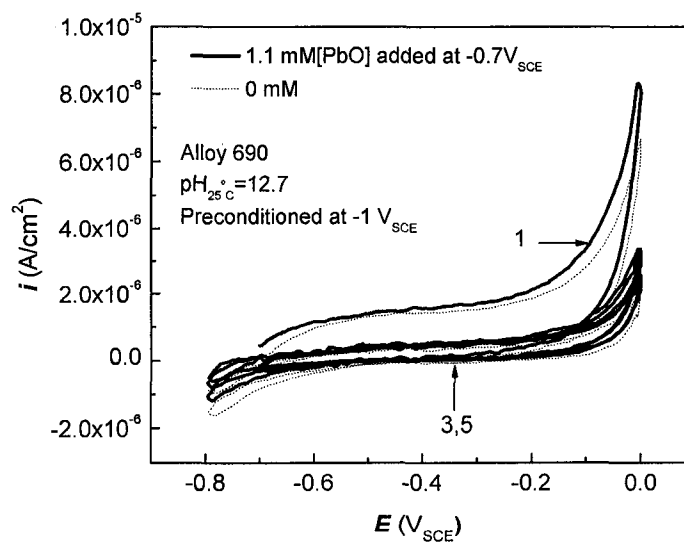


Figure 4-18 Effect of dissolved Pb^{2+} (added at -0.7 V_{SCE}) on the voltammetric behavior of Alloy 690.

(2) Dissolved lead species added at $-0.7 V_{SCE}$

Figure 4-18 shows 1, 3, 5 cycles of cyclic voltammograms when dissolved Pb^{2+} impurities were added at $-0.7 V_{SCE}$. Above this potential lead oxide is stable. The possible lead species in the high pH range is $HPbO_2^-$ according to the potential-pH diagram. The anodic current densities with and without lead impurities are very close for every scan. The dissolved lead species display no detrimental effect on the corrosion behavior of Alloy 690 when added at this potential.

(3) Dissolved lead species added at $-0.2 V_{SCE}$

According to the potential-pH diagram, further oxidation of chromium occurs around $0 V_{SCE}$ at pH 12.7 at room temperature. Above this potential, the effect of chromium on the protective character of the passive film weakens quickly. In Figure 4-19, it is found lead exhibits some kind of inhibiting effect at high potential range. Lead contamination actually decreases passive current density when nickel and iron oxides are the main components of the passive film, implying that the impact of lead on the passive films may change when the composition of the passive film is different.

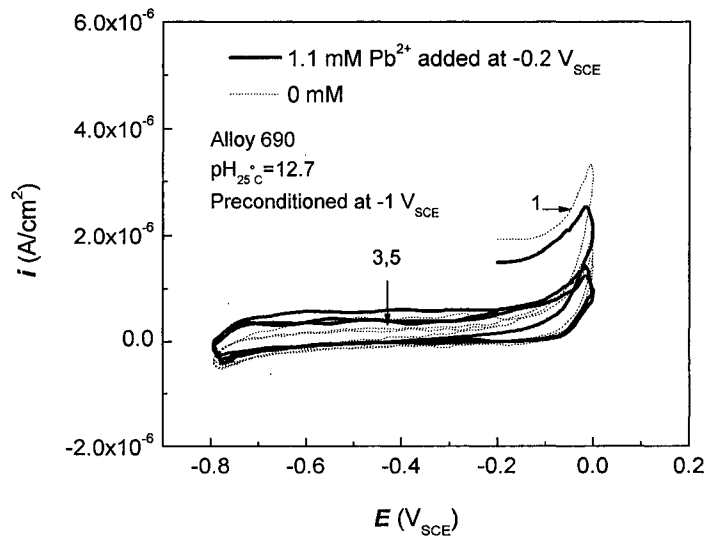


Figure 4-19 Effect of dissolved Pb^{2+} (added at $-0.2 V_{SCE}$) on the voltammetric behavior of Alloy 690.

4.1.6 Effect of lead on the semiconductive behavior of Alloy 690

Since passive films on nickel alloys act as semiconductors, the electronic properties of the passive films were investigated. The capacitive behaviors of passive films formed on Alloy 690 at different pH with and without lead are presented from Figures 4-20 through 4-22. The negative slopes of $1/C^2$ vs. E plots indicate the surface films obtained in acidic, neutral and alkaline conditions are all p-type semiconductors. This means the charge carrier resulted from an acceptor in these films.

The semiconductive type of the passive film is fundamentally determined by its composition. Usually capacitive response of iron oxide is acknowledged as a n-type semiconductor (Craig 1991), nickel oxide is p-type (Sikora et al. 2002), and chromium oxide reveals both types of semiconductivity (Goodlet et al. 2004). Da Cunha Belo and co-workers assessed the effects of alloying elements on the Mott-Schottky behavior of nickel alloy in borate buffer. It was found chromium does not change the p-type capacitive behavior of pure Ni and has little influence in a more positive potential domain, while the effect of iron on pure Ni is opposite, yielding strong n-type character in the high potential region. As a consequence, the simultaneous addition of Fe and Cr in a nickel-based alloy results in the development of a heterojunction in the passive film, whose nature and properties highly depend on the composition (Da Cunha Belo et al. 1999). This structure model is also supported by other publications (Montemor et al. 2000, Ferreira et al. 2002).

In Ni-Cr-Fe alloys it is theoretically possible to show either p-type or n-type semiconductive response because of the formation of bimetallic oxides (spinel) on the alloy surface. The spacious crystal structure of spinels allows cations to enter the interstitial lattice sites. The accumulation of cations facilitates the formation of a n-type semiconductor, while the lack of cations results in a p-type semiconductor (Beverkog et al. 1999). Obviously, the testing conditions play a key role in determining the specific type of surface films. In other words, for Alloy 690 the nature of film semiconductivity strongly depends on the composition and structure of the oxide film.

In the present experiment, only p-type capacitive response is observed. It may be associated with the type of spinel oxides formed in specific chemistries. $NiFe_2O_4$ and $FeCr_2O_4$ are two of the most stable bimetallic oxides at high temperature on nickel alloys. $NiFe_2O_4$ has n-type semiconductor behavior, while $FeCr_2O_4$ processes p-type semiconductor properties (Craig 1991). Because $FeCr_2O_4$ forms near the hydrogen equilibrium line, which is lower than the stable zone of $NiFe_2O_4$ and close to the OCP of nickel alloys (Beverkog et al. 1999), it is possible that $FeCr_2O_4$ (p type) is the predominant phase in the surface films, since all corrosion films in this section were obtained at the OCP of Alloy 690.

According to Equation 2-5, the slope change of the Mott-Schottky plot is basically determined by the acceptor density N_A and the dielectric constant ϵ . Various oxides in the passive film give rise to different values of the dielectric constant, for instance, NiO (11.9), Cr_2O_3 (~12), FeO (14.2), Fe_2O_3 (12) and Fe_3O_4 (20). Lead, which processes a higher value of 25.9 (PbO) (CRC Handbook 2006), may incorporate into the lattice structure of the films and essentially change their electronic nature. The complexity of film composition may profoundly alter semiconductive properties of a Pb-doped passive film. From this point of view, surface analysis is necessary to further explore the nature of the films in lead-contaminated conditions.

Experimental results also show that the effect of lead is different when the pH value of the solution is changed, which is summarized in Table 4-2. Since the composition of the passive films can't be determined, it is impossible to calculate the dielectric constant ϵ of a mixture as discussed above. Hence, the absolute values of slopes in Figure 4-20 through 4-22 are used for comparison. In acidic chemistry the acceptor density slightly increases with lead; in neutral chemistry lead incorporation sharply decreases the acceptor density; while in alkaline chemistry lead contamination significantly increases the acceptor density. Higher carrier density means a larger number of defects in the passive film. These results indicate the passive film in neutral solution naturally processes fewer defects and is more stable than others. It was reported that Alloy 690 is

almost immune to PbSCC in neutral environments in most field and lab reports (Staehele 2004a); this observation is in agreement with the stability sequence of passive films in different pH conditions.

Table 4-2 Effect of lead on the parameters in Mott-Schottky measurements

| Chemistry | $\frac{Slope_{Pb}}{Slope_{Pb-free}}$ | Effect of lead on absolute slope value | Effect of lead on carrier density |
|-----------|--------------------------------------|--|-----------------------------------|
| Acidic | 0.58 | decrease | slightly increase |
| Neutral | 3.87 | increase | substantially decrease |
| Alkaline | 0.15 | decrease | sharply increase |

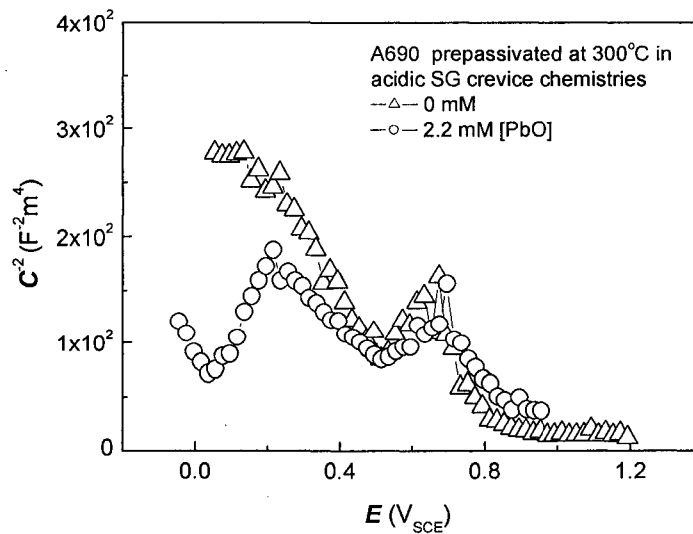


Figure 4-20 Mott-Schottky plots of Alloy 690 prepassivated in acidic SG crevice chemistry with and without Pb at 300°C.

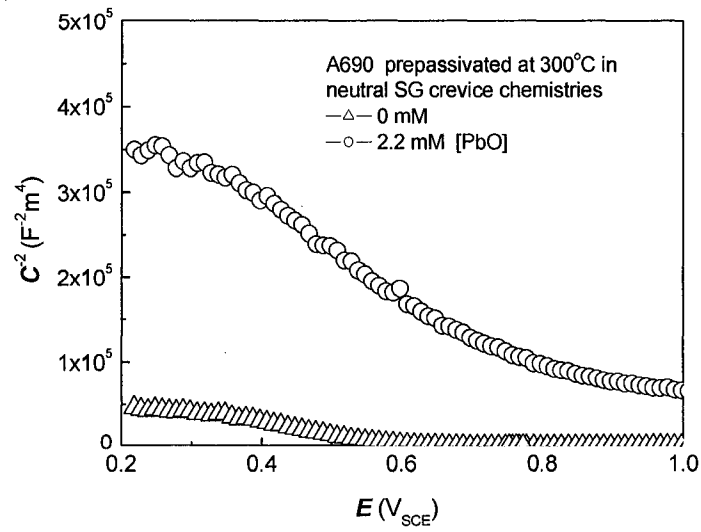


Figure 4-21 Mott-Schottky plots of Alloy 690 prepassivated in neutral SG crevice chemistry with and without Pb at 300°C.

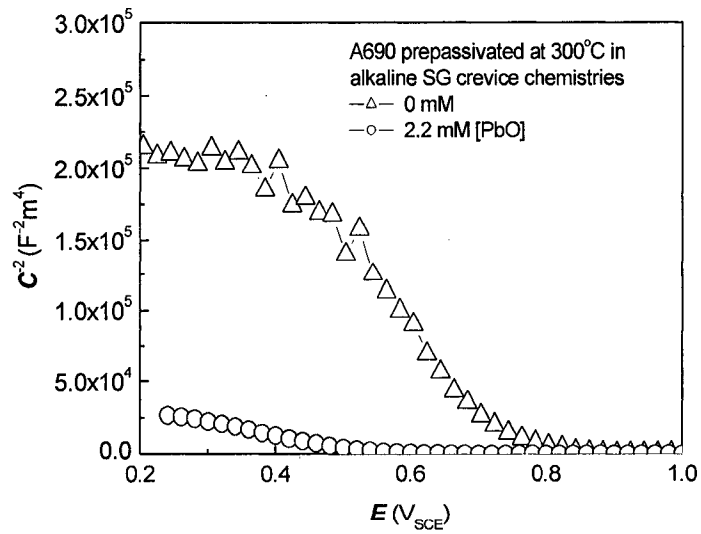


Figure 4-22 Mott-Schottky plots of Alloy 690 prepassivated in alkaline SG crevice chemistry with and without Pb at 300°C.

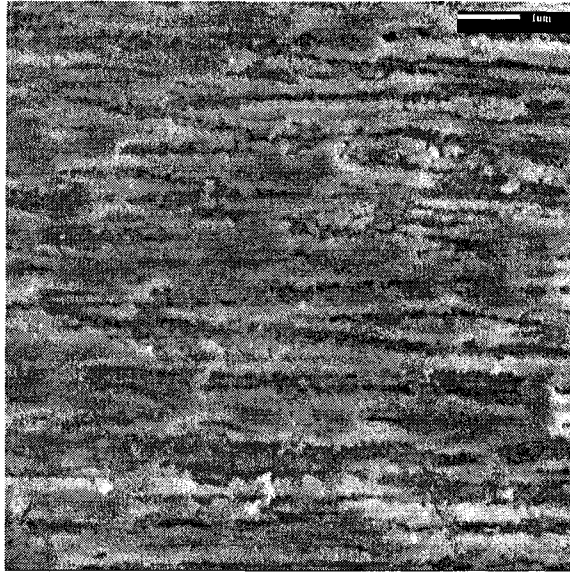
4.2 Surface analysis of Alloy 690 in lead-containing environments

4.2.1 Effect of lead on the surface morphology of passive films

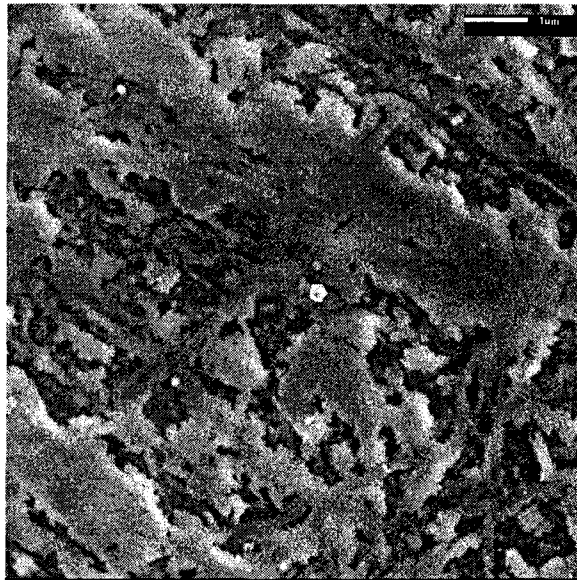
Figure 4-23 shows the morphologies of passive films formed on Alloy 690 in acid crevice chemistries. The samples were immersed in solutions with and without lead at 300°C for 24 hours, respectively. Both films are rough except that the prepassivation in lead-contaminated chemistry gives rise to a coarser morphology. In Figure 4-24, when the samples are prepassivated in the neutral lead-free and lead-contaminated chemistries, a fine crystalline-like structure has been observed for both samples. The only difference is that in the solution with lead, there are some precipitated particles scattered on the sample surface. It suggests that the impact of lead on the morphology is still limited. When the alloy was prepassivated in high pH solutions, noticeable differences in the morphology is observed. There is a crystal-like outer layer for the sample prepared in the alkaline solution without lead, as shown in Figure 4-25. With the addition of lead, a needle-like external layer covers the surface, indicating a significant modification of the morphology by lead. Comparing the film morphologies illustrated in Figure 4-23, 4-24 and 4-25, it can be seen that the influence of lead impurities is more evident if the material is exposed to the alkaline crevice environment.

4.2.2 Effect of lead on the composition and structure of passive films

The composition-depth profiles of Alloy 690 prepassivated in acidic crevice chemistries with and without lead at 300°C are presented in Figure 4-26 and 4-27, respectively. Experimental results show there is a double layer structure for passive films formed in both conditions. The outer layer is enriched with Cr and depleted with Fe and Ni. This observation is in line with the electrochemical measurement, which indicates Fe and Ni suffer active dissolution. In the inner layer Ni concentration steadily increases and the Cr content gradually decreases to nominal percentage. In this condition, it seems the ingress of lead does not change the film structure and composition distribution.

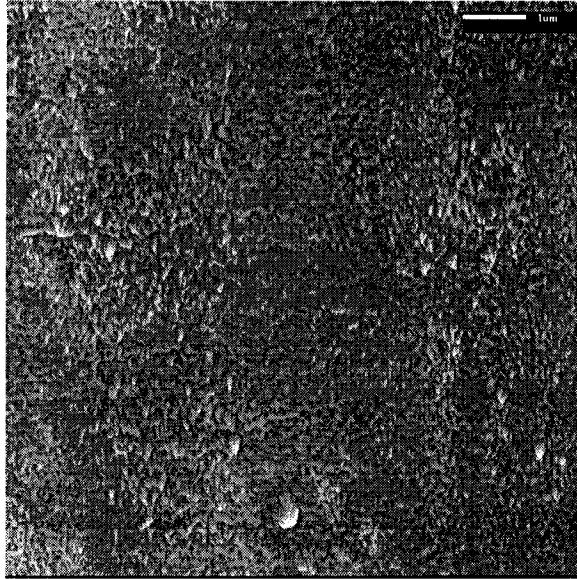


(a)

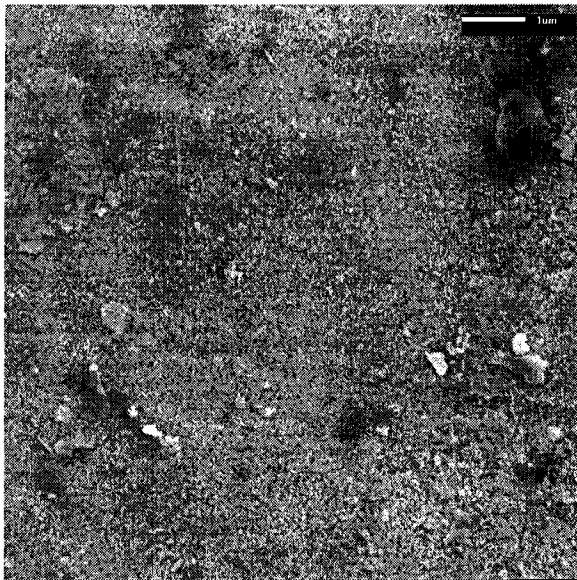


(b)

Figure 4-23 SEM images of passive films formed on Alloy 690 in acidic conditions. The samples were immersed in neutral SG crevice solutions (a) without PbO (b) with 2.2 mM PbO at 300°C for 24 hours.

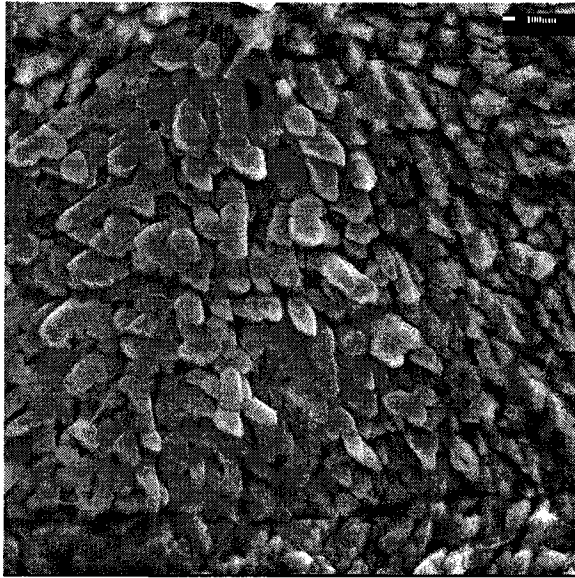


(a)

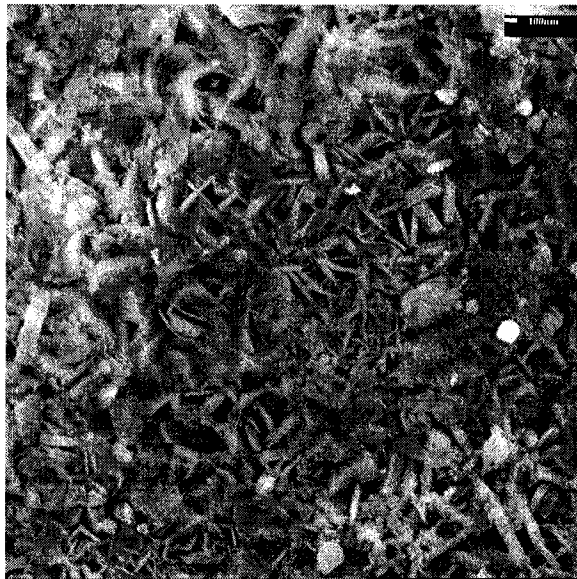


(b)

Figure 4-24 SEM images of passive films formed on Alloy 690 in neutral conditions. The samples were immersed in neutral SG crevice solutions (a) without PbO (b) with 2.2 mM PbO at 300°C for 24 hours.



(a)



(b)

Figure 4-25 SEM images of passive films formed on Alloy 690 in alkaline conditions. The samples were immersed in neutral SG crevice solutions (a) without PbO (b) with 2.2 mM PbO at 300°C for 24 hours.

When Alloy 690 was prepassivated in neutral crevice chemistries at 300°C, it is found lead substantially modifies the Ni depth profile but has no influence on Cr and Fe, as indicated in Figure 4-28 and 4-29. The content of Ni at the outermost layer drops from about 10% to 1% with lead incorporation, suggesting there exists a Pb-enhanced dissolution of Ni in the neutral condition. Comparing Figure 4-26 with 4-27, the double layer structure has been obscured in the lead-free chemistry and no chromium enrichment can be observed.

In the case of alkaline condition, the impact of lead on the composition and structure of the film is significant. The passive film formed in the lead-free solution also comprises a duplex layer structure, as shown in Figure 4-30. The external layer is enriched with Cr but depleted with Fe and Ni. The inner layer is a Cr-depleted layer, characterized with a sharp increment of Fe as a result of the mass balance. Chromium itself is not stable in a high pH environment from a thermodynamic point of view. This phenomenon was also reported in other work (Staeble 2003a, 2004b). The accumulation of chromium at the outermost layer may be due to the formation of spinel oxide, which is a function of pH, chemistry, temperature. However, in alkaline crevice chemistry with lead the Cr content in the inner layer has been raised significantly so that the double layer structure has been completely erased.

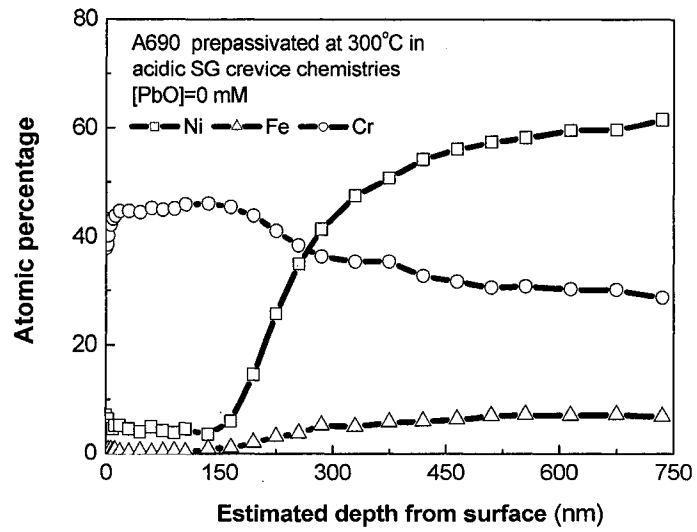


Figure 4-26 Composition-depth profile for the passive film on Alloy 690 prepassivated at 300°C in acidic SG crevice chemistry free of lead.

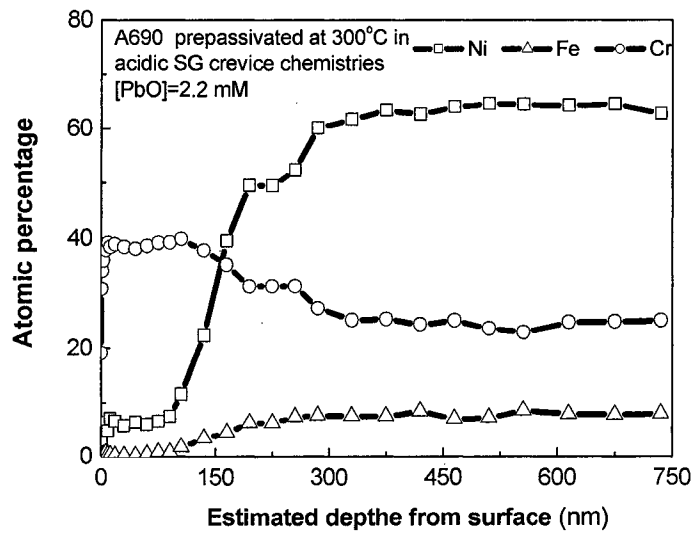


Figure 4-27 Composition-depth profile for the passive film on Alloy 690 prepassivated at 300°C in acidic SG crevice chemistry with lead contamination.

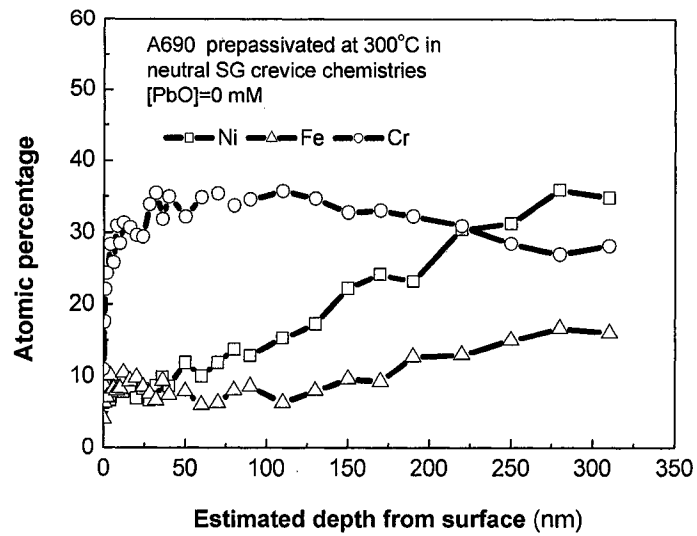


Figure 4-28 Composition-depth profile for the passive film on Alloy 690 passivated at 300°C in the neutral SG crevice chemistry free of lead contamination.

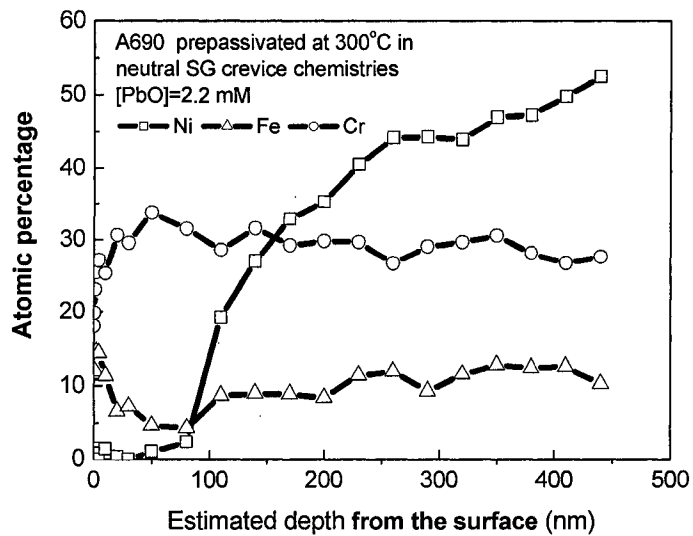


Figure 4-29 Composition-depth profile for the passive film on Alloy 690 passivated at 300°C in the neutral SG crevice chemistry with 2.2mMPbO.

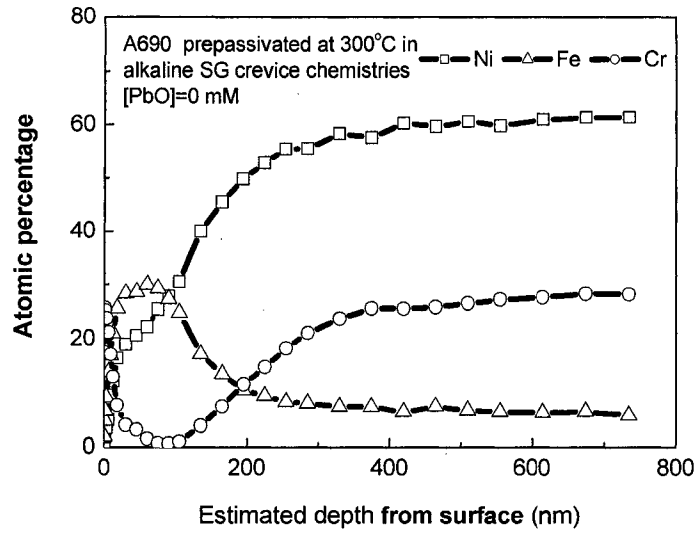


Figure 4-30 Composition-depth profile for the passive film on Alloy 690 prepassivated at 300°C in alkaline SG crevice chemistry free of lead contamination.

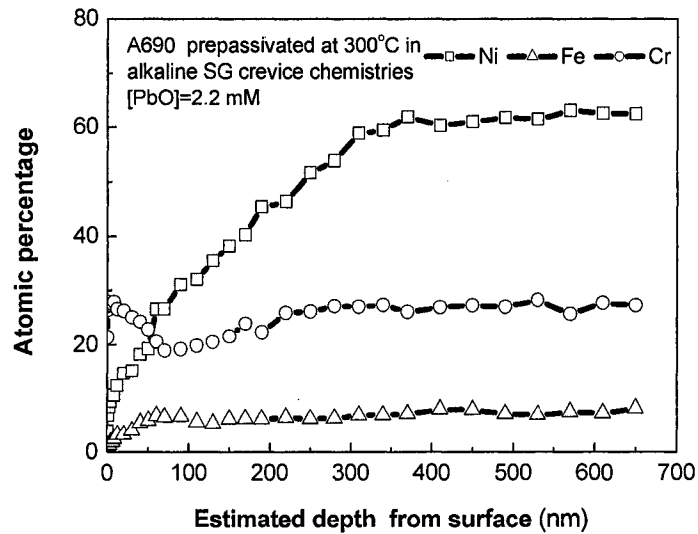


Figure 4-31 Composition-depth profile for the passive film on Alloy 690 prepassivated at 300°C in alkaline SG crevice chemistries with 2.2mM PbO.

4.2.3 Effect of lead on the thickness of passive films

To evaluate the protective quality of the passive film, it is important to depict the thickness of the oxide film. The thicknesses of passive films usually can be estimated according to 50% oxygen content by atomic percentage. As shown in Figure 4-32, lead decreases the film thickness in acidic and neutral chemistries. Especially in acidic condition, the reduction of passivation thickness is up to 50%. However, the impact of lead on the film thickness in alkaline chemistry is opposite; the film is slightly thicker with a 9% increment. Naturally, the passive film is not only a physical layer to separate the metal from the electrolyte, but also affects the mass transport rate and the distribution of the electronic field in the film (Chao et al. 1981). Similar experimental observations were reported by analyzing the effect of lead on the film depth of Alloy 600 and 690 in solutions with pH 10 at 90°C (Hwang et al. 2002). A significant increase of the film depth was detected for both materials, and it ascribed to the detrimental effect of lead. In the pH range of 3 to 7 at 280°C, it was also pointed out that lead decreased the film thickness of Alloy 600 in HCl solution (Sakai et al. 1992a). Actually, the passive film thickness is not determined only by one environmental or metallurgical factor. Although no interpretation of this lead effect is available to date, the modification of film thickness by lead can't be neglected in the investigation.

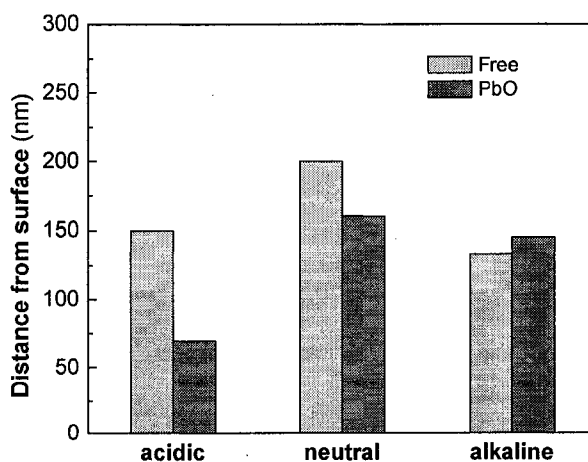


Figure 4-32 Passive film thickness on Alloy 690 obtained at 300°C in different crevice chemistries.

4.2.4 Distribution of lead in the passive films

Figure 4-33 shows the ingress of lead in the passive films obtained in different SG crevice chemistries at 300°C. It can be seen that lead can enter the passive film in all the testing conditions, but the lead content varies with the pH value. The neutral chemistry gives rise to the highest lead concentration in the film, while the ingress of lead in the acidic chemistry is the lowest. This result implies the incorporation of lead in the passive film also depends on environmental conditions. A widely accepted evidence of PbSCC is that lead can be detected throughout the crack, but few investigations address the feature of lead distribution in the surface film. Although anodic dissolution rate of Alloy 690 is higher at 300°C in SG alkaline solution than that in neutral solutions (Lu 2005), the maximum concentration of lead in the oxide film is six times lower than that in neutral chemistry. This result suggests the degradation of passive films is not solely determined by the lead concentration in the electrolyte or the lead content in the passive film. The decrease of corrosion resistance results from the interaction of lead and possibly oxides in the passive film.

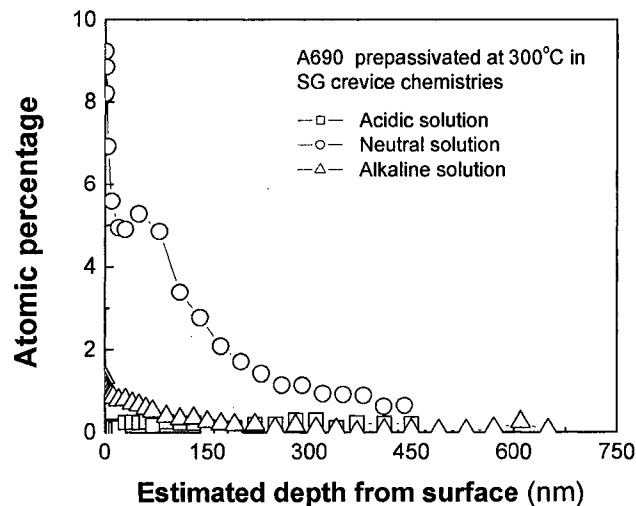


Figure 4-33 Depth profiles of Pb in the passive films on Alloy 690 prepassivated at 300°C in different pH conditions.

4.2.5 Effect of lead on the chemical state of oxygen in the passive film

XPS high resolution spectra can provide information about the chemical state of elements by identifying the shift of binding energy. There are generally three types of bonds in passive films, which are O-M, OH-M, H₂O-M (Okamoto et al. 1978). Accordingly, the O 1s signal is not a single peak. The curve fitting theoretically shows three components at 530~531 eV, 531~532 eV and 532~533 eV (Moulder et al. 1992), which corresponds to the binding energy of oxygen in M-O, M-OH and H₂O-M bonds, respectively. The quantitative evaluation of O²⁻ and OH⁻ is based on the integrated intensities (peak areas) determined from curve fitting of the detailed XPS spectra.

In Figures 4-34 through 4-36, it can be seen that the lead effect on the OH⁻ content in the film strongly depends on the pH value of testing solutions. Lead shows little contribution, if any, to the ratio of OH⁻ and O²⁻ in acidic condition, but significantly increases this value in neutral and alkaline conditions, implying a substantial increase of M-OH bonds in the film in the higher pH range.

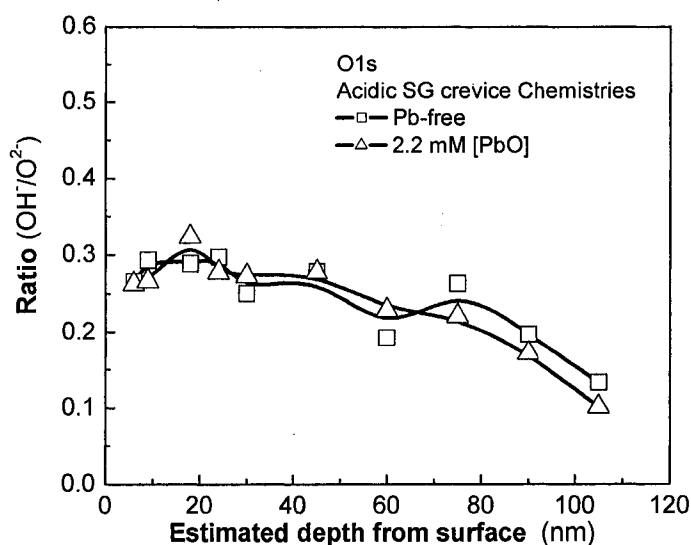


Figure 4-34 Estimated distribution of OH⁻ and O²⁻ in the passive film obtained in acidic crevice chemistries at 300°C with and without lead.

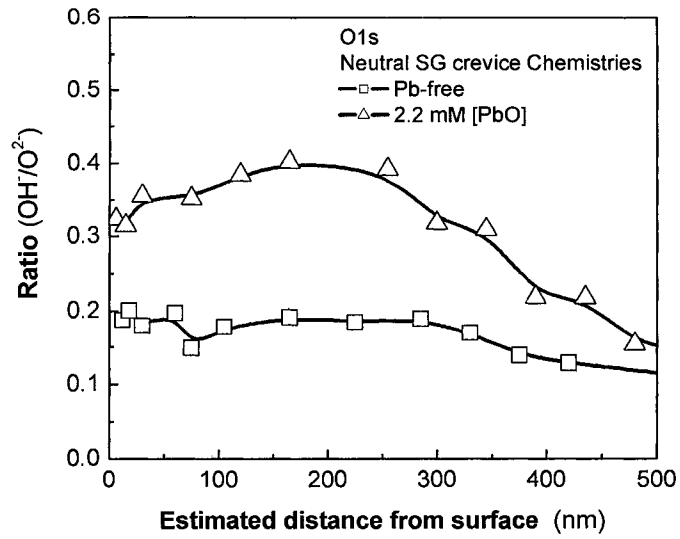


Figure 4-35 Estimated distribution of OH⁻ and O²⁻ in the passive film obtained in neutral crevice chemistries at 300°C with and without lead.

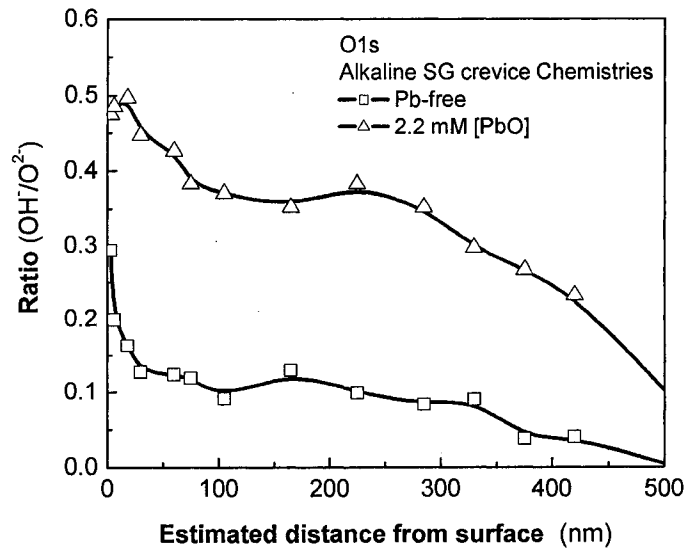


Figure 4-36 Estimated distribution of OH⁻ and O²⁻ in the passive film obtained in alkaline crevice chemistries at 300°C with and without lead.

At the early stage of oxidation on nickel alloys there is an ultra-thin oxide layer covered by a hydroxide layer. The growth of the oxide layer is by consumption of the outer layer (Machet et al. 2004). In the Ni-Cr-Fe system, the aging process will promote the development of a crystalline inner layer, which contains spinel oxide (Machet et al. 2002). It has been suggested that a crystalline passive film possesses higher resistance to passivity breakdown and pitting corrosion due to a high degree of dehydration (Marcus and Maurice, 2001). According to Okamoto et al., H₂O-M is the most active bond while the M-O bond is the most stable one (Okamoto et al. 1978). Therefore, the dehydration reaction in the film plays an important role on the passivity of nickel alloys. The higher dehydration degree the passive film achieves, the lower corrosion susceptibility it obtains. In Figure 4-37, it can be seen that lead significantly retards the completion of dehydration at high pH range. This deleterious effect may lead to instability of the passive film and increasing SCC susceptibility.

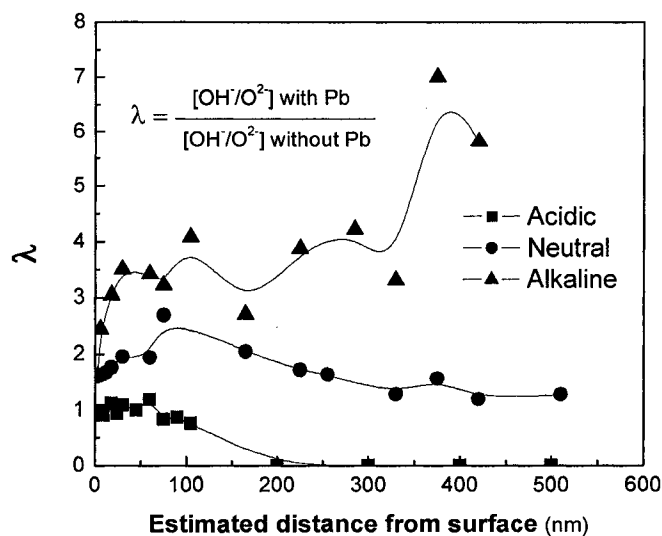
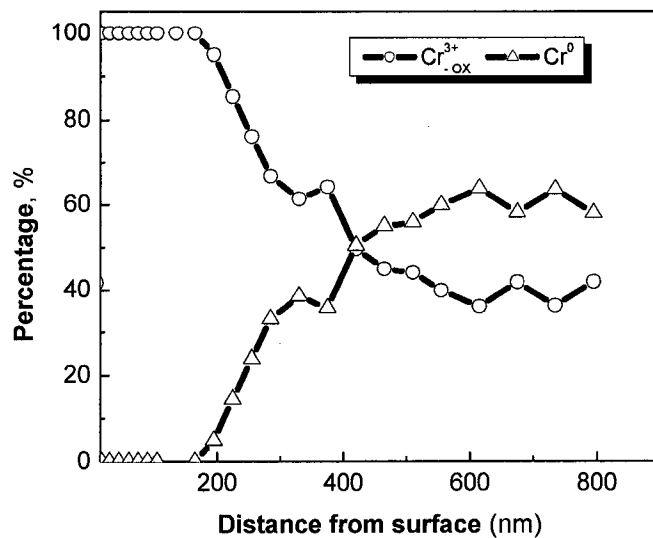


Figure 4-37 Effect of lead on the dehydration degree of passive films in different pH values.

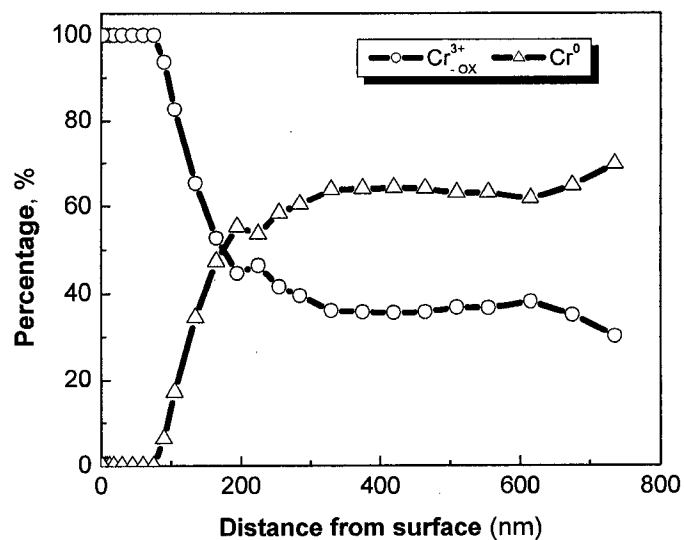
4.2.6 Effect of lead on the chemical state of chromium in the passive film

The effect of lead on the chemical state of chromium can also be identified by the same method. Cr 2p_{3/2} core level generally can be decomposed into three contributions, a hydroxide one, an oxide one and a metallic one with binding energies located at 577.4±0.5 eV, 576.0±0.5 eV, 574.0 ±0.1 eV (Dutta et al. 2002, Carmezim et al. 2005, Moulder et al. 1992). In the films obtained in acidic solutions, no hydroxide can be detected regardless of the presence of lead, as shown in Figure 4-38. The impact of lead is not pronounced at this pH value. Under neutral condition, there is a steady increase of metallic chromium in the film by lead as presented in Figure 4-39, but no hydroxide can be found. In Figure 4-40, a large amount of hydroxide appears in the film obtained in alkaline solutions. With the presence of lead, the hydroxide concentration is substantially increased.

Photoelectrochemical investigation reveals that chromium compounds in the film possess different band gap energies, which are $E_{g(\text{Cr}(\text{OH})_3)} \approx 2.4$ eV, $E_{g(\text{Cr}(\text{OOH}))} \approx 3.1$ eV and $E_{g(\text{Cr}_2\text{O}_3)} \approx 3.5$ eV (Schmuki et al. 1993). It can be seen the band gap energy increases with increasing degree of dehydration. A passive film with higher band gap energy basically contains fewer structural defects, thus possesses higher corrosion resistance. Therefore, it has been suggested that the stability of passive films on stainless steels can be evaluated by their band gap energies (Schmuki et al. 1992). In other words, Cr₂O₃ may naturally offer better corrosion protection than Cr(OOH) and Cr(OH)₃.

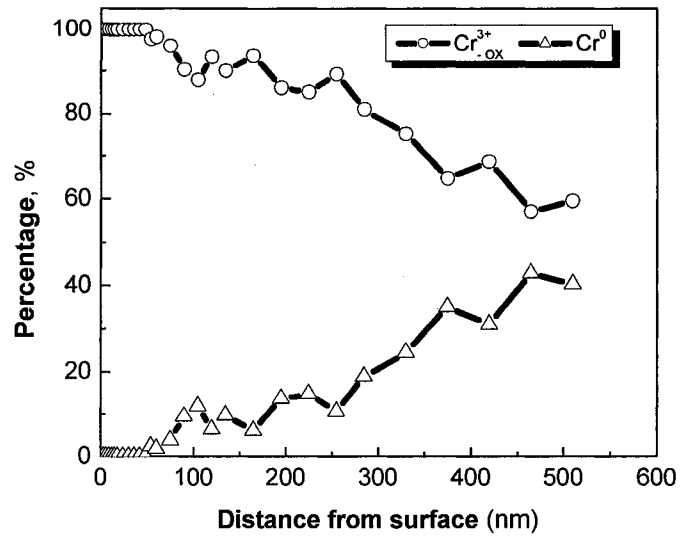


(a)

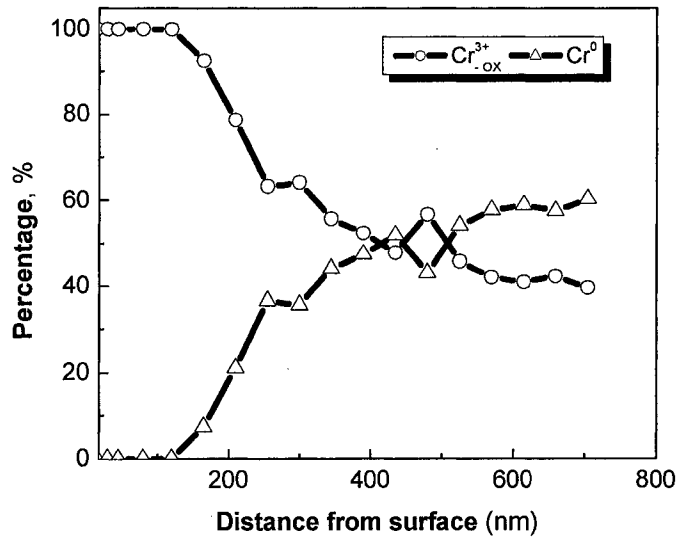


(b)

Figure 4-38 Decomposition of XPS Cr 2p_{3/2} spectra for samples prepassivated in acidic chemistry at 300°C (a) without and (b) with lead.

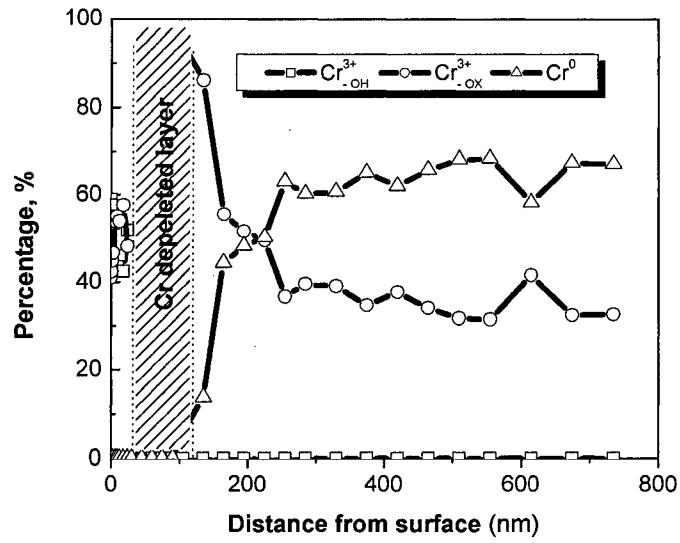


(a)

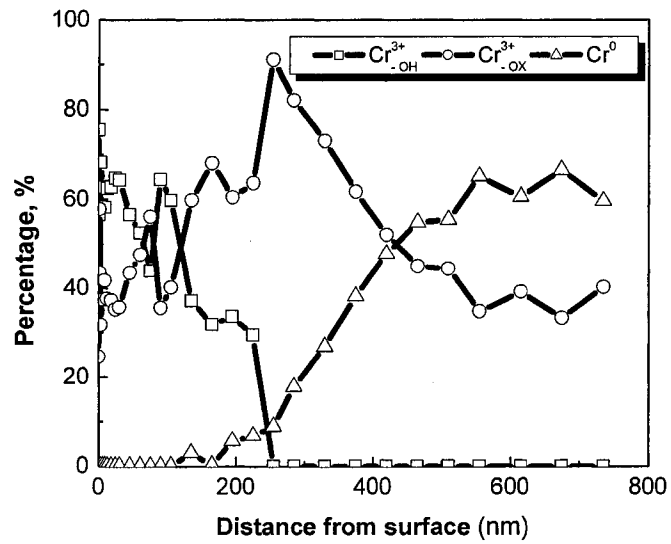


(b)

Figure 4-39 Decomposition of XPS Cr 2p_{3/2} spectra for samples prepassivated in neutral chemistry at 300°C (a) without and (b) with lead.



(a)



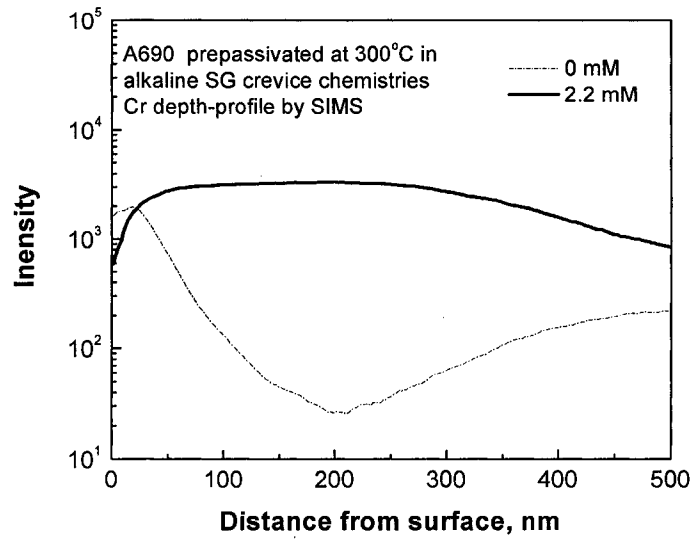
(b)

Figure 4-40 Decomposition of XPS Cr 2p_{3/2} spectra for samples prepassivated in alkaline chemistry at 300°C (a) without and (b) with lead.

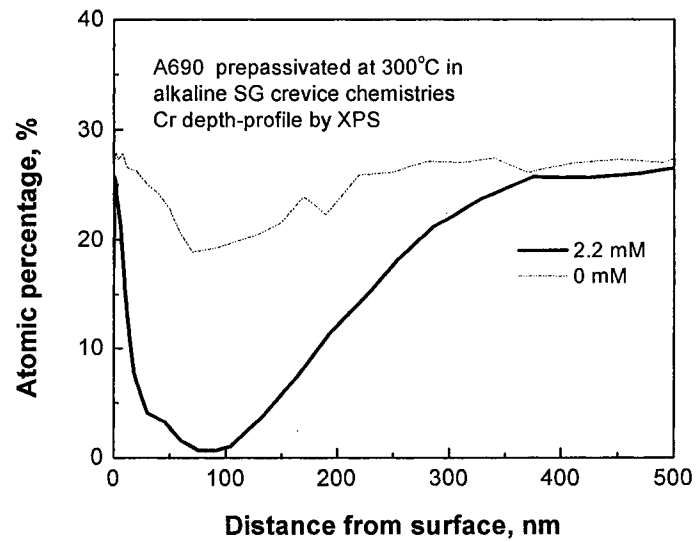
4.2.7 SIMS analysis

In order to verify the XPS results, composition profiles of Alloy 690 samples were further analyzed by the SIMS technique. In the examination, only samples prepassivated in alkaline solutions were focused because of the significant effect of lead under this condition. From Figure 4-41, it can be seen the results of SIMS and XPS analysis are consistent with each other. Both Figure 4-41(a) and 4-41(b) indicate lead decreases chromium concentration in the surface film in alkaline solution. Figure 4-42 further illustrate SIMS profiles of hydroxide and hydrogen in passive films obtained in alkaline solutions at 300°C, in which both species contents are increased by lead.

It is worthy to note that the increasing content of hydroxide in the lead-containing environment is associated with an increase of hydrogen. Hydrogen is also considered to play an important role in the occurrence of SCC for nickel alloys at elevated temperature and passive film formation (Takumi et al. 2003). Literature review shows that extensive studies have been carried out to investigate effects of hydrogen on the passivity of pure iron, steels (Yu et al. 2001, 2003; Li et al. 2003) and stainless steels (Yang et al. 2003). It has been found that hydrogen not only increases corrosion rate, but also decreases breakdown potential for those materials (Zeng et al. 2004). Hydrogen is a contributor to increase the $\text{OH}^-/\text{O}^{2-}$ ratio and donor density in the passive film. In a chloride solution, halide ions adsorbed on the surface can easily migrate into the surface film by substituting hydroxyl ions. As a consequence, the dissolution of metals is enhanced by the formation of soluble chloride-metal species (Yu et al. 2001). Further investigation is necessary to clarify the role of hydrogen in SCC of nickel alloys tubing materials.

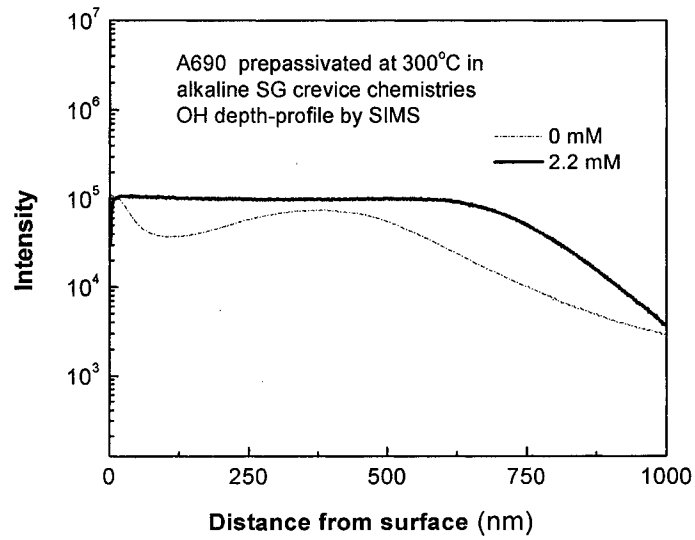


(a)

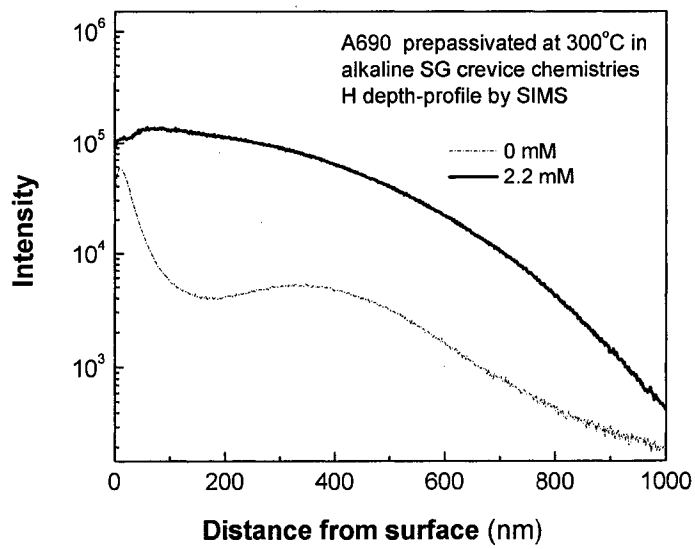


(b)

Figure 4-41 Composition profile of Cr in alkaline solution (a) by SIMS and (b) by XPS



(a)

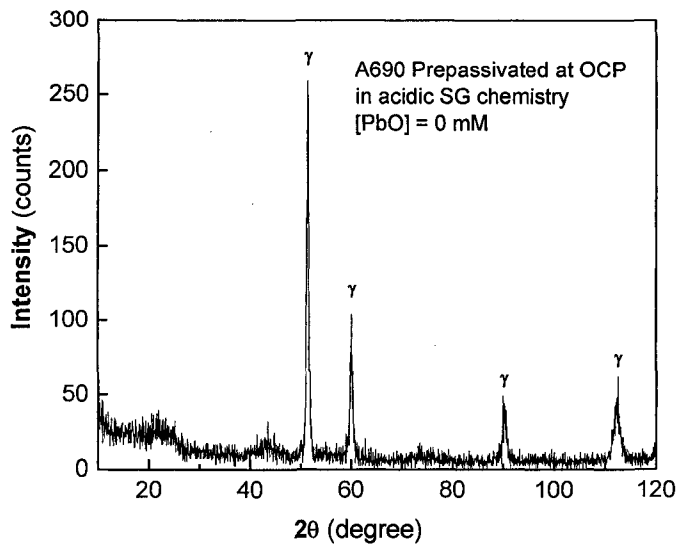


(b)

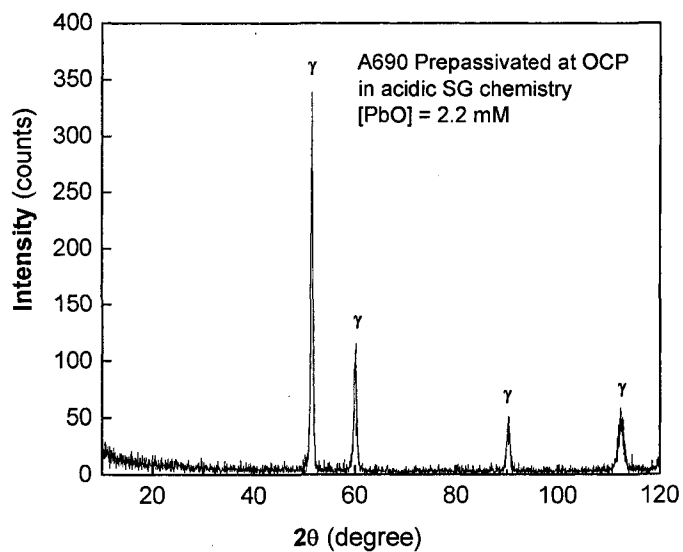
Figure 4-42 Distribution profiles of OH and H in samples immersed in alkaline solution at 300°C (a) with lead (b) without lead.

4.2.8 XRD analysis

At high temperature, aging of a passive film will lead to the formation of spinel oxides on nickel alloys. To identify the influence of lead on the crystalline structure on the alloy surface, low angle XRD examination was carried out for samples prepassivated at high temperature conditions. In acidic condition, as shown in Figure 4-43, the ingress of lead has no impact on the structure of passive films on Alloy 690. The peaks of γ phase reflect signals excited from the substrate. No oriented structure is detected in the passive film regardless of the absence of lead. This is consistent with the visible appearances of acidic samples in Figure 4-23. In neutral condition, crystalline NiCr_2O_4 is observed in the passive film obtained in lead-free solution in addition to the substrate peaks, as indicated in Figure 4-44. However, the presence of lead eliminates this phase and it seems some amorphous structure is generated in the film. In the case of alkaline condition, spinel structure clearly appears in the passive film passivated in the solution without lead as presented in Figure 4-45, whereas lead impurities completely inhibit the formation of the bi-metal oxides in the same chemistry. Comparing the effect of lead at different pH values, it can be seen that lead strongly prevents the formation of spinel oxides in the high pH range. This pronounced and detrimental effect is not evident at low pH range, because no spinel can be found in acidic solutions. It is well acknowledged that the production of crystalline oxides in a passive film is highly dependent on the dehydration reaction during the aging process. Therefore, the inhabitation of crystallization by lead is naturally a result of retarded dehydration in the passive film. Taking into account the increasing chromium and hydroxide contents in the passive film in alkaline solution by lead, it implicates that in a lead-containing environment the instability of the passive film on Alloy 690 results from the detrimental effect of lead. The efficient use of chromium in the material is drastically interrupted by lead impurities, accompanied by fundamentally modification of structural, ionic and electronic properties of the passive film.

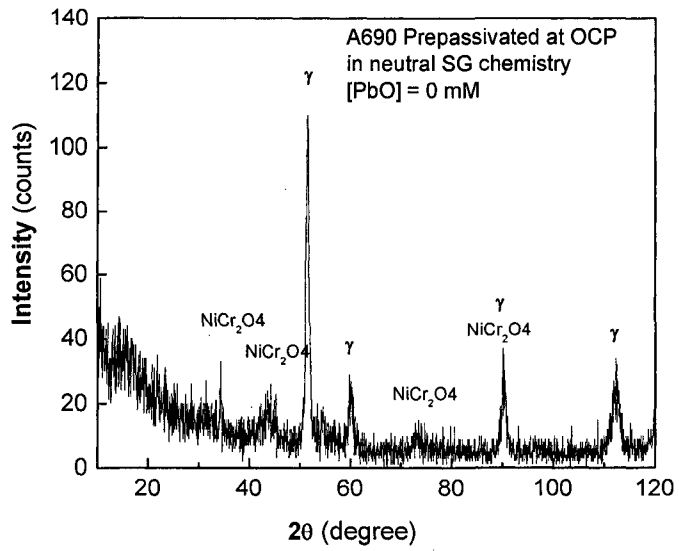


(a)

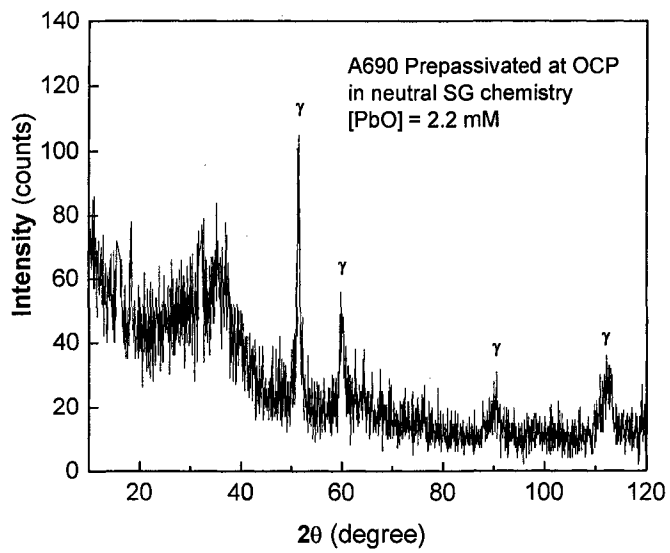


(b)

Figure 4-43 XRD patterns of samples prepassivated in acidic chemistry at 300°C (a) without and (b) with lead.

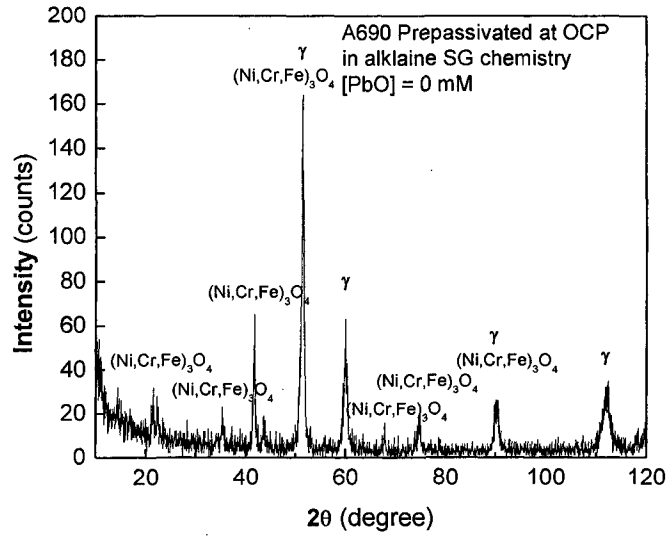


(a)

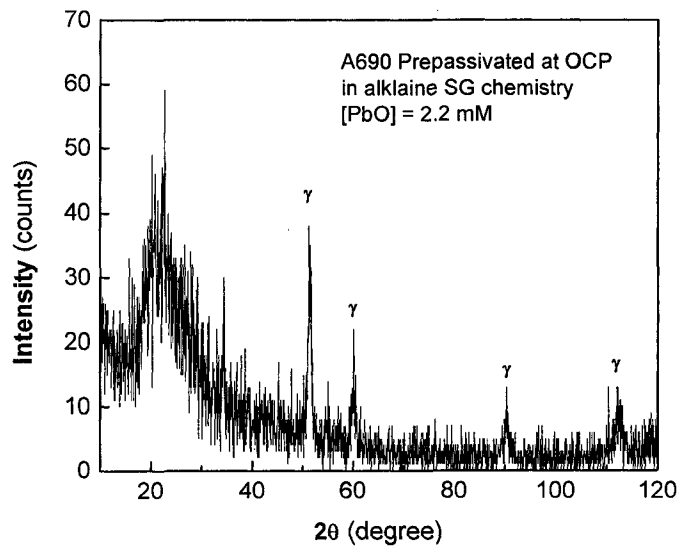


(b)

Figure 4-44 XRD patterns of samples prepassivated in neutral chemistry at 300°C (a) without and (b) with lead.



(a)



(b)

Figure 4-45 XRD patterns of samples prepassivated in alkaline chemistry at 300°C (a) without and (b) with lead.

4.3 Effect of lead on the mechano-chemical properties of passive films

The initiation and propagation of SCC is related to the rupture of passive films on metals which leads to the exposure of a bare metal surface to the corrosive surrounding. As a consequence, a current transient is often observed in corrosion monitoring when the bare metal surface is exposed to the aggressive environment. The advance of cracks is essentially a competition between the anodic dissolution rate and the repassivation rate of metals. Scratch test is a common technique used to study repassivation kinetics of metals in a corrosive environment. However, it is impossible for this method to reflect the mechanical integrity of the passive film. In recent years, nanoindentation has become a widely applied technique to evaluate mechanical response of thin films and coatings with a thickness range from nanometer to micrometer. Literature review shows there is no report to date concerning mechanical properties for the surface film on nickel-based alloys. Therefore, it is of great significance to investigate the effect of lead on the mechanical response of the oxide film.

The hardness and reduced modulus of Alloy 690 samples prepassivated in acidic SG chemistries are shown in Figures 4-46 and 4-47. The peak load is in the range of 500-3000 μN . When penetration depth is small, both values decrease regardless of the presence of lead. This phenomenon is acknowledged as the indent size effect (ISE) (Flick et al. 1993, 1994), which reveals that when indentation depths are less than 5 μm , the hardness of metallic materials decreases with increasing indentation depths. Although data collected from the surface film without Pb ingress are more scattered, it is evident the hardness and reduced modulus of this film are lower with the incorporation of lead. This result indicates a deleterious effect of Pb on the mechanical properties of the surface film. However, the mechanical degradation of surface film by Pb is absent in Figures 4-48 and 4-49, suggesting lead has no influence on the hardness and reduced modulus for Alloy 690 samples prepassivated in neutral SG chemistries. As mentioned before, the susceptibility of PbSCC is the lowest in neutral media. This phenomenon is in line with the nanoindentation observation. In the case of Alloy 690 samples prepassivated in alkaline SG chemistries, Pb significantly modifies mechanical characteristics of the film,

as shown in Figures 4-50 and 4-51. Note that the hardness of this sample free of lead is around 8 GPa. This value is very close to the hardness of spinels, which is 7.8 GPa (CRC handbook, 2006-2007), whereas the hardness and reduced modulus value of the lead-containing film are three times lower. XPS analysis has indicated that high pH values facilitate the modification of passive film by lead. That means lead can more easily be involved in the film formation. However, the mechanical degradation can't be explained solely by the amount of lead in the film, because in neutral solution the highest lead content does not give rise to a big change in the hardness and modulus.

It is also worthy to note that the hardness and reduced modulus of the surface film obtained in neutral solution are the highest among the three test pH values. In addition, the difference of mechanical properties induced by lead is larger in alkaline condition. The decrease of hardness and modulus in alkaline solution is almost three times bigger than that in acidic solution.

The mechanical properties of local sites on a passive film are closely related to the breakdown and repair of the passive layer. It has been pointed out that the hardness difference of a passive titanium surface between in-situ and ex-situ nanoindentation can be attributed to different repassivation rates at the film rupture sites (Seo et al. 2003). High hardness results from high repassivation rate, because the repair of the rupture sites can be accelerated when the repassivation rate is high, especially for anodic oxide film in electrolytes. Although testing the repassivation behavior of nickel alloys in high temperature and deaerated conditions is not possible now, it has been reported that the repassivation rate of Alloy 690 can be reduced by lead in pH 4 and 10 solutions (Ahn et al. 2005). According to the experimental observations, repassivation kinetics and mechanical properties of the film may be essentially important in the fracture process for an anodic oxide film.

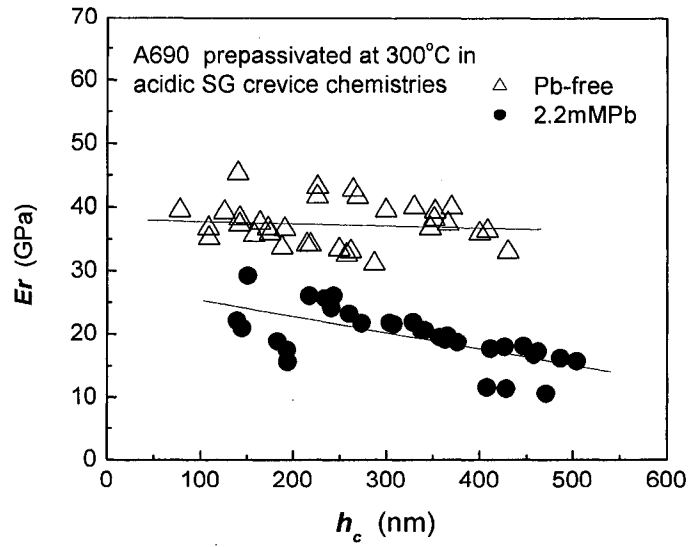


Figure 4-46 Reduced modulus of the passive film on Alloy 690 prepassivated in acidic SG crevice chemistry with and without Pb at 300°C.

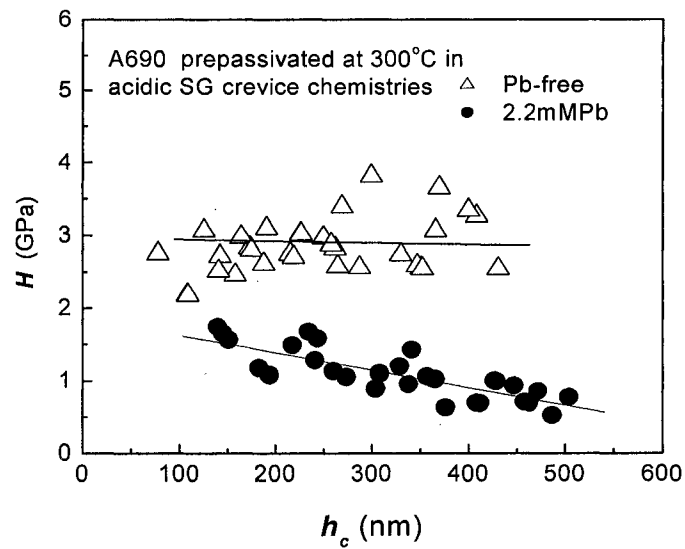


Figure 4-47 Hardness of the passive film on Alloy 690 prepassivated in acidic SG crevice chemistry with and without Pb at 300°C.

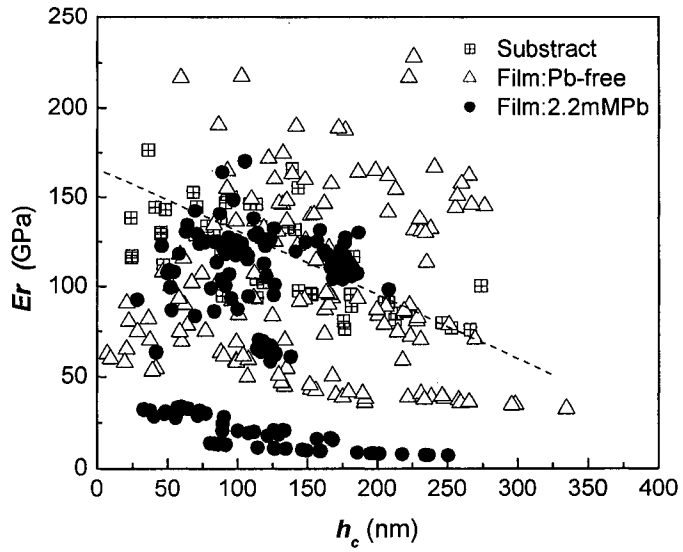


Figure 4-48 Reduced modulus of the passive film on Alloy 690 prepassivated in neutral SG crevice chemistry with and without Pb at 300°C.

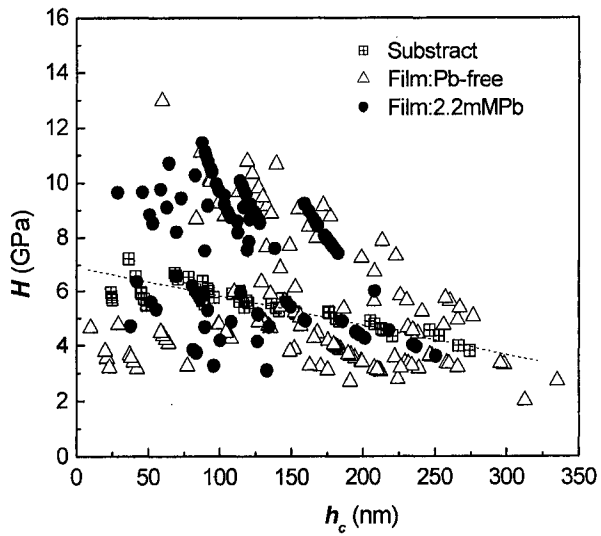


Figure 4-49 Hardness of the passive film on Alloy 690 prepassivated in neutral SG crevice chemistry with and without Pb at 300°C.

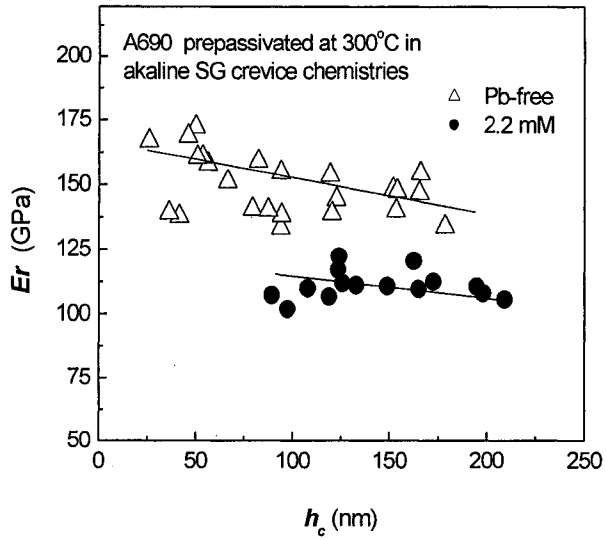


Figure 4-50 Reduced modulus of the passive film on Alloy 690 prepassivated in alkaline SG crevice chemistry with and without Pb at 300°C.

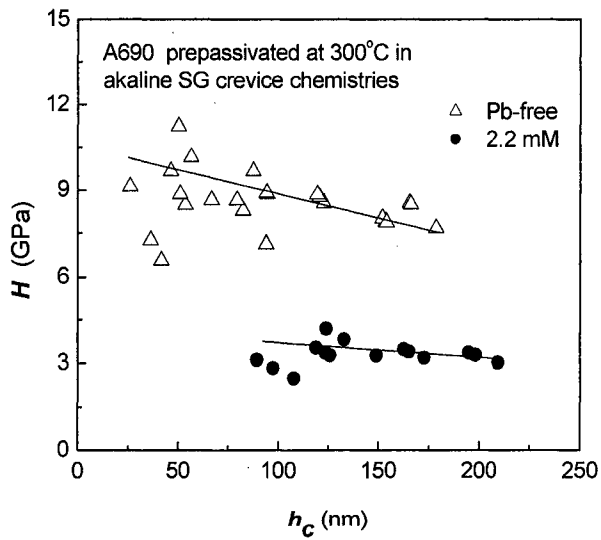


Figure 4-51 Hardness of the passive film on Alloy 690 prepassivated in alkaline SG crevice chemistry with and without Pb at 300°C.

Chapter 5

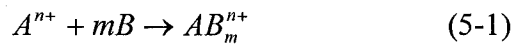
5.1 Mechanism of lead-induced passivity degradation

The increasing SCC susceptibility of nickel-based alloys in lead-containing environments has been acknowledged to be the result of the instability of passive films on the alloys. However, experimental results have revealed that the lead-induced passivity degradation is very complicated. Even though seven parameters (pH, potential, chemistry, concentration, temperature, microstructure and stress) were employed to evaluate the lead-induced SCC and passive film breakdown, there is no comprehensive theoretical explanation available to date.

Since passive films on nickel alloys naturally behave as semiconductors in all testing conditions, the electronic properties of the passive films should be taken into account when investigating the passivity and passive film breakdown of these materials. It has been well established that the passive film on nickel acts as a p-type or p-n heterojunction semiconductor in the electrolyte, in which the major charge carrier is the electron hole (Montemor et al. 2003, 2000). While for n-type semiconductors the major charge carrier is the electron, like the passive film on iron. The charge carrier of different type semiconductors is donated by completely different contributors. In the passive film electrons mainly come from oxygen vacancies. All oxygen vacancies are the same no matter what metal ions they are combined with. Therefore, it is possible to propose some principles concerning the passivity and breakdown of the n-type passive film. Electron holes are provided by cation vacancies in the passive film. For alloys, different oxides may be involved in the film formation depending on the testing conditions. Each metal ion possesses different electronic characteristics, and plays a different role in the alteration of charge carrier density. When a Fe^{3+} ion substitutes the position of a Ni^{2+} ion in the lattice, the result is that one electron is missing. The dopant atom is able to accept an electron nearby, thus an electron hole can be generated. Whereas a Pb^{2+} ion occupies the lattice site of a Cr^{3+} ion, the opposite event will take place. As a consequence, it is hard to yield a general theoretical model to interpret the passivity degradation of p-type

passive films. The following discussion is based on the present experimental observations and is the preliminary step to obtain a better understanding of the instability of passive films in a lead-contaminated environment.

It has been proposed that the effect of metal ions on the stability of passive films is closely related to their chemical hardness (Zhang et al. 2005). According to the Lewis rule of acids and bases, metal ions are acids and act as electron acceptors, while ligands are bases and behave as electron donors (Lewis 1923, 1938). The reaction between acids and bases leads to the formation of metal complexes.



Acids and bases can be further quantitatively characterized by their hardness and soft nature based on the Hard and Soft Acid and Base (HSAB) concept. For metal ions, the chemical hardness x can be expressed as

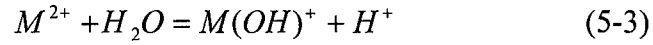
$$x = \frac{\left[x_m^0 + (\sum I_n)^{1/2} \right]^2}{10} \quad (5-2)$$

where x_m^0 is electronegativity of the metal atom, and I_n is ionization potential from the neutral metal atom to the given oxidized state, n . The stability of an A:B combination essentially depends on the intrinsic strength of A and B. In HSAB theory, it is assumed a hard-hard bond or a soft-soft one will generate a higher stabilization than a hard-soft bond.

At the beginning of passivation, the surface film is hydrated oxides with a gel-like structure. There are basically three types of oxygen bridges, O-M-O, OH-M-OH and H₂O-M-OH₂, in the passive film with different reactive capabilities as shown in Figure 2-9 (Marcus et al. 2001). Dehydration in the film, i.e. the loss of bound water, will reduce the content of OH-M-OH and H₂O-M-OH₂ bonds, and finally lead to the formation of

stable oxides in the surface film. If the dehydration reactions are blocked in an aging process, protective properties of the passive film can be seriously damaged because the transformation to the perfect oxide is retarded.

The first step of the deprotonation process can be expressed as Reaction 5-3. The equilibrium constant, K , of this reaction can be calculated according to Equation 5-4 (Zhang et al. 2005).



$$K = \frac{[M(OH)^+] \cdot [H^+]}{[M^{2+}]} = \frac{[M(OH)^+] \cdot K_w}{[M^{2+}] \cdot [OH^-]} = \frac{K_w}{K_{instab}} \quad (5-4)$$

where K_w and K_{instab} are the ion product of water and the instability constant of MOH^+ , respectively.



$$K_w = [H^+] \cdot [OH^-] \quad (5-6)$$



$$K_{instab} = \frac{[M^{2+}] \cdot [OH^-]}{[M(OH)^+]} \quad (5-8)$$

In the Ni-Cr-Fe-Pb system, the hardness sequence is $Fe^{3+} > Cr^{3+} > Ni^{2+} > Fe^{2+} > Pb^{2+}$ (Misono et al. 1967). Hard metal ions prefer to attract H_2O and OH^- in the passive film, which are classified as hard bases. Experimental evidence shows that the equilibrium constant, K , increases with the cation hardness (Zhang et al. 2005), which indicates that a harder cation can easily replace the proton of the H_2O in the passive film by bridging

the OH^- ions. Based on the hardness sequence, Cr is expected to combine with OH^- or H_2O quickly in a lead-free solution and enhance the repassivation of the alloy. When Pb occupies the vacancies of metal ions in the film, the deprotonation reaction of $\text{M}^{2+} \cdot \text{H}_2\text{O}$ may be inhibited due to the lower affinity of Pb and OH^- , as indicated in Figure 5-1. Pb ions have less capability to attract the electron pair of the oxygen atom in the OH bonds; therefore, it is hard to reduce the binding strength between O-H bonds. Consequently, there will be more HO-M-OH bonds in the passive film in the presence of lead, which is supported by the XPS results showing an increase of the OH/O^{2-} ratio in the passive film by lead at high pH range (Figures 4-34 through 4-36). Furthermore, the detrimental effect of lead is also reflected by an increase in HO-Cr-OH bonds in the passive film formed in alkaline solution, as shown in Figures 4-38 through 4-40. The suppression of dehydration in the lead-contaminated alkaline environment essentially leads to the degradation of the passive film.

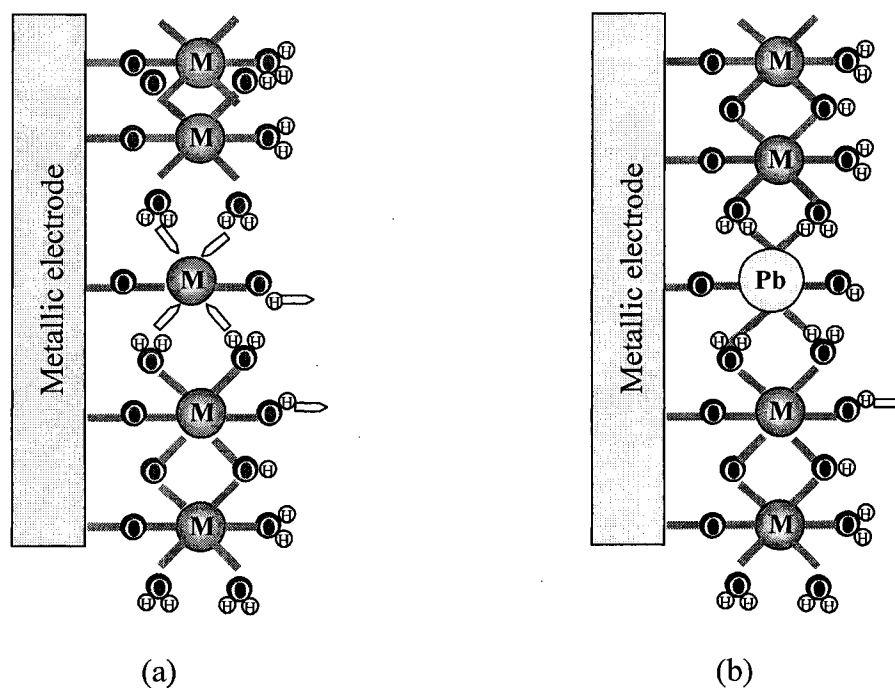
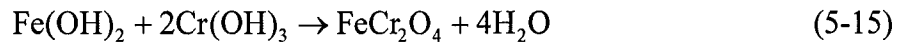
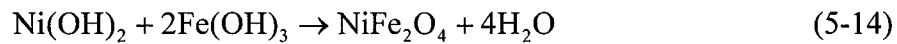
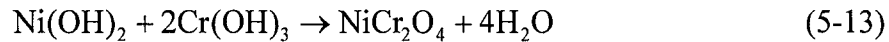


Figure 5-1 The gel-like structure of Pb-doped passive film

The main components in Alloy 690 are nickel, chromium and iron. At the early stage of passivation, these elements may be dissolved in the alkaline electrolyte and the gel-like structure can be generated rapidly. Deprotonation of adsorbed species may occur via the following reactions:



The continuation of further deprotonation eventually leads to an oxide layer on the electrode surface. For Ni-Cr-Fe based alloys, bimetallic oxides with spinel structure can be formed in the dehydration process.



It is well accepted that SCC usually initiates at the defective sites of passive films. A large number of experimental results indicate that, in general, the defect densities decrease in the film with aging time (Craig 1991). For nickel alloys, the dehydration and aging lead to an increase in the spinel oxides. As a consequence, improved SCC resistance can be expected.

In a lead-containing environment, the accumulation of lead at the electrode surface is possible considering the high adsorption capability of lead species. Lead ions can be involved in the formation of a gel-like structure near the alloy surface at the initial stage of passivation. The stability of $[M(OH)]^+$ can also be estimated by the equilibrium constant, K_{const} , of corresponding deprotonation reactions as listed in Table 5-1. Higher

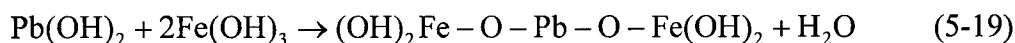
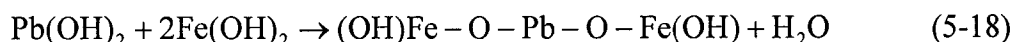
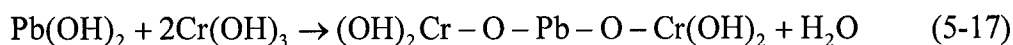
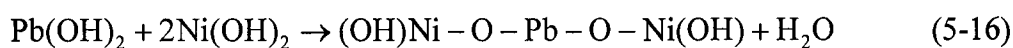
equilibrium constants give rise to less stable hydrated oxides adsorbed at the electrode surface, which means the deprotonation process is easier. Among all the reactions, the equilibrium constant of lead ions is the lowest at 300°C, implying the affinity between lead and OH⁻ is very weak in this system. Deprotonation is inhibited when lead is present in the gel-like mixtures, resulting in increasing anodic dissolution of alloys and the delay of the formation of an oxide film.

Table 5-1 Equilibrium constants for the deprotonation reactions*

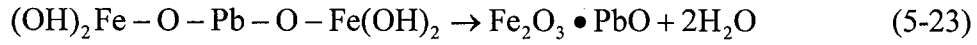
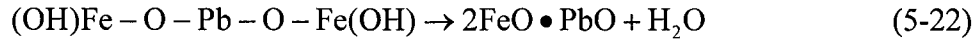
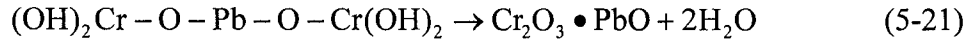
| T (°C) | K_{const} | | | | |
|-----------|--|--|---|---|---|
| | $Fe^{3+} \cdot H_2O \rightarrow [Fe(OH)]^{2+} + H^+$ | $Cr^{3+} \cdot H_2O \rightarrow [Cr(OH)]^{2+} + H^+$ | $Ni^{2+} \cdot H_2O \rightarrow [Ni(OH)]^+ + H^+$ | $Fe^{2+} \cdot H_2O \rightarrow [Fe(OH)]^+ + H^+$ | $Pb^{2+} \cdot H_2O \rightarrow [Pb(OH)]^+ + H^+$ |
| 25 | 6.8×10^{-3} | 9.5×10^{-5} | 1.8×10^{-10} | 4.8×10^{-10} | 6.8×10^{-7} |
| 300 | 2.8×10^1 | 1.3×10^0 | 2.0×10^{-5} | 1.7×10^{-5} | 6.2×10^{-8} |

*Calculated with HSC software

Furthermore, the dehydration of lead-containing hydroxides may gradually evolve into the development of a lead-doped surface film.



Further maturation leads to the accomplishment of a lead-doped oxide film, which may hold different electrochemical and mechano-chemical properties. The detrimental effects of lead have been already demonstrated in electrochemical studies and film investigation in Sections 4.1 and 4.3.



In addition, it is also possible for lead to enter the surface film at the stable state of passivation. At this stage of passivity, the phase transport at the electrolyte/film and film/metal interface reach a balance and can be interpreted by the PDM model (Macdonald, 1992). The introduction of Pb ions in the p-type film can be expressed by the following defect reactions.



It can be seen that Pb^{2+} can occupy the lattice sites of Ni, Cr, and Fe, and decreases the cation vacancy concentration. Theoretically, the electron hole concentration and conductivity of the film will be modified by means of the doping of lead. This phenomenon is shown from Figure 4-20 through Figure 4-22, which manifests as significant changes of charge carrier density with the addition of lead. However, it should be realized the influence of lead is complicated and the amount of lead in the film is very small. It is wise to consider that the degradation of passive films in the lead-containing environment is the synergistic effect of lead and environmental factors such as pH, chemistry and potential.

5.2 Film rupture model of lead-induced SCC

To study the mechanism of lead-induced SCC, the majority of available results are listed below.

- Lead significantly increases anodic dissolution in high pH media.
- Composition and structure of a passive film can be modified by lead, resulting in lower corrosive protection.
- Lead degrades mechanical properties of passive films, except neutral condition.
- Lead decreases the repassivation rate in high temperature water (Ahn et al., 2006).
- Lead does not exert any impact on the pre-formed film.

To date, there is no universally accepted mechanism of PbSCC, but prior studies in similar systems may offer some insight into the occurrence of PbSCC. In a boiling water reactor system (BWR) a film rupture model has been proposed to describe SCC with emphasis on passive film slip and metal dissolution (Ford et al. 1994). Considering the key observations in this work, combined with other publications, it is reasonable to draw an analogy and construct a similar framework of a film/rupture model based on the available experimental evidence.

In the film rupture model, it is assumed the crack tip advances by anodic dissolution while the crack wall is repassivated during this course. The average crack velocity can be calculated by Equation (5-28) (Ford et al. 1994).

$$CGR = \frac{M}{zF\rho} \frac{Q_f}{\varepsilon_f} \dot{\varepsilon}_{ct} \quad (5-28)$$

where M the atomic weight, z the valence of solvated species, F the Faraday's constant, ρ the density of the metal, Q_f the oxidation charge density passed between film rupture events, ε_f fracture ductility of the anodic film, $\dot{\varepsilon}_{ct}$ creep rate at the crack tip.

According to this equation, the advance of cracks is determined by the passivation/anodic dissolution rate, oxide rupture rate and crack tip creep rate. It was found in pressurized water system these parameters are influenced by the alloy/passive film composition. The increase of Cr bulk concentration results in an increase of repassivation rate and the required strain to rupture the oxide; at the same time it reduces the crack tip strain rate. A lower SCC susceptibility has been finally generated by the synergistic effect of these factors (Attanasio et al. 1999). PbSCC, which takes place in a similar condition, may also undergo such a model in caustic environments due to the composition and structure changes of passive films caused by lead incorporation. It is well accepted lead increases corrosion susceptibility under most laboratory testing conditions (Hwang et al. 1997, Sakai et al. 1998, Lu 2005). It has also been reported that a slower repassivation rate was observed in lead-containing alkaline solution (Ahn et al. 2006). A higher magnitude of oxidation charge density, Q_f , thus can be expected. Another strong argument is the nanoindentation result, which indicates clearly a mechanical degradation of the Pb-doped surface film. Other laboratory tests show that mechanical properties of thin films can be properly estimated via nanodentation measurements (Van Vliet et al. 2001) and, obviously, the mechanical properties of corrosion films are highly dependent upon their composition (Rosecrans et al. 2001, Kai et al. 2004).

This model for SCC on Alloy 690 in lead-containing alkaline environments can be interpreted as follows.

- Assume the rupture of the passive film on Alloy 690 can take place under tensile stress.
- In alkaline solutions, a lead complex such as HPbO_2^- is stable and lead species can be adsorbed at the exposed fresh surface.
- Lead ions will migrate into the gel-like hydrated oxide layer and occupy the cation vacancies.
- Lead is involved in the film formation process, resulting in the passivity degradation. The instability of the passive film is reflected by enhanced anodic dissolution and slow repassivation rate. As a consequence, an accelerated crack

growth rate and creep rate can be expected.

- The Pb-doped passive film possesses more sensitive mechanical properties, which increases the probability of localized passive film breakdown.
- This process repeats and eventually leads to premature failure of tubing materials.

Chapter 6

6.1 Conclusions

The objective of this work, as proposed in Chapter 1, is to evaluate the influence of lead on the electrochemical behavior of nickel alloys and obtain a better understanding of the mechanism of PbSCC. Electrochemical experiment results show that lead significantly increases the passive current density of Alloy 690 in alkaline SG crevice solution, but this effect is not very noticeable in acidic solution. For the same solutions, anodic dissolution of pure alloying elements was also analyzed. It indicated that there is an enhanced active dissolution of pure iron with the addition of lead in low pH condition, while the same phenomenon was detected on pure nickel in high pH condition. Anodic polarization measurements reveal that when Alloy 690 was prepassivated in the caustic solution, no difference in the polarization behavior could be monitored irrespective of the presence of lead. Mott-Schottky measurements further show that lead can modify the electronic structure of passive films formed on Alloy 690 depending on the specific testing conditions. Furthermore, by XPS and SIMS analyses, it was found that the hydroxide content in the passive film decreases in lead-containing neutral and caustic media. From XRD examination, the formation of a crystalline structure was observed in neutral to alkaline pH range without lead, but crystalline oxide disappeared in lead-containing solutions. Based on the above experimental results, the main conclusions in this work can be drawn as follows:

- The role of lead in corrosion processes is strongly dependent on the pH value of testing solutions. Detrimental effects of Pb are more significant in caustic environments than in acidic media.
- Selective dissolution of nickel alloys has been observed in simulated SG crevice chemistries. In acidic condition, lead promoted anodic dissolution of iron, while in alkaline condition it enhances anodic dissolution of nickel.
- The detrimental effects of lead seem more obvious when fresh metal surface is exposed. Lead has limited impact on the pre-formed passive film on nickel alloys.

- Mott-Schottky measurements indicate lead can change the electron hole concentration in the passive film, but there is no pH dependence with respect to the semiconductor behavior of the films. The effect of lead on the electronic structure of passive films on nickel alloys should be evaluated with respect to test conditions.
- XPS and SIMS analyses reveal that lead substantially modifies the composition and structure of the passive film. With the presence of lead, nickel depletion in neutral solution and chromium depletion under alkaline condition were detected.
- XRD results reveal that the degree of crystalline structure generated in the surface film increases with the pH value. The presence of lead eliminates the formation of spinel on the alloy surface, which plays a key role in the passivity of nickel alloys.
- When passivated in acidic and alkaline solutions, the mechanical properties of passive films decrease with the presence of lead. However, the differences of hardness and reduced modulus are not evident in neutral condition.
- Passivation degradation of the surface film in alkaline solutions with lead may be attributed to the block of dehydration processes in the film, resulting in lower corrosion resistance, instability of the passive film and high PbSCC susceptibility.
- The presence of lead also increases hydrogen content in the passive film in alkaline solution, which may play an important role in the degradation of passivity.

6.2 Future work

The available experimental evidence shows that PbSCC can be interpreted by the film rupture mode. On the other hand, it is necessary that more in-situ experiments should be conducted at high temperature to investigate the electrochemical and mechanical response of nickel alloys and alloying elements. Film rupture frequency and crack propagation rate in a lead-containing solution can be monitored in an autoclave, which provides a simulated high temperature environment. The equipment has been

successfully set up in the laboratory, and the following experiments can be performed to further study the characteristics and mechanism of PbSCC on nickel-based alloys.

- Investigate in-situ SCC behavior on Alloy 690 in lead-containing solutions at high temperature. By combining the multi-meter monitoring system and electrochemical noise technique, it is possible to monitor the crack growth rate and electrochemical noise caused by film rupture at the same time. This experiment is expected to clarify how lead affects the stability of passive films at high temperature.
- Study semiconductor behavior of pure Ni, Cr and Fe in high temperature environments with lead. The breakdown of a passive film is essentially determined by electronic transport across the film/electrolyte interface. Mott-Schottky measurements can provide information on the electronic structure of passive films on alloys, which is useful in evaluating the role of lead at elevated temperature.
- Assess repassivation rate of tubing materials in simulated SG crevice solutions. This parameter is crucial to evaluate the crack growth rate. The effect of lead on the repassivation process may have a large influence on the propagation of cracks.

References

Ahn S.J., Shankar Rao V., Kwon H.S., Kim U.C., Effects of PbO on the repassivation kinetics of Alloy 690, Corrosion science, Vol. 48, 2006, 1137 - 1153

Anderson T.L., Fracture mechanics: fundamental and applications, 3rd edition, 2005

Beverkog B., Puigdomenech I., Pourbaix diagrams for the ternary system of Iron-Chromium-Nickel, Corrosion, Vol. 55, No. 1, 1999, 1077-1087

Brundle C.R., Evans C.A. Jr., Wilson, S, Encyclopedia of Materials Characterization - Surfaces, Interfaces, Thin Films, 1992

Carmezim M.J., Simoes A.M., Momntemor M.F., Da Cunha Belo M., Capacitance behavior of passive films on ferritic and austenitic stainless steel, Corrosion science, vol. 47, 2005, 581-591

Castano-Marin M.L., Gomez-Briceno D., Hernandez-Arroyo F., Influence of lead contamination on the stress corrosion resistance of nickel alloys, Proc. 6th International Symposium on Environmental Degradation of Materials in Nuclear Power System-Water reactors, 1993, 189-196

Chao C.Y., Lin L.F., Macdonald D.D., A Point Defect Model for anodic passive films, J. Electrochem. Soc., Vol. 128, No. 6, 1981, 1187-1194

Chung K.K., Lim J.K., Moriya S., et al., Lead induced stress corrosion cracking of Alloy 690 in high temperature water, Proc. 7th International Symposium on Environmental Degradation of Materials in Nuclear Power Systems--Water Reactors, August, 1995, 233-244

Chung K.K., Characteristics of lead induced stress corrosion cracking of Alloy 690 in high temperature, NACE International Annual Conference and Exposition, 1996, paper No. 93

Copson H.R., Dean S.W., Corrosion, Vol. 21, 1965, p1

Costa D., Talah H., Marcus P., Interaction of lead with nickel-base alloys 600 and 690, Proc. 6th International Symposium on Environmental Degradation of Materials in Nuclear Power System-Water reactors, 1995, 199-207

Craig B.D., Fundamental aspects of corrosion films in corrosion science (New York, NY: Plenum Press, 1991

CRC Handbook of chemistry and physics, Permittivity (dielectric constant) of inorganic solids, 87th Edition, 2006-2007

Da Cunha Belo M., Hakiki N.E., Ferreira M. G.S., Semiconducting properties of passive films formed on nickel-base alloys type Alloy 690: influence of the alloying elements, Electrochimica Acta Vol. 44, 1999, 2473-2481

Dutta R.S., Lobo A., Purandare R., Kulkarni S.K., Dey G.K., Corrosion of austenitic Alloy 690 under anodic and cathodic potentials, Metallurgical and materials transactions, Vol. 33A, May 2002, 1437-1447

Electric Power in Canada, Natural Resources Canada, 1997

Flick N.A., Hutchinson J.W., A phenomenological theory for strain gradient effects in plasticity, J. Mech. Phys. Solid., Vol. 41, 1993, 1825-1857

Flick N.A., Muller G.A., Ashby M.F., et al., Stresses, deformations and porosities in standard fracture specimens, Acta Metall. Mater, Vol. 42, 1994, 475-487

Ford F.P., Andresen P.L., Corrosion in Nuclear Systems: Environmentally Assisted Cracking in Light Water Reactors, in "Corrosion Mechanisms", Ed. P. Marcus & Ouder, M. Dekker, 1994, 1x501-546

Garcia-Mazario M., Lancha A.M., Hernandez M., et al. Effect of lead on Inconel 600 and Incoloy 800 oxide layers formed in simulated steam generator secondary environments, Nuclear engineering and design, Vol. 167, 1996, 155-167

Goodlet G., Faty S., Cardoso S., et al. The electronic properties of sputtered chromium and iron oxide films, Corrosion science, Vol. 46, 2004, 1479-1499

Harrod D.L., Gold R.E., Jacko R.J., Alloy optimization for PWR steam generator heat-transfer tubing, Journal of the Minerals, Metals and Materials Society, Vol. 53, 2001, 14-17

Helie M., Lambert I., Santarini G., Some consideration about the possible mechanism of lead assisted stress corrosion cracking of steam generator tubing, Proc. 7th International Symposium on Environmental Degradation of Materials in Nuclear Power Systems - Water Reactors, 1995

Helie M., Lead assisted stress corrosion cracking of alloys 600, 690 and 800, Proc. 6th International Symposium on Environmental Degradation of Materials in Nuclear Power Systems - Water Reactors, 1993

Hwang, S.S., Kim, H.P., Kim, J.S., Degradation of Alloy 690 steam generator tubes in operating pressurized water reactor nuclear power plants, Corrosion, Vol. 59, No. 9, 2003, 821-827

Hwang S.S., Kim J.S., Electrochemical interaction of lead with Alloy 690 and Alloy 690 in high-temperature water, Corrosion, Vol. 58, No. 5, 2002, 392-398

Hwang S.S., Kim H.P., Lee D. H., The mode of stress corrosion cracking in Ni-base alloys in high temperature water containing lead, *Journal of Nuclear Materials*, 275, 1999, 28-36

Hwang S.S., Kim U.C., Park Y.S., The effects of Pb on the passive film of Ni-base alloy in high temperature water, *Journal of Nuclear Materials*, 246, 1997, 77-83

Jones R.H., *Stress-corrosion cracking, Materials performance and evaluation*, 1992

Kai A., Takegoshi M., Shoji T., In situ Micro Raman Spectroscopy for characterization of oxide film formed on the new surface and for measurements of the stress of oxide film formed on 304L stainless steel, *Key Engineering Materials*, v 261-263, Proc.5th International Conference on Fracture and Strength of Solids, 2004, 913-918

Kim U.C., Kim K.M., Lee E.H., Effects of chemical compounds on the stress corrosion cracking of steam generator tubing materials in a caustic solution, *J. of nuclear materials*, 341, 2005, 169-174

King P.J., et al., Stress corrosion cracking experience in steam generators at Bruce NGS, Proc. 6th international symposium on environmental degradation of materials in nuclear power systems, 1993, 233-240

Kilian R., Influence of lead on the SCC behavior of SG tubing materials, IAEA specialist meeting on steam generator problems and replacement, Madrid Spain: International Atomic Energy Agency, 1993, p 137

Lemire R.J., McRae G.A., The corrosion of Alloy 690 in high-temperature aqueous media-thermodynamic considerations, *J. Nuclear materials*, 294, 2001, 141-147

Lewis G.N., *Valence and Structure of Atoms and Molecules*, Chem. Catalogue Co. Inc., New York, 1923

Lewis G.N., J. Franklin Inst., 226, 293, 1938

Li L., Luo J.L., et al., Effects of hydrogen on current oscillations during electro-oxidation of X70 carbon steel in phosphoric acid, *Electrochemistry Communications*, v 5, n 5, 2003, 396-402

Lu Y.C., Effect of lead contamination on steam generator tube degradation, Proc. of 12th international conference on environmental degradation of materials in nuclear power systems - water reactors, 2005

Lumsden J., McIlree A., Eaker R., Thompson R., Slosnerick S., Effects of Pb on SCC of Alloy 690 and Alloy 690 in prototypical steam generator chemistries, *Materials Science Forum*, Vols. 475-479, 2005, 1387-1392

Macdonald D.D., The Point Defect Model for the passive state, *J. Electrochem. Soc.*, Vol. 139, No. 12, 1992, 3434-3449

Machet A., Galtayries A., Marcus P., et al., XPS study of oxides formed on nickel-base alloy in high-temperature and high-pressure water, *Surface and interface analysis*, 34, 2002, 197-200

Machet A., Galtayries A., Zanna S., et al., XPS and STM study of the growth and structure of passive films in high temperature water on a nickel-base alloy, *Electrochimica Acta*, v 49, 2004, 3957-3964

Maeng W.Y., Kang Y.H., Kook I.H., et al., The effects of thermal treatment and composition on the IGSCC behaviour of Inconel alloys in simulated nuclear environment, THERMEC'97. International Conference on Thermomechanical Processing of Steels and Other Materials, 1997, pt. 2, vol. 2, 1689-95

Marcus P., On some fundamental factors in the effect of alloying elements on passivation of Alloys, *Corrosion Science*, Vol. 36, No. 12, 1994, 2155-2158

Marcus P., Maurice V., The structure of passive films on metals and alloys, *Proc. 8th international symposium: passivity of metals and semiconductors*, 2001, 30-56

Mirzai M., Maruska C., Pagan S., Lepik O., Stress corrosion cracking/corrosion fatigue/fatigue in Alloy 690, *Proc. 8th international symposium on environmental degradation of materials in nuclear power systems - water reactors*, 1997, 11-18

Misono M., Ochiai E., Saito Y., and Yoneda Y., A new dual parameter scale for the strength of Lewis acids and bases with the evaluation of their softness, *J. Inorg. Nucl. Chem.*, Vol. 29, 1967, 2685-2691

Montemor M.F., Ferreira M.G.S., Walls M., et al., Influence of pH on properties of oxide films formed on Type 316L stainless steel, Alloy 690, and Alloy 690 in high-temperature aqueous environments, *Corrosion*, Vol. 59, No. 1, 2003, 11-21

Montemor M.F., Ferreira M.G.S., Hakiki N.E., et al., Chemical composition and electronic structure of the oxide films formed on 316L stainless steel and nickel based alloys in high temperature aqueous environments, *Corrosion science*, Vol. 42, 2000, 1635-1650

Moulder J.F., Stickle W.F., Scobol P.E., Bomben K.D., *Handbook of X-ray Photoelectron Spectroscopy*, 1992

O'Connor D.J., Sexton B.A., Smart R.St.C., *Surface analysis methods in materials science*, 2nd edition, 2003

Okamoto G., Shibata T., Passivity and the Breakdown of Passivity of Stainless Steel, Passivity of Metals, R. Frankenthal and J. Kruger, Electrochemical Society Princeton, New Jersey, 1978, 646-677

Parkins R.N., in Corrosion'95, paper no. 183, NACE, Huston, 1995

Parkins R.N., in Corrosion'00, paper no. 00363, NACE, Huston, 2000

Pourbaix M, Atlas of Electrochemical Equilibria in Aqueous Solutions, NACE, Houston, 2nd, Edition, 1974

Psaila-Dombrowski M.J., Hua F.H., Lead assisted stress corrosion cracking of Alloy 690, Proc. 9th international symposium on environmental degradation of materials in nuclear power systems - water reactors, 1999, 703-710

Radhakrishnan H., Carcea A.G., Newman R.C., Influence of Pb⁺⁺ ions on the dissolution and passivation of nickel and Ni-21 Cr in acidic solutions, Corrosion science, Vol. 47, 2005, 3234-3248

Rosecrans P.M., Duquette D.J., Formation kinetics and rupture strain of Ni-Cr-Fe alloy corrosion films formed in high-temperature water, Metallurgical and Materials Transactions A: Physical Metallurgy and Materials Science, v 32, n 12, 2001, 3015-3021

Sakai T., Aoki K., Shigemitsu T., Kishi Y., Effect of Lead Water Chemistry on Oxide Thin Film of Alloy 690, Corrosion, Vol.48, No. 9, 1992a, 745-750

Sakai T., Senjuh T., Aoki K., et al., Lead-induced stress corrosion cracking of Alloy 600 and 690 in high temperature water, Proc. 5th international symposium on environmental degradation of materials in nuclear power systems - water reactors, 1992b

Sakai T., Nakagomi N., Kikuchi T., et al., Mechanism of lead –induced stress corrosion cracking of nickel-based alloys in high-temperature water, *Corrosion*, Vol. 54, No. 7 1998, 515-523

Schmuki P., Bohni H., Metastable pitting and semiconductive properties of passive films, *J. Electrochem. Soc.*, v 139, 1992, 1908-1913

Schmuki P., Bohni H., Mansfeld, F., Photoelectrochemical investigation of passive films formed by alternating voltage passivation, *J. Electrochem. Soc.*, v 140, 1993, L119-L121

Seo M., Kurata Y., Nano-mechano-electrochemical properties of passive titanium surfaces evaluated by in-situ nano-indentation and nano-scratching, *Electrochimica Acta* 48, 2003, 3221-3228

Shreir L.L., Jarman R.A., Burstein G.T., *Corrosion (3rd Edition) Volumes 1-2*, 1994

Sikora E., Macdonald D.D., Nature of the passive film on nickel, *Electrochim. Acta*, 2002, 48, 69-77

Staehele R.W., Gorman J. A., Quantitative assessment of submodes of stress corrosion cracking on the secondary side of steam generator tubing in pressurized water reactors: Part1, *Corrosion*, Vol. 59, No.11, 2003 (a); Part 2, *Corrosion*, vol. 60, No.1, 2004 (a); Part 3, *Corrosion*, vol. 60, No.2, 2004 (b)

Staehele R.W., Assessment of and proposal for a mechanistic interpretation of the SCC of high nickel alloys in lead-containing environments, *Proc. 11th international symposium on environmental degradation of materials in nuclear power system-water reactors*, 2003 (b), 381-424

Takamatsu H., Matsunaga T., Miglin B.P., et al., Study on lead-induced stress corrosion cracking of steam generator tubing under AVT water chemistry conditions, *Proc. 8th*

international symposium on environmental degradation of materials in nuclear power system-water reactors, 1997, 216-223

Takumi T., Nobuo T., Takuyo Y., et al., Influence of dissolved hydrogen on structure of oxide film on Alloy 690 formed in primary water of pressurized water reactors, *Journal of Nuclear Science and Technology*, Vol. 40, No. 7, 2003, 509-516

Thomas L.E., Bruemmer S.M., Observation and insights into Pb-assisted stress corrosion cracking of Alloy 690 steam generator tubes, *Proc. 12th international symposium on environmental degradation of materials in nuclear power system-water reactors*, 2005, 1143-1154

Uhlig H.H., Revie R., *Corrosion and corrosion control*, 3rd edition, 1985, p. 61

Van Vliet K.J., Gouldstone A., Mechanical properties of thin films quantified via instrumented indentation, *Surface Engineering*, v 17, n 2, 2001, 140-145

Wright M.D., Mirzai M., Lead-induced SCC propagation rates in Alloy 690, *Proc. 9th international symposium on environmental degradation of materials in nuclear power system-water reactors*, 1999, 657-664

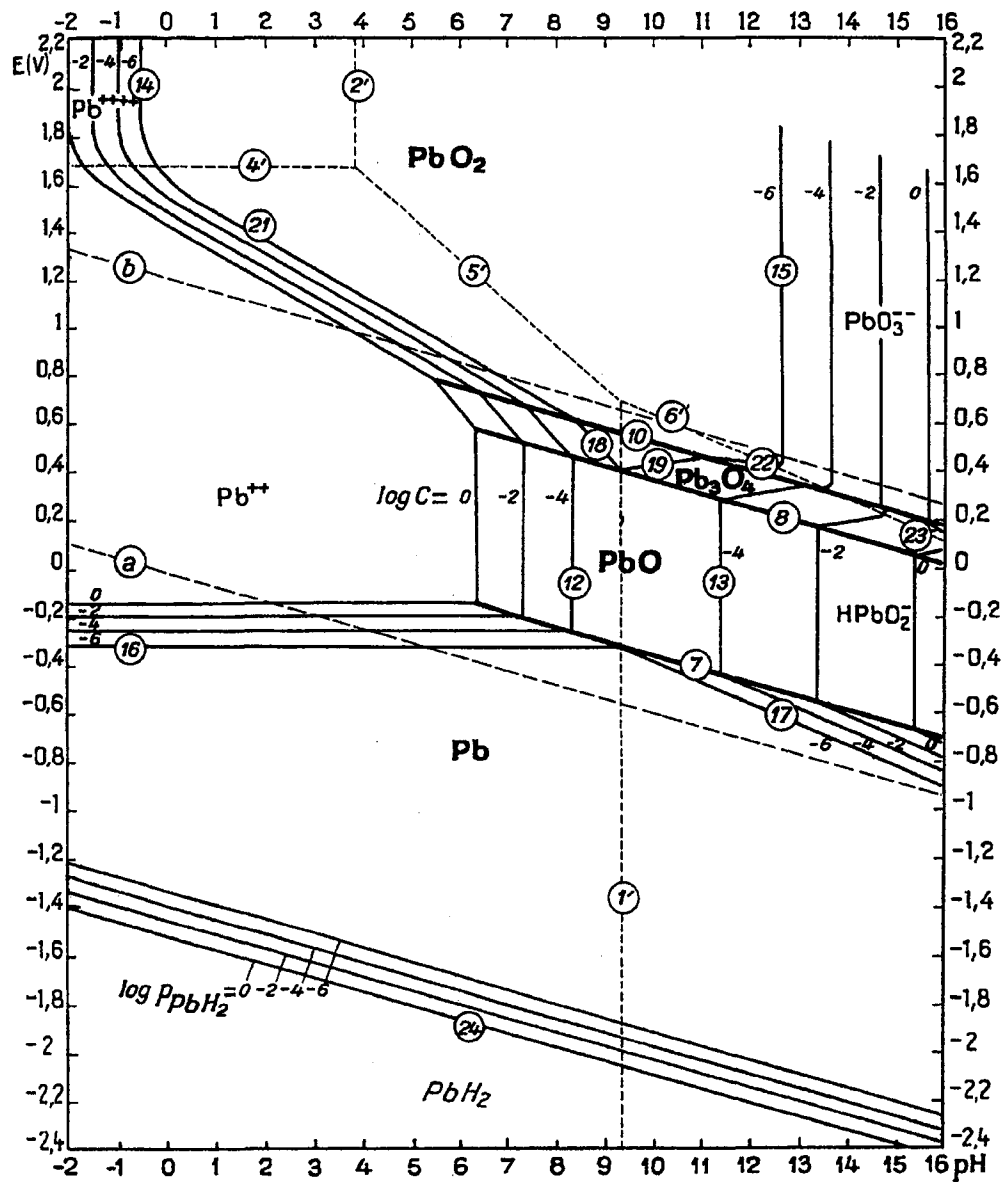
Yang Q., Yu J.Y., Luo J.L., The influence of hydrogen and tensile stress on passivity of type 304 stainless steel, *JES*, v 150, n 8, August, 2003, p B389-B395

Yu J.G., Luo J.L., Norton P.R., Effects of hydrogen on the electronic properties and stability of the passive films on iron, *Applied Surface Science*, v 177, n 1-2, 2001, 129-138

Yu J.G., Zhang C.S., Luo J.L., Norton P.R., Investigation of the effect of hydrogen on the passive film on iron by surface analysis techniques, *JES*, v 150, n 2, 2003, B68-B75

Zeng Y.M., Luo J.L., Norton P.R., Initiation and propagation of pitting and crevice corrosion of hydrogen-containing passive films on X70 micro-alloyed steel, *Electrochimica Acta*, v 49, n 5, 2004, 703-714

Zhang S.H., Shibata T., Haruna T., Inhibition effect of metal cations to intergranular stress corrosion cracking of sensitized Type 304 stainless steel, *Corrosion science*, Vol. 47, 2005, 1049-1061



Potential-pH equilibrium diagram for the system lead-water at 25°C. The reference electrode is standard hydrogen electrode (from Pourbaix 1974).